11-17-2016

Quantitative Proteomic Investigation of Disease Models of Type 2 Diabetes

Mark Gabriel Athanason
University of South Florida, athanason@mail.usf.edu

Quantitative Proteomic Investigation of

Disease Models of Type 2 Diabetes

by

Mark Gabriel Athanason

A dissertation submitted in partial fulfillment
of the requirements for the degree of
Doctor of Philosophy
Department of Cell Biology, Microbiology, and Molecular Biology
College of Arts and Sciences
University of South Florida

Major Professor: Brant R. Burkhardt, Ph.D.
Stanley M. Stevens, Jr, Ph.D.
Meera Nanjundan, Ph.D.
Patrick Bradshaw, Ph.D.

Date of Approval:
November 4th, 2016

Keywords: PANDER, proteomics, phosphoproteomics, stable-isotope labeling

Dedication

The work contained in this dissertation is dedicated to my love and companion, Tori. Her presence illuminates paths through the most challenging endeavors, which I myself could not navigate alone. Additionally, I also dedicate this work to my loving mother, Despina, and father, Gary, for their unrelenting and constant support.

Acknowledgments

I would like to thank my mentor, Dr. Brant Burkhardt for his guidance and support not only through the chaos of the scientific world, but also for providing guidance for every day challenges, too. I also thank my mentors and committee members: Dr. Meera Nanjundan, Dr. Patrick Bradshaw, and especially Dr. Stanley Stevens for his expert knowledge and mentorship that made this project possible. From Dr. Stevens's lab I thank my colleagues and friends, Dr. Dale Chaput and Jenny Guergues. From my own lab I thank Dr. Whitney Ratliff, Dr. Melanie Kuehl, Katie MarElia, Tiffany Shemwell, Arielle Sharp, Ramsey Grace, and Amanda Fernandez for their friendship and comradery, I wish them all the best.

Table of Contents

List of Tables..... iv

List of Figures..... vi

Abstract..... ix

Chapter 1 – Introduction..... 1

Discovery and Characterization of Pancreatic Derived Factor..... 1

The Pander Gene..... 4

Structure of the Pander Protein..... 6

Physiological Role of Pander in the Pancreas..... 7

Pander Expression, Localization and Regulation in Comparision to Insulin..... 8

Physiological Role of Pander in the Liver..... 9

Liver Derived Pander Impacts Hepatic Insulin Signaling in Murine Models..... 10

Pancreatic Derived Pander Impacts Hepatic Insulin Sensitivity and Lipid Metabolism..... 12

Initial Proteomic Analysis of The Pander Transgenic Mouse Liver using Super Silac Aml-12 Cells..... 16

Liver X Receptor Modulates Pander Induced Hepatic Lipogensis..... 21

Hepatic Insulin Resistance in Type 2 Diabetes..... 25

Proteomics and Type 2 Diabetes Research..... 29

Gel-Based Proteomics..... 29

Quantitative Mass Spectrometry Based Proteomics..... 32

Innovation..... 41

Chapter 2 – Generation of The Pander Transgenic Model for Identification of Pander-Induced Hepatic Proteome..... 44
Abstract..... 44
Materials and Methods..... 45
Generation of the Pander Transgenic Animal Colony... 45
Metabolic Treatment of The Pander Transgenic Mouse..... 46
Hepatic Protein Isolation..... 47
Sample Digestion, Desalt, and Scx Fractionation..... 47
Acquisition of Hepatic Proteome by Lc-Ms/Ms..... 48
Database Search for Identification and Quantification of Proteins..... 49
Results..... 50
Discussion..... 76

Chapter 3 – Investigation of The Pander Transgenic Hepatic Proteome..... 78
Introduction..... 78
Materials and Methods..... 81
Statistics And Pathway Analysis..... 81
Hepatic Phosphoproteomic Analysis of The Insulin Stimulated PANTG Mouse..... 84
Immunoblotting..... 86
Cell Culture and Transient Transfection..... 87
Results..... 88
Network and Pathway Analysis..... 88
Proteomic Identification of Pander-Induced Hepatic LXR Pathway..... 93
Validation of Pander-Induced Hepatic LXR Pathway and Fatty Acid Synthase Expression..... 94
Pander Stimulates LXR Transcriptional Activity In-Vitro..... 97
Phosphoproteomic Analysis Reveals Increased Phosphorylation of Glycogen Synthase..... 106
Discussion..... 109

Chapter 4 – Exploring Proteomic Changes in the Fatty Liver... 116
Abstract... 116
Introduction... 117
Materials and Methods... 120
Animals and Diet... 120
Glucose and Insulin Tolerance Testing... 120
Proteomic Experimental Design... 121
Statistical and Pathway Analysis... 121
Results... 122
Metabolic Phenotyping... 122
Proteomic Characterization of the HFD Liver and Network Analysis... 129
Proteomic Analysis: Effects After 2 Weeks HFD... 129
Proteomic Analysis: Effects After 9 Weeks HFD... 135
Discussion... 139

Chapter 5 – Conclusions and Future Directions... 147
Overview and Summary of Major Findings... 147
Hepatic Proteome Characterization of the PANTG Mouse... 147
Pander Affects LXR Promoter Activity... 149
Hepatic Phosphoproteome Analysis of the PANTG Mouse Liver... 150
Metabolic and Proteomic Evaluation of High Fat Diet Fed Mice... 154

Future Directions... 157
Unexplored Information In The PANTG Proteomic Dataset... 157
Improvement of the Experimental Design... 159
Proteomic Evaluation of Other Tissues in the PANTG Mouse... 161
Proteomic Evaluation of the PANKO Mouse... 161
Pander as a Therapeutic Target For T2D... 161

References..... 163

Appendix I: Permissions..... 183

Appendix II: Additional Data..... 196

List of Tables

Table 1: Differentially expressed proteins in the fasted state..... 54

Table 2: Differentially expressed proteins in the fasted state..... 62

Table 3: Differentially expressed proteins in the fasted state..... 69

Table 4: Affected metabolic functions in the insulin stimulated state..... 91

Table 5: Differentially expressed proteins in the fasted state..... 107

Table 6: Proteins modulated by LXR activation after 2 weeks HFD..... 134

List of Figures

Figure 1: North analysis of PANDER mRNA in human tissues 2

Figure 2: Immunogold electron microscopy localization of PANDER in secretory granules 3

Figure 3: DNA sequence from -829 to +29 5

Figure 4: PANDER structure 6

Figure 5: Metabolic phenotype of the PANTG mouse 13

Figure 6: Mechanism of PANDER induced diabetes 15

Figure 7: Proteomic analysis of PANTG mouse 19

Figure 8: Classical LXR activation 24

Figure 9: Pathophysiology of T2D 28

Figure 10: Typical mass spectrometry based proteomic workflow 36

Figure 11: SILAC proteomic experimental approach for investigation of PANTG 52

Figure 12: Distribution of proteins across metabolic conditions 53

Figure 13: IPA determination of altered molecular and cellular functions with the PANTG liver 90

Figure 14: Network analysis of significantly differentially expressed lipogenic associated proteins during insulin stimulator conditions in PANTG liver 92

Figure 15: Canonical pathway analysis of significantly differentially expressed proteins during all metabolic conditions in PANTG liver 93

Figure 16: Western blotting and validation of LXRα and LXR targets (FASN and CYP7A1) in insulin stimulated PANTG mice 96

Figure 17: PANDER increased LXRE transcriptional activity in BNL-CL2 cells 99

Figure 18: PANDER increased LXRE transcriptional activity in 1.1B4 cells 100

Figure 19: PANDER increased LXRE transcriptional activity in 1.1B4 cells 101

Figure 20: T0901317 and/with PANDER increased LXRE transcriptional activity in 1.1B4 cells 102

Figure 21: T0901317 and/with PANDER increased LXRE transcriptional activity in 1.1B4 cells 103

Figure 22: GSK 2033 and/with PANDER increased LXRE transcriptional activity in 1.1B4 cells 104

Figure 23: GSK 2033 and/with PANDER increased LXRE transcriptional activity in 1.1B4 cells 105

Figure 24: Increased phosphorylation of glycogen synthase at Ser627 108

Figure 25: Weight gain of HFD or NC fed mice 123

Figure 26: Physical signs of fatty liver 124

Figure 27: GTT after one week on high fat chow 125

Figure 28: GTT after two weeks on high fat chow 126

Figure 29: ITT after one week on high fat chow 127

Figure 30: ITT after two weeks on high fat chow 128

Figure 31: Cellular functions altered after 2 week HFD exposure 130

Figure 32: Disease functions altered after 2 weeks HFD 133

Figure 33: Proteins involved in the synthesis and metabolism of triacylglycerol and lipids after 9 weeks on HFD 136

Figure 34: Disease functions altered after 9 weeks HFD 137

Figure 35: Heat-map of proteins involved in NAFLD 138

Abstract

PANcreatic DERived factor (PANDER, FAM3B) is a member of a superfamily of FAM3 proteins that are uniquely structured and strongly expressed from the endocrine pancreas and co-secreted with insulin. Unique animal models available to our lab have indicated that PANDER can induce a selective hepatic insulin resistant (SHIR) phenotype whereby insulin signaling is blunted yet lipogenesis is increased. The complexity of the biological networks involved with this process warranted the logical approach of employing quantitative mass spectrometry based proteomic analysis using stable isotope labeling of amino acids in cell culture (SILAC) to identify the global proteome differences between the PANDER transgenic (TG) overexpressing murine model to matched wild-type mice under three metabolic states (fasted, fed and insulin stimulated). Additionally, this technique was used to compare the hepatic proteome of mice on a high fat diet to elucidate early and late mechanisms of disease progression. The "spike-in" process was employed by equal addition of lysate obtained from livers of heavy L-Lysine (13C6, 97%) fed mice to the mice liver protein lysate (PANTG and WT) for relative quantitative analysis. Upon acquisition of the

dataset by use of liquid chromatography tandem mass spectrometry (LC-MS/MS, LTQ Orbitrap), geometric means and Uniprot Protein identification numbers were uploaded to Ingenuity Pathway Analysis (IPA) to reveal the effect of PANDER on hepatic signaling. IPA identified lipid metabolism and fatty acid synthesis as top cellular functions differentially altered in all metabolic states. Several molecules with a role in lipid metabolism were identified and include FASN, ApoA1, ApoA4, SCD1, CD36, CYP7A1 and ACC. Furthermore, central to the differentially expressed proteins was the revealed activation of the liver X receptor (LXR) pathway. In summary, our SILAC proteomic approach has elucidated numerous previously unidentified PANDER induced molecules and pathways resulting in increased hepatic lipogenesis. In addition, we have demonstrated strong utility of this approach in comprehensively phenotyping animal models of hepatic insulin resistance. PANDER may potentially propagate pro-hepatic lipogenic effects by LXR activation in contrast to increased LXRα expression. This can be evaluated through the use of LXR agonists (T0901317) antagonists (GSK 2033). LXR activity can be measured by luciferase assays using an LXRE response plasmid. Our central hypothesis is that PANDER induces activation of LXR and is measured and predicted in our line of experiments. In general, PANDER induced LXR activation will be

enhanced by T0901317 and diminish effects of GSK 2033 along with direct correlation of downstream metabolic effects such as increased hepatic lipogenesis and fatty acid metabolism. Taken together, PANDER strongly impacts hepatic lipid metabolism and may induce a SHIR phenotype via the LXR pathway. Additionally, phosphoproteomic analysis uncovered large-scale differences in protein phosphorylation states as PANDER impacts insulin signaling. A notable finding was the increased phosphorylation of glycogen synthase (GSK), possibly responsible for the decreased hepatic glycogen content in the PANTG mouse. In an effort to map out critical molecules involved in non-alcoholic fatty liver disease (NAFLD) pathogenesis, the same proteomic approach was carried out, providing a unique dataset of differentially expressed hepatic proteins due to a high at diet.

Chapter 1 – Introduction

Discovery and Characterization of Pancreatic Derived Factor

PANcreatic-DERived Factor (PANDER) is a well characterized secreted hormone that was discovered through the use of the algorithm Ostensible Recognition of Folds (ORF) which predicted novel cytokine-like proteins based on secondary structure homology of several cytokines such as IL-2 - 7, -9, -10, and -13. The secondary structure of many cytokines can be described as a four-helix bundle with up-up-down-down topology [2]. Therefore, ORF identified a novel family of proteins predicted to possess the secondary structure typical to many cytokines: FAMily with sequence similarity 3 (FAM3). The family of proteins consists of four constituents: FAM3A, FAM3B, FAM3C, and FAM3D. Northern blot analysis revealed mRNA expression to exist mainly in the pancreas of human and mouse (Figure 1) [1]. Further immunohistological staining revealed localization of PANDER in the Islet of Langerhans in both α and β-cells, specifically co-localizing with insulin in secretory vesicles (Figure 2); FAM3B was later coined PANDER due to these features [1, 3, 4].

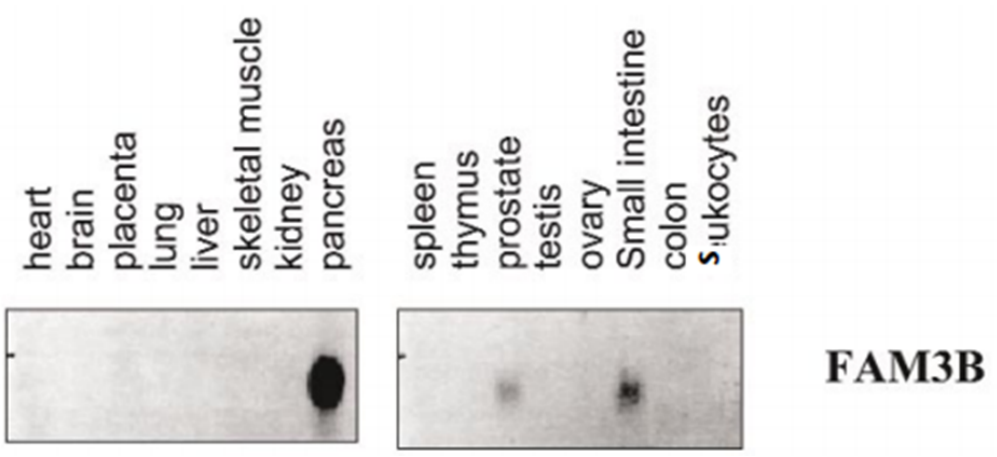

Figure 1: North analysis of PANDER mRNA in human tissues. PANDER indicated a high level of mRNA in pancreas, and to a lesser extent in small intestine and prostate. Figure from *Zhu* et al. [1].

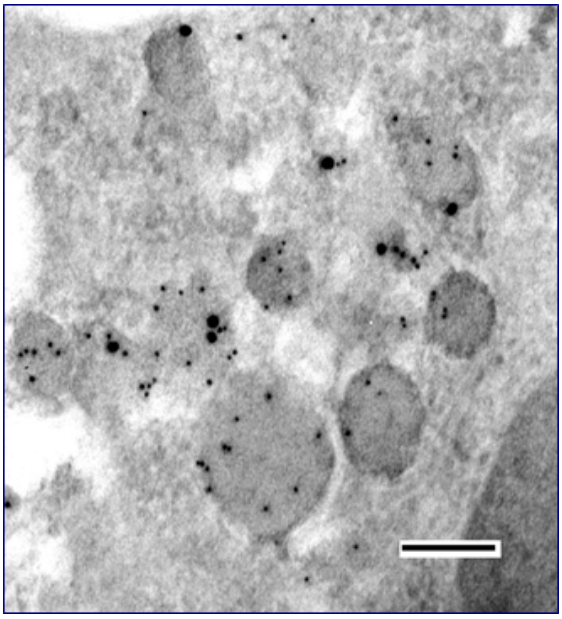

Figure 2: Immunogold electron microscopy localization of PANDER in secretory granules. Mouse islets were stained with rabbit anti-PANDER and mouse anti-insulin antibodies, followed by gold-conjugated secondary antibodies, prior to electron microscopy. PANDER was labeled with 18 nm gold particles, insulin with 6 nm gold particles. The bar is 100 nm. Figure from *Xu* et al. [4].

The Pander Gene

In humans, PANDER is located on the chromosome 21q22 [1]. The murine gene is located on chromosome 16B-C4 and consists of eight exons spanning approximately 32 kilo-base pairs [3]. In mice, the pancreatic transcriptional start site (TSS) is located 520 base pairs upstream of the translational start codon in β-cells. The murine promoter, between -335 and +523 relative to the pancreatic TSS, contain binding sites for A and E box elements, hepatic nuclear factors (HNF) 1 and 4α, and signal transducer and activation of transcription (STAT) 3, 5, and 6 (Figure 3) [3]. More recently, an additional TSS has been identified as determined from examination of PANDER expression within primary hepatocytes. The hepatic PANDER TSS was located 26 base pairs upstream of the PANDER translational start site [5]. Under high glucose conditions, carbohydrate response element binding protein (ChREBP) has been shown to bind to the PANDER promoter and promote PANDER gene expression [5]. In the pancreas, the A box elements have been shown to confer tissue specific expression of PANDER in the pancreas by allowing for the interaction of the transcriptional factor Pancreatic/Duodenal Homeobox domain-1 (PDX-1) with the PANDER promoter [6]. Overall, the PANDER gene demonstrates strong expression by both the pancreatic islets and liver and is

heavily determined by regulatory elements within the promoter region many of which serve functions in metabolic regulation.

B

```
TGGGCTCCTT GGAAGAGGAG GAACAAGGAT GGAATAGAAT TCCTACAGCT -779
                           HNF-1                    A box
GGACTGGAGT CTCAGCTTGC CTTAGTTACT TAAGACCACT GTGACTCTAA -729
        HNF-4/STAT5                                 A box
TGAGCTAAAA AGTTCTGTGA AAACCTGAAC CCTGGAGATT GAGAGGGTAC -679

TGTGCCTACT CAGGTGGAAG GGTGGGTAAA CCTAGGAAGC CTTCACCCAT -629
                                              Oct-1
TCACTTGACA CCATTTCTGA GTCCCATGTC CTTGTATATA CATATCCCAA -579
                                 STAT3      A box
GGGACCTGGA GCTCTTTCTC ACCTCATTTC CCTAAAATAA TCATCCCATC -529
                                          +1 (pancreatic)
AGTAAAGAAG GAAGGGGTTG GCACCACACT GGGTCACATG TCAGCAAGGG -479

GGCAGTGTGA CGACTTTGGA CACAATGTAG AGCCTTGGCA TTTGGAGCAG -429

GAGCTTTGCT CTAGGATTCT GTGTTCATGA GGCTTGAGCC AGTCTATACT -379
           STAT6
TTACTGCCAT TTCTTGTGAA ACTAAGGTCG GGAATACTAT TGTTAGGGGC -329

GCCTTAAAGT AAACTCTTGG TGTTCTTTCT CTGATTACAT TAGCTCTAGC -279
HNF-4 (-)            E Box
CTTTGGCCGT CTGTAGCCCC AGGTGAACAG GACAGAAAGT GCCTCCTGCT -229
                                    E Box
TCTTAGGTGA CCCTGGAGCT CCAGGGTGCT ACCAGCTGTG CAGCCCCACC -179

CATACCTGCT AGCCTGCCAG TCTGCCAGCT ACTCTGAACC TTCCTGCTTT -129
             E Box
ATGGATCCTC CCATTTGCTG GGAATTGGTC CACCCTTTTC TGCCTGCCCC -79
           A Box
AAGGGCGGTC ATAATCTATG TGCAGCTCAA GCAGGTAGGC CAGCTTTCAT -29
                                  +1 (hepatic)
AGGTCCCTGG GGATTGCAGC CAAGAGCTGT GAGCTCCGCG AGCAGTTTCT +21

GGAAGATG +29
```

Figure 3: DNA sequence from -829 to +29. The identified transcriptional start site is bolded and denoted by +1 hepatic. The previously identified pancreatic start site is denoted by +1 pancreatic. Putative transcription factor binding sites as predicted by MatInspector 7.0 (Genomatix) are shown and underlined. These sites include A and E box elements, hepatocyte nuclear factor (HNF), signal transducer and activator of transcription (STAT) and octamer binding protein-1 (Oct-1). The PANDER translational start codon ATG is italicized and located at the end of the nucleotide sequence. Figure from *Ratliff* et al. [5]

Structure of the Pander Protein

In humans, PANDER contains 235 amino acids and shares a 78% sequence homology (including 4 conserved cysteines) with the murine form. Amino acid sequence homology ranges between 31.6% - 53.3% amongst the FAM3 constituents and has no sequence homology to any known cytokine [7]. In 2013, the crystal structure of secreted PANDER was determined and revealed a unique globular β-β-α fold as a major structural motif (Figure 4). This structure is conserved in all four constituents of FAM3 proteins. The crystal structure of PANDER contradicts the original assumption of the protein resembling a typical cytokine; therefore the structure of FAM3 represents a novel class of signaling molecules and is unlike that of any known cytokine [8].

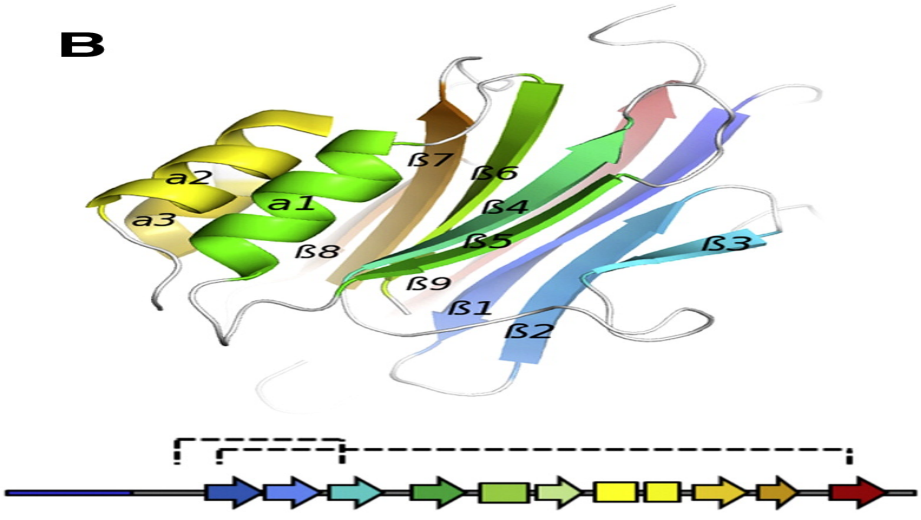

Figure 4: PANDER structure. Murine PANDER structure above with diagram below colored from blue to red from N terminus to C terminus. Disulphide topology is indicated by dashed lines. Figure from *Johansson* et al. [8].

Physiological Role of Pander in the Pancreas

An initial *in-vitro* evaluation of the autocrine function of PANDER demonstrated that overexpression, either by exogenous recombinant PANDER treatment or PANDER adenoviral delivery in human, mouse, and rat islets, along with β-TC3 cells, induced apoptosis [7, 9]. Apoptotic mediators involved in cytokine-induced apoptosis such as Akt, STAT1, *NF*-κB, and Fas were not affected. Instead, a caspase-dependent mechanism was observed, with cleavage of caspase-3 being central without the production of either Ca^{2+} or nitric oxide (NO), suggesting a non-canonical apoptotic pathway [7, 10]. Furthermore, a microarray study on PANDER-treated vs. control mouse islets revealed twenty-two genes with association to cell death to be differentially expressed [11]. Cyclin-dependent kinase inhibitor 1A (CDKN1A), also known as p21, was the most affected gene. The downregulation of p21 has been associated with cell death in other cell types [12]. Additionally this analysis revealed the activation of caspase-3, a molecule critically involved in β-cell death in autoimmune disease [13]. Caspase-3 has been demonstrated to cleave p21, which is an important mechanism for death-associated cyclin A/Cdk2 activation in various cell types [14]. Taken together, the marked downregulation of p21 and simultaneous activation of caspase-3 are central players in the PANDER-induced mechanism of apoptosis in islet cells [11].

Pander Expression, Localization and Regulation in Comparison to Insulin

Initial evidence strongly supported the concept that PANDER is involved in glycemic regulation. In particular, PANDER was identified within the secretory granules of the pancreatic β-cells in conjunction with insulin. As previously mentioned, PANDER is localized in the β-cell insulin granules which suggest that PANDER is co-secreted with insulin in response to glucose. Glucose treatment, in a time and dose dependent manner, increased PANDER and insulin secretion in β-cell lines. Treatment with insulin secretagogues, such as potassium chloride, markedly increased PANDER secretion. Glucose stimulation on mouse islets overexpressing PANDER in β-cells also significantly increased PANDER secretion [10, 15]. Previous studies have demonstrated a role of PANDER impacting insulin secretion from β-cells, in turn affecting glucose metabolism. In β-TC3 cells, recombinant PANDER treatment decreased basal insulin secretion, however had no effect on β-cell glucose metabolism or glucose stimulated secretion [1]. Additional experiments demonstrated the ability of PANDER overexpression to amplify signals of glucose stimulated insulin secretion (GSIS) by altering calcium signaling in pancreatic β-cells. This was demonstrated by overexpressing PANDER in murine islets by exogenous recombinant PANDER application or adenoviral

PANDER delivery, where this had no impact on GSIS, however did impair insulin secretion in the presence of glucose with various insulin secretagogues such as carbachol or potassium chloride [9]. Taken together, PANDER secretion from pancreatic β-cells is thought to be regulated in a manner similar to that of insulin.

Physiological Role of Pander in the Liver

^{125}I-PANDER saturation and competitive binding assays revealed the liver membrane as the primary target tissue involved in PANDER signaling. Similar analyses on brain, kidney, adipose, and pancreatic membrane tissue samples were performed with no significant positive findings; however, the receptor remains unknown. In the human hepatoma cell line HepG2, recombinant PANDER treatment impacted insulin signaling by suppressing activation of several signaling molecules: insulin receptor-β (IRβ), insulin receptor substrate-1 (IRS-1), phosphatidylinositol-3′-OH-kinase (PI3K), and Akt [16]. In primary mouse hepatocytes, either treated via adenoviral delivery or by exogenous treatment of PANDER, elevated gluconeogenic gene expression and glucose output was observed, accompanied by increased levels of cyclic adenosine monophosphate (cAMP) and cAMP-responsive element binding protein (CREB) signaling [17]. Although exogenous hepatic PANDER influences metabolic functions, the liver is the suggested novel target tissue of PANDER secretion from the endocrine pancreas

[16]. We hypothesized that the pathophysiological conditions of metabolic disease increase circulating levels of PANDER; another group has reported evidence of this in an Asian population with varying degrees if insulin resistance. We now hypothesize that increased PANDER levels can act on the liver, promoting dangerous metabolic functions contributing to the pathophysiology of liver disease.

Liver Derived Pander Impacts Hepatic Insulin Signaling in Murine Models

There have been several animal models created in order to investigate the role of PANDER in the context of glucose and lipid metabolism in the liver with varying results being observed. In PANDER-deficient mice (PANKO), glucose intolerance was observed due to impaired insulin secretion from pancreatic β-cells [18]. However, in a similar study these mice also displayed increased hepatic insulin sensitivity due to decreased hepatic glucose production compared to wild-type mice in a hyperinsulinemic-euglycemic clamp assay [19, 20]. Conversely, liver-specific overexpression of PANDER increases the expression of important gluconeogenic genes such as phosphoenolpyruvate carboxykinase (PEPCK) and glucose-6-phosphatase (G6Pase), overall increasing hepatic gluconeogenesis [17]. Viral overexpression of PANDER in the liver of C57BL/6 mice increased lipogenesis, which was attributed to the decreased activation of

Akt and AMP-activated protein kinase (AMPK) and concordantly increasing levels of forkhead box 1 (FOXO1) protein expression [19]; a similar observation was made *in vitro*, where cultured murine hepatocytes overexpressing PANDER had suppressed insulin-stimulated activation of Akt and subsequent FOXO1 inactivation. In these same mice, hepatic PANDER overexpression led to increased serum levels of very low density lipoprotein (vLDL) triglycerides causing global insulin resistance. Small interfering RNA (siRNA)-mediated knockdown of hepatic PANDER attenuates almost all of the effects observed during viral-mediated overexpression of PANDER in diabetic mice. Hepatic steatosis is markedly decreased; PANDER knockdown increases activation of Akt and AMPK, while causing a reduction in FOXO1 protein expression. PANDER knockdown also improved insulin resistance globally by reducing levels of circulating glucose and vLDL [19]. Taken together, it is difficult to distinguish if the physiological impact PANDER has on the liver is driven by islet or hepatic derived PANDER. Significant promoter activity of PANDER has been observed in hepatic cell lines [3]. As previously mentioned, our lab recently discovered a liver specific TSS of the PANDER gene in primary murine hepatocytes [5]. While some data does support liver derived PANDER as having an important role in insulin signaling and hepatic glucose production (HGP), the actual physiological impact and mechanisms

driving it remains largely unknown. However, the evidence more strongly supports islet derived PANDER acting on the liver via endocrine signaling interaction. In an effort to clear up these discrepancies, our lab created the only transgenic animal model stably overexpressing PANDER specifically in the endocrine pancreas.

Pancreatic Derived Pander Impacts Hepatic Insulin Sensitivity and Lipid Metabolism

The PANDER transgenic (PANTG) animal model has proven invaluable in the ongoing effort to better understand the endocrine function of pancreatic derived PANDER and its putative role in hepatic insulin signaling. These mice over-express PANDER from the pancreatic β-cells of the Islets of Langerhans and display elevated serum levels of PANDER [21]. As previously discussed, there is overwhelming evidence to support the liver as being the target organ of PANDER endocrine signaling and affecting the metabolism of glucose and lipids in the liver [5, 16, 19, 21, 22]. Due to elevated circulating levels of PANDER in the blood of PANTG mice, males display fasting hyperglycemia and hyperinsulinemia as well as glucose intolerance during a glucose tolerance test. These same mice display increased hepatic glucose production and overall insulin resistances compared to wild-type mice during a hyperinsulinemic-euglycemic clamp study (Figure 5).

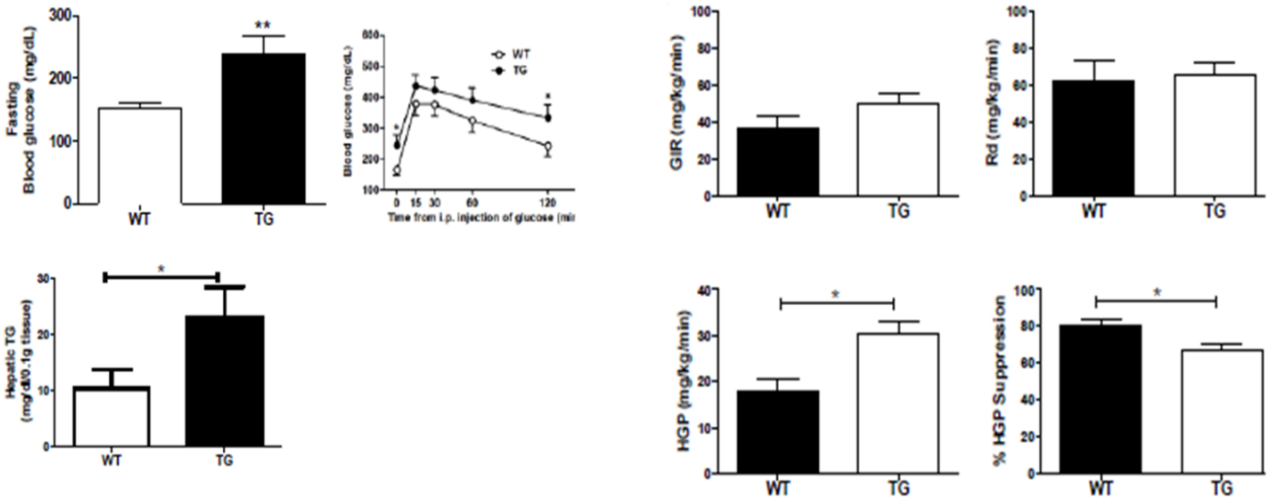

Figure 5: Metabolic phenotype of the PANTG mouse. PANTG mice display fasting hyperglycemia (left, top left) as well as glucose intolerance after a glucose tolerance test (left, top right) as compared to the wild-type mouse. Hepatic triglyceride content was significantly increased in the PANTG mouse livers (left, bottom right). HEC assays revealed steady glucose infusion rate (GIR) and glucose disposal (Rd) (right, top left and right, respectively, N=8). HEC assays also revealed impaired insulin signaling whereby hepatic glucose production is increased and HGP suppression decreased significantly (N=6-8, $P<0.05$ by students two-tail t-test). Figure from *Robert-Cooperman* et al. [21].

Additionally, and very interestingly, an increase in triglyceride content was observed in the livers of the PANTG mouse [21]. Type 2 diabetes is mainly characterized by insulin resistance in several organs, including the liver. Normal insulin signaling promotes hepatic lipogenesis, however in the state of T2D a metabolic anomaly occurs where insulin signaling selectively promotes hepatic lipogenesis but fails to suppress HGP, or selective hepatic insulin resistance (SHIR) [23, 24]. Considering the metabolic triad of type 2 diabetes, including hyperglycemia, hyperinsulinemia, and hyperlipidemia, SHIR is a severe metabolic defect and the mechanism driving its progression is largely unknown and will be discussed in greater detail later. Taken together, the PANTG mouse displays a very similar SHIR phenotype. The pleiotropic effect of PANDER overexpression causing increased hepatic triglyceride and glucose production could be attributed to decreased activation of Akt [16] and AMPK and ACC in the fasted state as shown by western blotting [21]. However, to comprehensively investigate the complex nature of the PANDER induced metabolic effects observed in the liver, our lab employed a quantitative mass spectrometry approach in order to compare the hepatic proteome of PANTG and wild-type mice. The metabolic pathology induced by PANDER overexpression is outline in Figure 6.

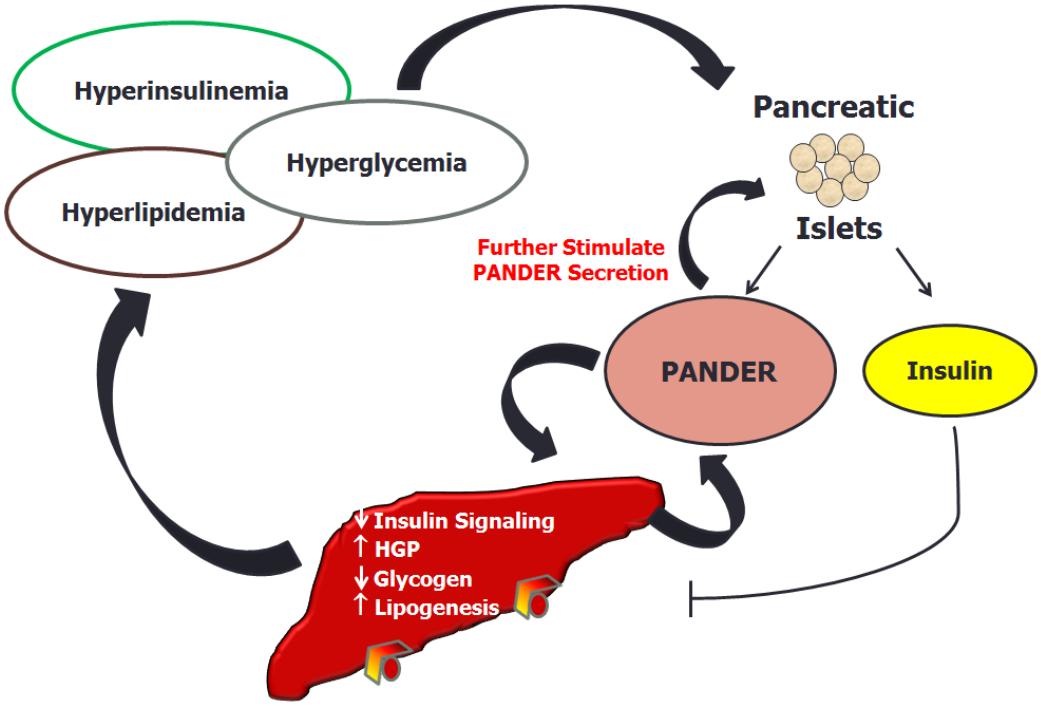

Figure 6: Mechanism of PANDER induced diabetes. The pathophysiological conditions of T2D can stimulate secretion of PANDER from the endocrine pancreas. PANDER overexpression has been shown to affect insulin signaling in the liver, whereby insulin signaling is blocked in terms of glucose metabolism yet lipogenesis is promoted mimicking a selective hepatic insulin phenotype.

Initial Proteomic Analysis of The Pander Transgenic Mouse Liver using Super Silac Aml-12 Cells

The initial phenotype of the PANTG mouse can be characterized by increased fasting and fed circulating glycemic levels and increased hepatic triglyceride content due to insulin resistance in the liver. This bifurcation of events mimics the selective hepatic insulin resistant (SHIR) state seen in type 2 diabetes. Insulin signaling is a highly complex process that activates a tyrosine phosphorylation cascade affecting numerous biological functions [25, 26]. Insulin impacts over 100 proteins, many of which are involved in metabolic and mitogenic regulation [26, 27]. Our hypothesis is that PANDER drives selective hepatic insulin resistance (SHIR) during pathophysiological conditions of type 2 diabetes. In order to detail the mechanism of PANDER induced hepatic signaling, we employed state of the art proteomic technology. The quantitative proteomic strategy, stable isotope labeling of amino acids in cell culture (SILAC), allows for the metabolic labeling of all proteins with either ^{13}C-lysine or ^{13}C-arginine in a system; either in cell culture or whole animals [28, 29]. “Spike-In” SILAC employs heavy labeled reference proteins or proteomes that are added to the proteomes (primary tissue) under investigation. These protein mixtures can then be analyzed by liquid chromatography tandem mass spectrometry (LC-MS/MS) for the identification of peptides in

the sample. Relative quantification is possible when overlapping labeled “heavy” and “light” unlabeled peptides exist in the same sample, allowing for the differences in spectral intensities to be used in the calculation. This method has become a relatively novel and highly useful tool because it allows one to take a molecular snap-shot of all the proteins in a mixture, or a proteome. The proteome can be used to identify networks of proteins that are differentially expressed and known to be involved in signaling cascades or metabolic pathways [29, 30], and the use of bioinformatics tools such as Ingenuity Pathway Analysis (IPA) greatly assist in doing so [31]. The initial proteomic analysis was performed on the liver lysate of six PANTG and wild-type mice using labeled ethanol-treated AML-12 cell lysate, a murine liver cell line, for spike-in. Roughly 1640 proteins were identified and quantified. Of those proteins, 88 proteins were upregulated and 9 downregulated in the PANTG mouse liver. IPA identified lipid metabolism (Figure 7) as the top significantly affected protein network involving 20 proteins, including sterol carrier protein (SCP2), acetyl CoA synthetase (ACSL1), ectonucleoside triphosphate diphosphohydrolase 5 (ENTPD5), and fatty acid binding protein (FABP1). Further research would be required to elucidate a precise mechanism from this information. ACSL1 is an isozyme of the long-chain fatty-acid-coenzyme A ligase family that convert

free long-chain fatty acids into fatty acyl-CoA esters, and serve a central role in lipid biosynthesis [32]. FABP1 and SCP2 serve as binding and carrier proteins involved in lipid homeostasis [33]. PRKAR2B and ENTPD5 are involved in the substrate production necessary for lipogenesis. In these instances, MS based proteomic techniques almost seem to have a drawback in that it provides too much information. However, the mass spectrometry (MS) method also revealed the upregulation of phosphoenol-pyruvate carboxykinase (PEPCK), up 3.5 fold in the PANTG mouse (Figure 7). PEPCK controls the rate limiting step in gluconeogenesis and suppression is expected under conditions of hyperglycemia and insulin secretion [34], however in the PANTG mouse liver the opposite is apparent, and is supported by both the results of the hyperinsulinemic euglycemic clamp study and glucose tolerance testing [21]. In this particular experiment, numerous factors existed that constrained us from get the best results, that is: most protein identification and mass accuracy. Despite these shortcomings, the MS based proteomic technique proved valuable in identifying key molecules involved in biochemical processes promoting the phenotype of PANDER overexpression. To circumvent this, we recently published a similar, refined study that was performed in order to analyze the PANTG mouse liver using age and gender matched mice in various controlled metabolic states [22].

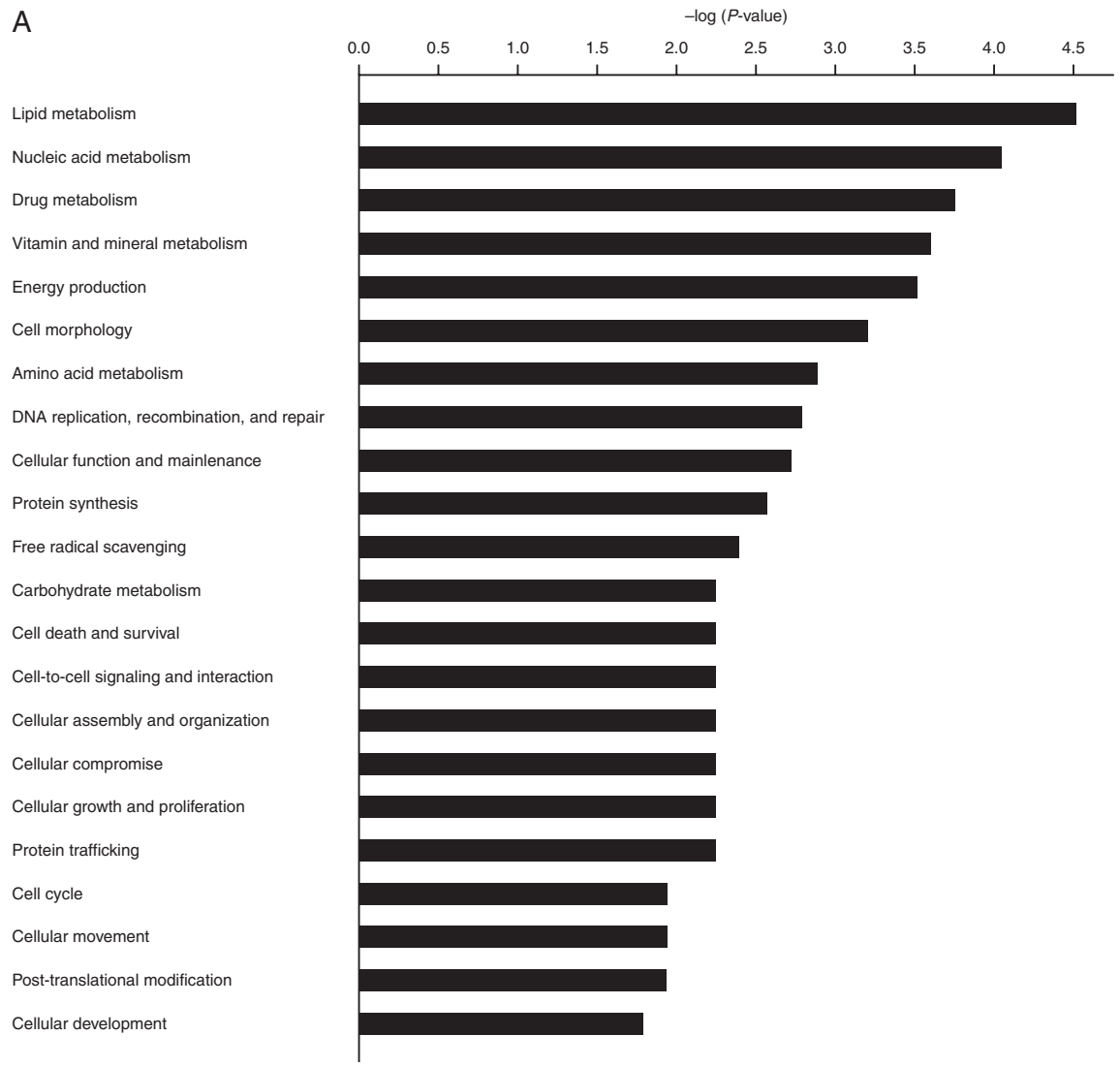

Figure 7: Proteomic analysis of PANTG mouse. Relative changes in the levels of identified proteins were determined by the ratio of PANTG to that of WT. (A) IPA analysis of predicted impacted metabolic functions indicates lipid metabolism as the top function altered in PANTG liver. (B) Differentially expressed hepatic proteins identified in PANTG predicted to act in concert to increase triglyceride production. (C) Network analysis of differentially expressed proteins that molecularly interact involved in triglyceride production. Figure from *Robert-Cooperman* et al. **[36]**.

B

Increased PANTG hepatic proteins	Fold change above WT
FABP1	2.8
PKA	2.8
PEPCK	3.5
SCP2	3.5
ACSL1	4.6
ENTPD5	8.3

C

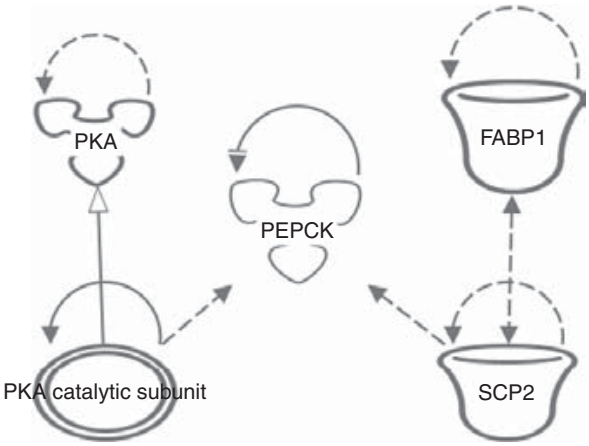

Figure 7: Continued

Liver X Receptor Modulates Pander Induced Hepatic Lipogensis

Our proteomic investigation provided strong evidence to suggest that lipid metabolism is increased in the liver of the PANTG mouse by analysis of differentially expressed proteins. Additionally, several of these proteins are known to be modulated by the liver X receptor (LXR), an important transcriptional factor regulating lipid metabolism. *In vitro*, exogenous PANDER treatment stimulated LXR transcription using LXR reporter constructs. Due to the pleotropic action PANDER signaling elicits on the liver, LXR is suggested to play a key role in PANDER induced lipogenesis. Liver X receptors (LXR) are transcription factors belonging to the class II nuclear receptor superfamily and are composed of 2 isoforms [37-39]. LXRα is highly expressed in the liver, intestine, and adipose tissues whereas LXRβ is ubiquitously expressed. Upon activation, LXRs form a heterodimer with the retinoid X receptor α (RXR) which binds to LXR response elements (LXREs) enhancing specific targeted gene expression in a functional dependent manner, outlined in Figure 8. Oxysterols are generally accepted as the endogenous LXR agonist in humans, with the most potent activators being 22(R)-hydroxycholesterol, 20(S)-hydroxycholesterol, 24(S)-hydroxycholesterol and 24(S), 25-epoxycholesterol [40-43]. LXR activity is not only governed by agonist and antagonists, but also by changes in expression which

LXR itself impacts by an auto-regulatory loop [44]. LXRs appear to regulate overall glucose, cholesterol, bile acid, and triglyceride homeostasis (Figure 8) [45]. LXRs were initially considered therapeutic targets for T2D but beneficial effects have been hampered with hyperlipidemia and hepatic steatosis [46, 47]. LXR agonists (such as T0901317) can directly activate critical genes necessary for hepatic *de novo* lipogenesis which serves as a contributor to triglyceride accumulation in non-alcoholic fatty liver disease (NAFLD) [48, 49] either indirectly by increasing expression of SREBP-1c [50] and ChREBP [51], and directly by promoting transcription of SCD1 [52], FasN [53], and ACC [54]. In addition, LXR governs cholesterol transport by impacting ATP-binding cassette transporter a1 (Abca1) [55], Abcg1 [56], Abcg5 [57], and Abcg8 [57], and bile acid metabolism by CYP7A1 [58]. Previous research (reviewed in [59-61]) has strongly supported the implication that PANDER is involved in the pathogenesis of NAFLD and T2D. Our proteomic analysis of the PANTG liver demonstrates that lipid metabolism is strongly altered when compared to the wild-type mouse. Additional computational analysis with IPA was performed to identify canonical functions impacting the mechanism for the increased lipogenic state and the activation of the LXR pathway was a top candidate during all metabolic states [21, 35]. FasN is considered one of the most critical genes involved in LXR

governed hepatic lipogenesis [53] and was demonstrated to be upregulated in all three metabolic states. In addition, SCD1 was increased in the PANTG by 5.5 fold [22, 35]. SCD1 is crucial for the lipogenic effect of LXRs [52]. Other differentially expressed proteins within the LXR predicted network included ACC, CD36 and CYP7A1 (FIG) [22, 35]. Western blotting analysis confirmed an increase expression of FasN and Cyp7A1, as well as an increase of LXR expression within the PANTG liver (FIG). *In vitro, r*eporter gene analysis was performed on BNL-CL2 liver-derived cells transfected with LXRE-luciferase plasmids exposed to increasing concentrations of purified secreted PANDER (AstraZeneca) followed by measurement of luciferase activity, which displayed an increased activity of the LXR promoter in a dose-wise manner [22]. Taken together, the proteomic analysis resulting from the PANTG and *in vitro* functional assays indicated that PANDER may potentially impact hepatic lipogenesis via the LXR pathway and will be discussed in greater detail in Chapter 3.

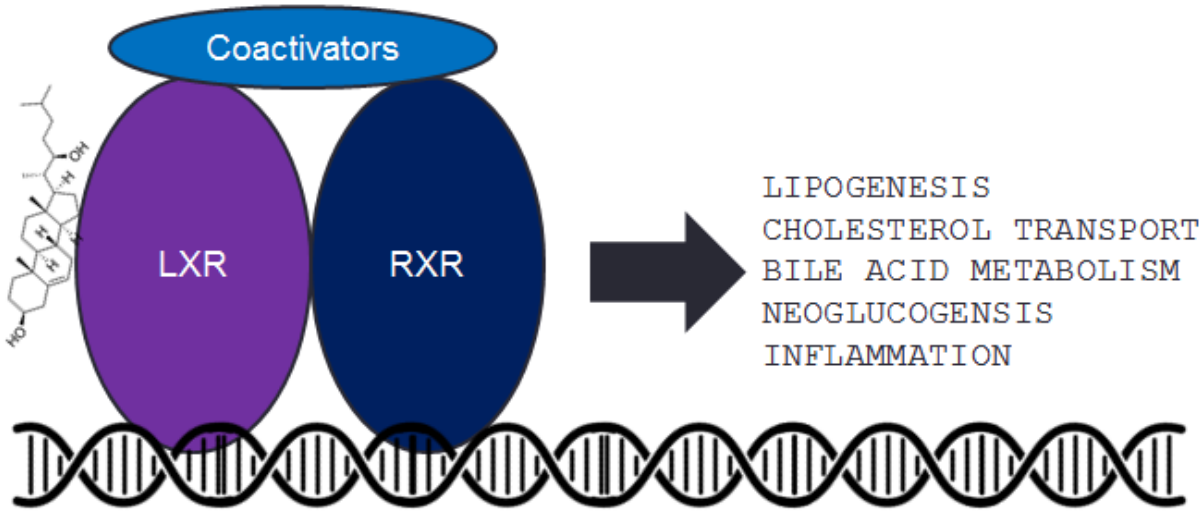

Figure 8: Classical LXR activation. In the presence of oxysterols, LXRs form a heterodimer with the RXRs which binds to LXR response elements (LXREs) enhancing specific targeted gene expression in a functional dependent manner.

Hepatic Insulin Resistance in Type 2 Diabetes

Type 2 diabetes has become one of the most major health epidemics of our time [62]. Incidence of T2D has increased drastically over the decades [63-65] with the pronounced changes in human behavior and the environment resulting in increased obesity to blame [66]. Humans with T2D exhibit the classic metabolic triad of hyperinsulinemia, hyperglycemia, and hypertriglyceridemia. Hyperglycemia in the presences of hyperinsulinemia is described as insulin resistance, with the major contributing organs being the liver, muscle, and adipose tissue. T2D has also been attributed to impaired β-cell function and/or loss of β-cell mass [67, 68]. In order to understand this metabolic dilemma, a rudimentary understanding of normal glycemic regulation is necessary (Figure 9). Under normal conditions, insulin is stored in the pancreatic β-cells until its release is required when blood glucose levels rise. Insulin signals for the muscle and liver to take up excess glucose which can then be used for cellular fuel or stored in the form of glycogen. Insulin signaling also suppresses hepatic glucose production and causes the release of fatty acids from adipocytes [69, 70]. In the diabetic state, however, almost every aspect of glucose and lipid metabolism goes awry (Figure 9). Impaired insulin secretion from pancreatic β-cells causes an overall decrease in insulin signaling, resulting in a lack of glucose

uptake which ultimately causes hyperglycemia. This decrease in insulin sensitivity results in impaired glucose tolerance, increased hepatic glucose production, and increased fatty acid release from adipose tissue. In order to combat this, the pancreas continues producing insulin to no avail, leading to hyperinsulinemia. High levels of glucose and fatty acids in the blood promote this dangerous positive feedback loop, further driving insulin resistance and worsening of the pathophysiological progression of T2D [71]. How organs act in concert to promote insulin resistance is weakly understood, however the liver is arguably the most significantly dysregulated organ in T2D. The liver is responsible for both glycogenolysis [72], the breakdown of glycogen for energy, and gluconeogenesis [73], the conversion of non-carbohydrate sources to glucose. Normally, insulin suppresses the release of fatty acids in the blood from adipocytes [70, 74] and decreases blood glucose levels, however in an insulin resistant state, this is not the case. The excess of these oxidized compounds can accumulate in the liver which can lead to other metabolic diseases such as nonalcoholic fatty liver disease and ultimately cirrhosis of the liver [75, 76]. The major contribution the liver has in T2D was briefly mentioned previously: selective hepatic insulin resistance. Normally, insulin signals two major events to take place in the liver. The first is the decrease in

gluconeogenesis, whereby insulin allows for the phosphorylation of FOXO1 which inhibits its translocation to the nucleus, downregulating genes such as PEPCK and G6Pase required for gluconeogenesis [77]. Additionally, hepatic insulin signaling activates genes necessary for lipid synthesis. Insulin activates the transcription factor SREBP-1c which facilitates the transcription of genes responsible for fatty acid synthesis, such as ACC and FasN [78, 79]. In the liver of T2D patients, the FOXO1 pathway becomes insulin resistant, whereby gluconeogenesis continues despite elevated blood glucose levels. Simultaneously, the lipogenic gene pathways modulated by SREBP-1c are maintained and fatty acid synthesis persists [80]. This increase in hepatic glucose output and fatty acid synthesis only further contributes to the positive feedback loop promoting insulin resistance and the T2D metabolic triad.

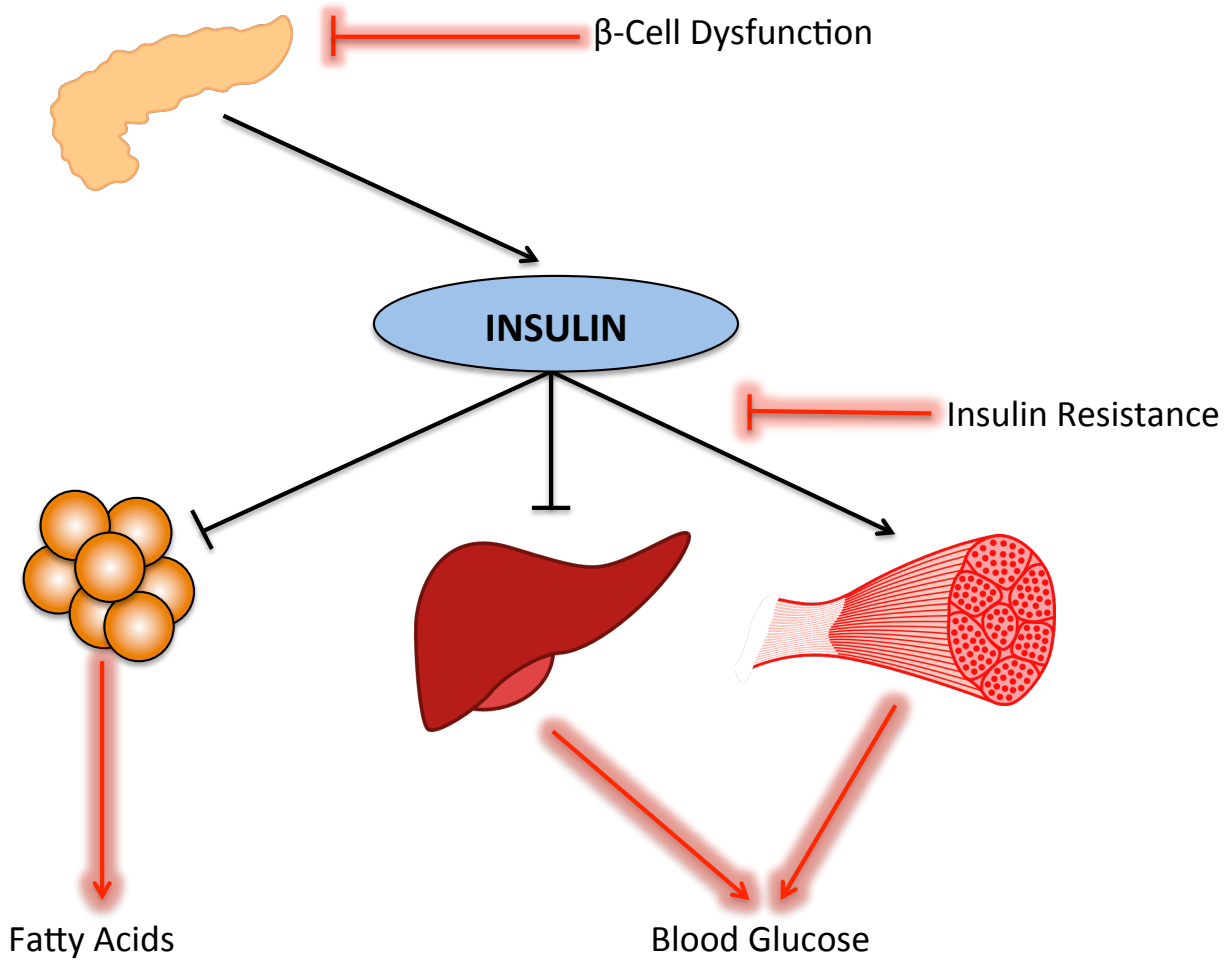

Figure 9: Pathophysiology of T2D. In healthy individuals, the pancreas secretes insulin in response to elevated blood glucose. In response to insulin, skeletal muscles uptake glucose into the cells, the glucose production within the liver is suppressed and adipose tissue is prevented from releasing free fatty acids into the blood. Under conditions of diabetes, β-cell dysfunction causes a partial loss of insulin production. Insulin resistance in the tissues results in insulin action not being completed within the cells. Both conditions result in an increase in free fatty acids and glucose within the blood. Figure from *Stumvoll et al.* [81].

Proteomics and Type 2 Diabetes Research

With the completion of the human genome project, the study of molecular biology is shifting into what has been coined the "-omics era", where the utilization of high throughput technology and large scale databases can allow researchers to compare entire biological systems of disease models. In this brief review, the application of proteomics will be the major focus especially as this technical application we employed within my dissertation.

Gel-Based Proteomics

In order to appreciate the impact proteomics has made in molecular research, one must be familiar with the origins of this science. The term *proteomics* was first coined in 1997 by then Ph.D. student Marc Wilkins [82]. Presently, proteomics is often used to describe the analysis of entire sets of proteins in a system, or *proteome*. The method to study proteomics at this time was dominated by two-dimensional gel electrophoresis (2DE), which separates proteins based on their isoelectric point and mass, coupled with mass spectrometry for the identification of proteins of interest [83, 84]. Briefly, a control and perturbed protein lysate is separated by 2DE and differential spot sizes can correspond to differences in protein expression. The spot can be excised and the protein within can be identified by mass spectrometry, fragmenting peptides and identifying the amino

acid sequence based on Edman degradation. Recent developments have even been made on this technique, utilizing multi-color fluorescent labeling of two protein samples (such as control vs. perturbed) which rids many limitations inherent to 2DE [85], referred to as differential gel electrophoresis (DIGE). 2DE is still widely used today and can allow for quantitative differential analysis of hundreds to thousands of proteins in a given sample [86]. Because of this, proteomics offers unmatched insight of molecular biological systems, compared to genomics and transcriptomics, as it bridges the gap between gene, gene transcription, and gene expression which ultimately is most useful for understanding disease mechanisms [87].

PROTEOMICS AND DIABETES USING 2DE

2DE-MS has proven to be a valuable tool in the context of diabetes research. *Sanchez* et al. used gel based techniques to build shareable databases and has provided reference proteomes for several species, including human and mouse [88]. A similar reporting by *Ahmed* et al. included 66 proteins identified in human pancreatic islets, several of which were not previously described [89]. Both demonstrated proteomic based techniques in their ability to greatly aid in the construction of useful databases that can be used in many contexts. 2DE-MS can provide quantitative data as well, as demonstrated by *Ahmed* et al. where they investigated glucose induced changes of mouse islets,

successfully identifying 77 differentially expressed proteins [90]. *Sparre* et al. performed a similar study where 82 differentially expressed proteins were identified out of 2,200 total proteins in BB rat islets treated with IL-1β [91]. Many proteins that were differentially expressed were involved in energy production, protein synthesis, signal transduction, and apoptosis. This study demonstrated the strong utility proteomics has in understanding molecular pathways, as IL-1β influences several cellular events that inhibit β-cell function and induce apoptosis.

Mechanisms of disease have been investigated using this method, where *Tilton* et al. described the changes in the renal cortical proteome in diabetic *db/db* mice. 147 proteins were differentially expressed and identified, most being involved in cellular metabolism [92]. *Douette* et al. described changes in the liver mitochondria proteome in steatotic *ob/ob* mice where 56 differentially expressed proteins were identified and are involved in acetyl-CoA regulation and oxidative stress [93]. Molecular mechanisms impacted by therapeutic drugs such as PPARα and PPARγ agonists, used to treat hypertriglyceridemia [94-98], have been investigated using 2DE by the Dahllöf group in obese and diabetic *ob/ob* mice. The study identified 14 differentially expressed proteins in the liver and was able to provide evidence

that PPARα induces β-oxidation and upregulates enzymes involved in lipogenesis [99].

The epigenetic effects of T2D have been explored, where skeletal muscle proteomes were compared in T2D and healthy individuals. The reporting from *Højlund* et al. concluded that cellular stress, alterations in mitochondrial metabolism, and ATP synthesis was dysregulated in skeletal muscle cells of T2D individuals as evident by the 10 differentially expressed proteins identified [100]. The application for proteomic studies is endless, with the only major drawback being the difficulty in interpretation following the accumulation of a complex compilation of differentially expressed proteins and potential networks. In the context of T2D, the mechanisms driving insulin resistance, β-cell dysfunction/death, and liver disease can be investigated as an entire system. The technology is certainly ever improving; recent advances in mass spectrometry, as well as liquid chromatography, have allowed for relative and absolute quantitation by either stable isotope labeling or label free techniques, drastically increasing the robustness of proteomic applications.

Quantitative Mass Spectrometry Based Proteomics

With the relative recent development of smaller, more accurate, and more economical mass analyzers, quantitative mass

spectrometry based proteomics has become a favorable high-throughput method to study the unbiased large scale changes in protein expression as well as post translational modifications (PTMs) in several types of biological samples. Quantitative MS-based proteomics relies on labeling techniques where one sample is labeled with a "heavy" reagent and the other a "light" (or unlabeled peptides) reagent which when mixed together can be analyzed by tandem mass spectrometry to identify the relative abundance, peptide identification, and origin of the peptide between the two samples (Figure 10). In the early nineties, these methods could only be carried out on the Fourier transform ion cyclotron resonance mass spectrometers (FTICR) or other complicated arrangements of mass analyzers, which was not a feasible option for most. However, the invention of the Orbitrap has allowed researchers to harness the same sensitivity of FTICR mass spectrometers and perform more complicated analyses in less time. For precursor ion fragmentation, Orbitrap mass spectrometers harness the exclusive higher-energy collisional dissociation (HCD) cell, which allows for sensitive detection of low molecular weight isobaric tag reporter ions [101, 102], a useful feature in isobaric tag based techniques for quantitative proteomics. Many sources of error can be eliminated by this method, as the labeled peptides act as an internal standard, reducing error caused by sample preparations, variance between

individual chromatography separations, and mass spectrometry analyses.

Gygi et al. first described a labeling method using isotope-coded affinity tags (ICAT) [103], based off the earlier isotope dilution assay methods [104]. Since then, several labeling techniques have been developed; one being stable isotope labeling of amino acids in cell culture (SILAC) developed by the Mann lab [105]. *Oda* et al. set the stage for this method in yeast cells [106], however SILAC allows mammalian cells to metabolically incorporate heavy or light amino acids into their proteomes during synthesis by providing the either labeled or non-labeled essential amino acids lysine and/or arginine in the cell culture medium. This allows for the simultaneous comparison of two different treatment groups during LC-MS/MS. SILAC was formally restricted to *in vitro* applications; however, methods have been developed where peptides labeled *in vitro* can be "spiked-in" to corresponding animal protein lysate [107]. Additionally, multiple labeled cell type lysates can be combined which increases the protein overlap when spiked-in to the protein lysate under investigation [108], referred to as superSILAC. superSILAC for spike-in has improved, where yeast, fruit flies, and mice have been metabolically labeled *in vivo* by providing them the isotope via feeding over several breeding generations [109-112]. Lysates from labeled animals are

therefore superior for protein coverage, however they poses the drawback of being labeled with only one isotopic amino acid. For the study of human tissue, *in vitro* methods such as isobaric tags for relative or absolute quantitation (iTRAQ) [113], or isotopic reductive demethylation labeling [114, 115], both *in vitro* labeling methods, allow for the chemical labeling of peptides with covalently bonded isobaric tags for quantitation. With ever advancing technology in liquid chromatography and mass spectrometry, label-free quantitative methods are becoming possible, eliminating the need for the labeling of peptides and subsequent experimental error from doing so [116].

Coupling mass spectrometry with high performance liquid chromatography, or multidimensional protein identification technology (MudPIT), allows for greater identification of proteins in a complex mixture [117, 118]. This is achieved by first fractionating samples for MS by HPLC to reduce sample complexity, usually by strong cation exchange (SCX) chromatography, and then performing HPLC again on each fraction directly inline to MS, usually based on a chromatography method exploiting other physical properties, such as reverse phase (RP) chromatography. This method has allowed for the drastic improvement of protein identifications and high-throughput analyses of complex proteomes. See Figure 10 for a general proteomics workflow.

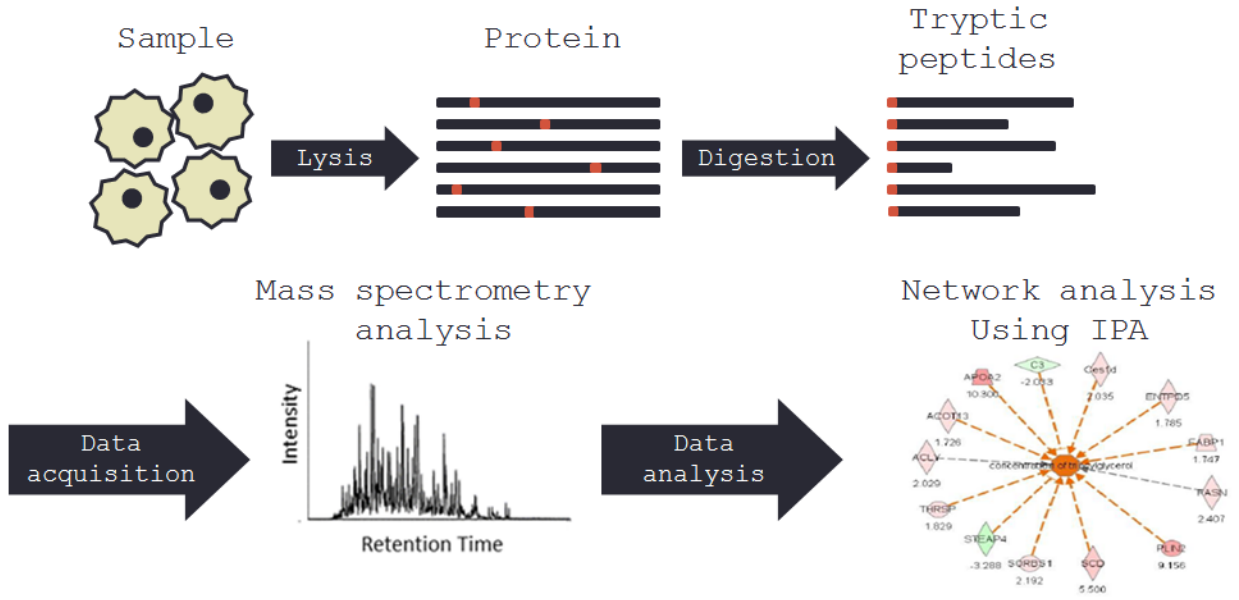

Figure 10: Typical mass spectrometry based proteomic workflow. Following sample preparation and protein extraction, purified proteins are digested, typically with the protease trypsin, generating tryptic peptides. The peptide mixture is then analyzed by mass spectrometry for the identification and abundance of protein. Differentially expressed proteins can be analyzed using IPA for the identification of differential protein networks and biochemical pathways.

PROTEOMICS AND DIABETES USING LC-MS/MS

As evident from the literature, there is sparse use of quantitative mass spectrometry based proteomics in an effort for the functional understanding T2D pathology; that is, to identify altered mechanisms based on differences in protein expression. However early uses of LC-MS/MS provided enhanced proteome coverage when used as a tool for tissue profiling, as demonstrated by *Metz* et al. [119]. 2D LC-MS/MS was employed for the proteomic characterization of human pancreatic islets, where over 29,000 peptides were identified which corresponded to 3,365 proteins, compared to the earlier mention of *Ahmed* et al. where only 66 proteins were identified [89, 119]. The significant highlights of this study included the observation of proteins involved in metabolic and cellular pathways, including MAP kinase, NF-κβ, and JAK/STAT signaling cascades. To date, this is the most comprehensive islet proteomic profiling analysis. To expand on this, *Brunner* et al. isolated insulin secreted granules from the rat insulin-secreting cell line INS-1E and identified 130 unique proteins by LC-MS/MS, in which 110 were not previously described [120]. Unfortunately, this investigation did not identify PANDER in their dataset.

In an effort to detail the functional changes in the islets of the MKR mouse (a model of T2D), *Lu* et al. employed iTRAQ to investigate proteomic differences in the islet compared to the

wild-type mouse [121]. 159 differentially expressed proteins were identified in the islets of the MKR mouse as compared to control islets. Many of these proteins suggested differential regulation of protein biosynthesis, endoplasmic reticulum (ER) stress pathways, insulin secretion, energy utilization, and metabolism. Additionally, several differentially expressed proteins were observed that are linked to insulin-secretory defects in T2D. Several proteins were described for the first time with an association to islet dysfunction, including the unfolded protein response proteins (ERP72, ERP44, ERP29, PPIB, FKBP2, FKBP11, and DNAJB11), endoplasmic reticulum-associated degradation proteins (VCP and UFM1), and multiple proteins associated with mitochondrial energy metabolism (NDUFA9, UQCRH, COX2, COX4I1, COX5A, ATP6V1B2, ATP6V1H, ANT1, ANT2, ETFA, and ETFB). Interestingly, this study also investigated the differential expression of mRNAs to corresponding proteins identified by MS using microarray and quantitative real time PCR, in which a low correlation was found [121]; this does suggest strong post-translational regulation, but without going off-topic, also serves as additional supportive evidence that proteomics provides unique and valuable insight of biochemical changes driving β-cell dysregulation and insulin resistance [122].

Yurong et al. investigated the proteome changes in liver mitochondria of mice on a high fat diet using iTRAQ. From this approach, 1508 proteins were identified, with 72 proteins predicted to be up-regulated and 20 proteins down-regulated [123]. Retinol metabolism was shown to be distinctly down-regulated and the mitochondrial structural proteins—components of mitochondrial inter-membrane space bridging complex (Mitofilin, Sam50, and ChChd3), and Tim proteins, essential for protein import, were shown to be significantly up-regulated in HFD fed mice [123].

More recently, a study by *Han* et al. utilized iTRAQ to compare the islet proteomes of Zucker Lean (ZL), Zucker Fat (ZF) and obese diabetic Zucker rats (ZDF) in an effort to propose potential factors mediating the progression of insulin resistance to T2D [124]. 54 and 59 differentially expressed proteins were observed between the ZDF vs. ZL and ZF vs. ZL, respectively. These proteins were involved in impaired insulin secretion, mitochondrial dysfunction, dysregulation of triglyceride/free fatty acid cycling, lipotoxicity, and microvascular dysfunction [124].

To outline critical proteins involved in islet differentiation/regeneration, *Jin* et al. utilized iTRAQ and microarray analysis to identify differentially expressed

proteins in a human β-cell line [125]. Many proteins identified are involved in cell cycle, cell structure and developmental processes which were significantly downregulated, while proteins involved in lipid, fatty acid, steroid, and nucleotide metabolism were upregulated [125]. The information obtained from this study aided in the development of a large scale protein interaction map using GenBank and all available islet proteomic data by *Levetan* et al., which additionally led to the development of a pro-islet peptide that stimulates β-cell population growth *in vitro* [126].

The study of proteomics has allowed for tremendous strides to be made in the understanding of biological mechanisms underlying disease. Gene regulation and expression is an extremely complex and multifaceted process, however the ability to observe the overall end product, proteins, logically allows for the most pertinent understanding of disease. In this dissertation, mass spectrometry based proteomics is used as a powerful heuristic tool to outline critical proteins involved in the pathogenic effects of PANDER overexpression. In an additional and rather unique study, the same approach was employed to shed light on important protein expression changes in the liver due to a high fat diet exposure, and will be discussed in chapter 5.

Innovation

Hepatic insulin resistance (HIRE) is a significant clinical hallmark of type 2 diabetes (T2D) that results in impaired insulin signaling, increased gluconeogenesis, hyperlipidemia, and progressive nonalcoholic fatty liver disease (NAFLD). The prevalence of NAFLD is approximately 30% of the US population and is a risk factor for T2D [127, 128]. NAFLD results in initial steatosis (fatty liver) due to increased hepatic lipogenesis [129]. Despite active investigation, therapeutic strategies are limited and there is much elucidation needed to determine the specific etiological molecules responsible for HIRE, NAFLD, and T2D. Over the past decade a wealth of data has been generated to support a role for pancreatic derived factor in the onset or progression of HIRE, NAFLD, and T2D [1, 4, 6, 9-11, 15, 18, 130-135]. Our published findings from the PANDER transgenic (PANTG) mouse that displays increased circulating PANDER revealed a phenotype containing several T2D characteristics such as fasting hyperglycemia, glucose intolerance, hepatic insulin resistance and increased triglyceride production [21, 22]. Hepatic PANDER overexpression can promote hepatic steatosis resulting in increased triglycerides and very low density lipoprotein production, yet this effect has not been determined for pancreas derived PANDER [3, 17, 19, 21, 22, 60]. PANDER is a uniquely structured

molecule that is strongly expressed and secreted from the endocrine pancreas and other tissues such as the liver and intestines. Based on recent crystallography data, PANDER has a unique globular β-β-α fold structure not found in any other class of proteins [8]. The physiological function of PANDER is to regulate glycemic levels via interaction with the liver and pancreas [16]. However, the precise signaling mechanism of how PANDER regulates this multitude of effects is unknown.

My innovative approach will hopefully have a high impact on the fields of liver metabolism and diabetes biology by identification of a causative molecule involved in hepatic insulin resistance and potentially T2D and NAFLD. These findings would also provide insight into novel mechanisms potentially regulating the liver X receptor (LXR) pathway. As strongly indicated by others, selective hepatic insulin resistance (SHIR) is a major uncharacterized problem in T2D and is a critical source of the cardiovascular complications identified with this disease [136, 137]. Our PANDER animal models and others [17-19, 21, 138] have provided evidence that PANDER may impact SHIR and therefore suggest that PANDER is a potential cofactor involved in this pathogenic paradox. These findings may also provide additional therapeutic avenues for clinical intervention of T2D and NAFLD. In addition, an understanding of PANDER induced lipogenesis may also provide insight into the LXR signaling

mechanism and this is valuable since LXR clinical application has been hindered due to this detrimental outcome (25). Furthermore, our laboratory has generated the first and only PANDER animal models that are currently established and available for analysis of this unique secreted protein.

Chapter 2 – Generation of The Pander Transgenic Model for Identification of Pander-Induced Hepatic Proteome

Abstract

PANcreatic-DERived factor (PANDER) is a member of a superfamily of FAM3 proteins modulating glycemic levels by metabolic regulation of the liver and pancreas. The precise PANDER-induced hepatic signaling mechanism is still being elucidated and has been very complex due to the pleiotropic nature of this novel hormone. Our PANDER transgenic (PANTG) mouse displays a selective hepatic insulin resistant (SHIR) phenotype whereby insulin signaling is blunted yet lipogenesis is increased, a phenomenon observed in type 2 diabetes. To examine the complex PANDER-induced mechanism of SHIR, we utilized quantitative mass spectrometry based proteomic analysis using Stable Isotope Labeling by Amino Acids in Cell Culture (SILAC) as a heuristic technique to reveal the global hepatic proteome differences within the PANTG under the metabolic states of fasting, fed and insulin-stimulated conditions. 3304 hepatic proteins were identified with analysis comparing PANTG versus wild-type hepatic proteomes within a specific metabolic condition. Of those, there were 228, 239 and 189 differentially expressed

proteins in the fasted, fed and insulin-stimulated conditions within the PANTG liver as compared to WT, respectively, as determined by the Significance A outlier test in Perseus ($P<0.05$, N=3, combined prior to outlier test).

Materials and Methods

Generation of the Pander Transgenic Animal Colony

The *Fam3b* (PANDER) gene cloned into the pCR2.1 cloning vector (Life Technologies) was kindly provided by GlaxoSmithKline. The PANDER gene was excised and ligated downstream of the Pdx1 promoter which drives the expression exclusively in the endocrine tissue of the pancreas. This vector was obtained from Dr. Maureen Gannon, Vanderbilt University. B6SJLF (strain generated from a cross between C57BL/6J females and SJL/J males) transgenic mice were produced according to the protocol of the University of Pennsylvania Transgenic and Chimeric Mouse Facility. During the course of this investigation, the laboratory and animal colony were moved to the University of South Florida (USF) from the Children's Hospital of Philadelphia. Frozen embryos of the PANTG were shipped to the Moffitt Stabile Vivarium on the campus of USF and implanted into pseudo pregnant females for subsequent rederivation of murine colony. Animals were fed standard chow from Purina and given water *ad libitum*. All animals were handled according to the

guidelines established by the Institutional Animal Care and Use Committee at the University of South Florida and Children's Hospital of Philadelphia before relocation. Offspring were screened by PCR to confirm transgenic integration using primers specific (forward 5′-GCT GGA CAG GGG CAC GTC AGG AAT GAG CTC-3′ and reverse 5′-TAC TCT GAG TCC AAA CCG GGC CCC TCT GCT-3′) for the β-globin intron and PANDER transgene resulting in a 300bp transgene-specific PCR product amplified from genomic DNA isolated from tail tissue (DNeasy Kit, Qiagen). All animals were born normally at the expected Mendelian frequency. Male mice aged 4 to 6 weeks were evaluated in this study and an effort was made to match mice by liter mates. Relative PANDER expression was determined by RT-PCR and western analysis (FIG).

Metabolic Treatment of The Pander Transgenic Mouse

The PANTG and wild-type mice were exposed to fasted, fed, and insulin stimulatory conditions prior to liver extraction and subsequent proteomic examination. All treatments were performed on PANTG and wild-type mice at six weeks of age. Fed and fasted mice were withheld from food for approximately 4 and 16 hours, respectively. Following the 4 hour fast, fed mice were provided with chow *ad-libitum* for 2 hours. Insulin-stimulated mice were fasted for 4 hours prior to insulin injection (Humulin®, 1 unit/kg). Insulin was diluted to a concentration of 20 units/ml and injected intraperitoneally with exposure for 15 minutes.

Mice were humanely euthanized by carbon dioxide asphyxiation and cervical dislocation following above described metabolic conditions. Livers were extracted immediately following exposure to described metabolic conditions, snap frozen and stored at -80°C prior to proteomic analysis.

Hepatic Protein Isolation

Approximately 40 mg of tissue was excised from a lobe of mouse liver for tissue lysis. Tissue was submerged in cold lysis buffer (100mM Tris-HCl, 100mM DTT, 4% SDS and 1x HALT protease inhibitor) and homogenized using a Qiagen TissueRupter. Cell lysate was then heated at 95°C for five minutes followed by brief sonication. The tissue lysate was cleared by centrifugation at 16000 × g for 5 min and the supernatant was collected and stored at -80°C prior to further analysis. The same procedure for protein purification was performed on the "heavy" labeled ($^{13}C_6$ L-Lysine) murine male liver (MT-LYSC6-ML-PK, Cambridge Isotope Laboratories, Inc.).

Sample Digestion, Desalt, and Scx Fractionation

Protein concentration was quantified using the Pierce 660 nm protein assay kit supplemented with the provided ionic detergent compatibility reagent (IDCR). Equal mass of labeled and unlabeled protein or "light" and "heavy" protein respectively, were combined and digested using the filter-aided sample

preparation (FASP) method (Expedeon). Briefly, 30 µL of the protein mixture (~12.5mg/ml) was added to the spin column. The lysate buffer was exchanged to 8M urea using centrifugation prior to iodoacetamide alkylation and then exchanged to 50 mM ammonium bicarbonate for trypsin/Lys-C digestion at a ratio of 1:40 (w/w). Digestion was carried out overnight in a humidified incubator at 37°C. Peptides were eluted off the column by addition of 0.5M NaCl followed by centrifugation. Samples were desalted using solid phase enrichment C18 columns (The Nest Group, Inc.). Briefly, columns were activated using 100% acetonitrile followed by equilibration with 0.1% formic acid in water. Samples were loaded onto the columns and washed three times using equal volumes of 0.1% formic acid in water. Samples were eluted using 90% acetonitrile / 0.1% formic acid in water and then concentrated in a vacuum concentrator (Thermo) prior to resuspension with 5 mM ammonium formate and 25% acetonitrile. Peptides were fractionated by strong cation exchange chromatography.

Acquisition of Hepatic Proteome by LC-MS/MS

Fractions were separated on a 10 cm × 75 µm I.D. reversed phase column packed with 5 µm C18 material with 300 Å pore size (New Objective) using 125 minute gradients of 2–40% ACN in 0.1% formic acid. Inline mass spectrometric analysis was performed on an Orbitrap XL (Thermo). Survey scans were performed at a

resolving power of 60000, and the top 10 most abundant peaks were selected for subsequent MS/MS analysis.

Database Search for Identification and Quantification of Proteins

Raw files were processed in MaxQuant 1.2.2.5 employing the Andromeda search algorithm and searched against the UniprotKB reference database for *Mus musculus*, concatenated with reversed protein sequences. A second database of known contaminants provided with the MaxQuant suite was also employed. All fractions for each biological sample were combined for analysis. Constant modification of carbamidomethylation of cysteine and variable modifications of oxidized methionine and acetylated protein N-termini were used. Additionally, Lys-6 for the spike-in internal standard was set as a label in the group-specific parameter section. A false discovery rate of 1% was used for peptides and proteins. A minimum peptide length of 6 amino acids was used. Razor and unique peptides were used for identification and quantification. Protein ratio values were reconstructed using median peptide ratio values across all three biological replicates for each experimental group where the final ratio for each protein was calculated by determining the ratio-of-ratio (PANTG/Internal Standard) / (WT/Internal Standard). Final ratios were input into the Perseus processing suite (Perseus version 1.2.0.13). Statistical analysis was performed using the

Significance A outlier test where statistical significance based on magnitude fold-change was established at $P < 0.05$. Ratio values and Uniprot Protein identification numbers of differentially expressed proteins were uploaded to Ingenuity Pathway Analysis (IPA) to determine canonical pathways, networks and upstream regulators in the liver affected by increased pancreas-secreted PANDER. The complete proteomic dataset, along with a modified proteinGroups spreadsheet has been deposited to the ProteomeXchange Consortium (http://www.proteomexchange.org) via the PRIDE partner repository with dataset identifiers PRIDE: PXD004171 and doi:10.6019/PXD004171 [35].

Results

To comprehensively examine the PANDER-induced hepatic proteome, we performed SILAC-based quantitative proteomics on our PANTG model. The PANTG mouse is an ideal candidate for our comparative investigation due to pancreatic-specific overexpression of PANDER resulting in robust increased circulating levels as compared to wild-type mice along with resultant impaired glucose tolerance, hepatic insulin resistance and increased hepatic triglyceride levels [21]. Our quantitative proteomic approach was performed on the PANTG model in comparison to WT mice in the context of 3 metabolic conditions of fasting, fed and insulin-stimulated to examine the impact of PANDER across numerous metabolic states. Following

exposure to the various metabolic conditions, livers from PANTG and age/gender matched wild-type mice were collected and subsequently processed by tryptic digestion, desalting and SCX chromatography followed by mass spectrometry as detailed in Figure 11. Across all metabolic conditions, the MaxQuant search identified a total of 19,423 unique peptides (Complete data files deposited to the ProteomeXchange Consortium via the PRIDE partner repository with the dataset identifier PXD004171 and 10.6019/PXD004171, Username: reviewer56976@ebi.ac.uk, Password: VtR5rnIR) correlating to a proteome of 3304 proteins identified from the liver. The distribution of these proteins in their respective metabolic state in the PANTG mouse liver proteome compared to that of the wild-type is displayed in Figure 12. Of those, there were 228, 239 and 189 significantly differently expressed and quantifiable proteins in the fasted, fed and insulin-stimulated conditions within the PANTG liver as compared to WT, displayed in tables 1, 2, and 3, respectively.

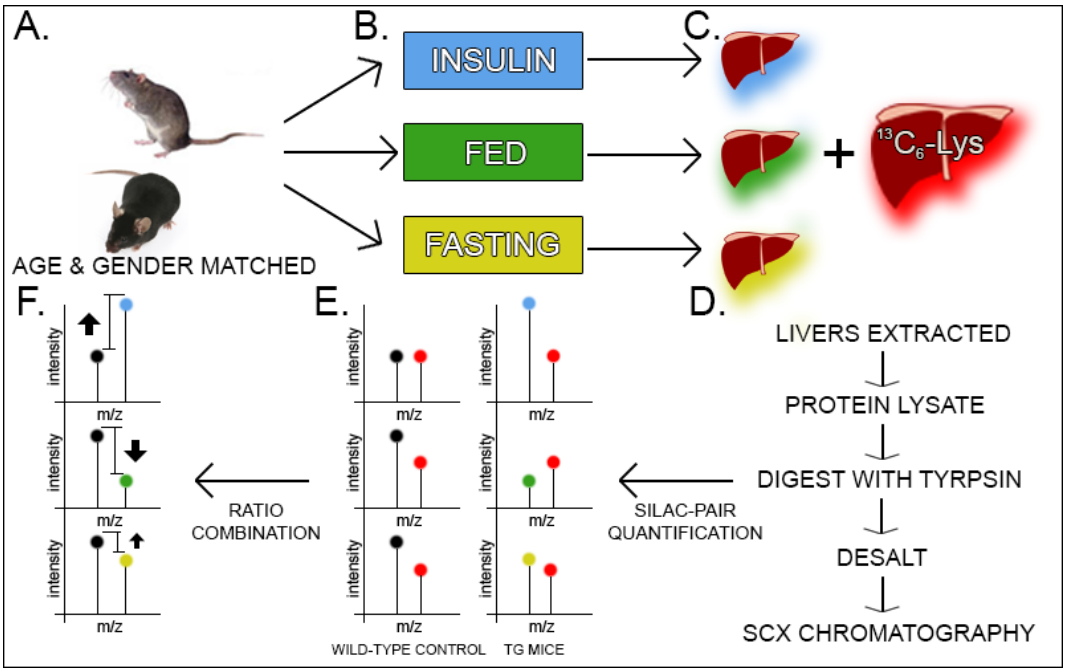

Figure 11: SILAC proteomic experimental approach for investigation of PANTG. A. & B. Age and gender matched PANTG and WT mice at six weeks of age (N=3 per condition) were exposed to three metabolic states prior to liver extraction: fed, fasted and insulin-stimulated. Livers were immediately extracted following exposure to described metabolic conditions, snap-frozen and stored at -80 °C. C. & D. 40 mg of liver tissue were lysed in cold lysis buffer (100 mM Tris-HCl, 100 mM DTT, 4% SDS and 1× HALT protease inhibitor) prior to heating at 95 °C for five minutes followed by brief sonication. Identical processing was performed on livers obtained from metabolically labeled "SILAC" mice (Cambridge Isotopes). The "heavy" protein lysate was combined with each experimental mouse liver protein lysate prior to tryptic digestion utilizing the FASP (Expedeon) method. Samples were desalted using solid phase enrichment C18 columns (The Nest Group, Inc.). Prior to LC-MS/MS, sample complexity was reduced by strong cation exchange chromatography. E. & F. Each biological sample was analyzed by tandem mass spectrometry. Normalized ratios from MaxQuant for each biological sample were inputted into the Perseus processing suite to determine statistical significance of quantitation values using Significance A outlier test ($P<0.05$).

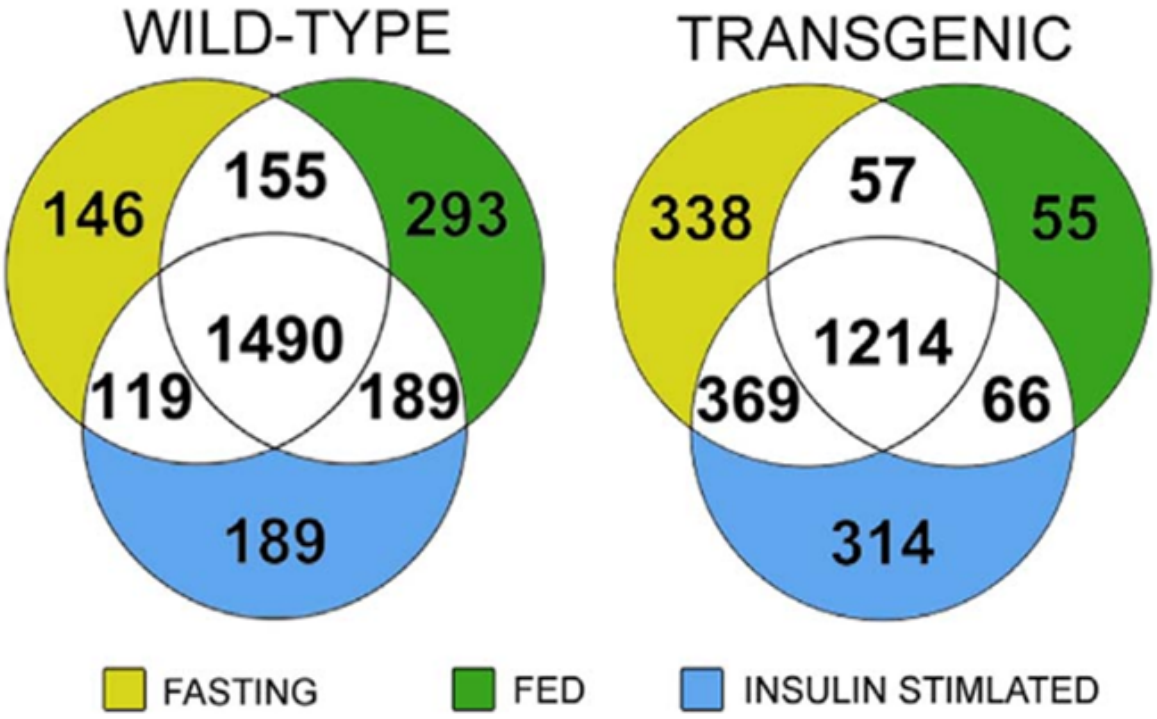

Figure 12: Distribution of proteins across metabolic conditions. Identification of unique proteins across metabolic states in the PANTG mouse liver. SILAC spike in fractionated protein extracts were analyzed by LC-MS/MS from age- and gender-matched wild-type and PANTG mice (N=3 per metabolic condition and genotype). Approximately 3300 proteins were confidently revealed that were shared across genotype and metabolic conditions with overlap indicated in Venn diagram.

Table 1: Differentially expressed proteins in the fasted state. Differentially expressed proteins (P<0.05 in a Significance A outlier test) in the PANTG liver compared to the wild type (n=3 for each). See methods for metabolic treatment (Pages 54-61).

Exp Fold Change	ID	Symbol	Entrez Gene Name
267.090	E9Q6Z0	CUL5	cullin 5
9.844	Q8BFW7	LPP	LIM domain containing preferred translocation partner in lipoma
6.164	O08663	METAP2	methionyl aminopeptidase 2
5.711	Q3TKD0	TNPO1	transportin 1
4.723	P49586	PCYT1A	phosphate cytidylyltransferase 1, choline, alpha
4.203	Q9D1P4	CHORDC1	cysteine and histidine-rich domain (CHORD) containing 1
4.004	P58467	SETD4	SET domain containing 4
3.595	P58281	OPA1	optic atrophy 1 (autosomal dominant)
3.476	Q9R099	TBL2	transducin (beta)-like 2
3.449	Q8BYU6	TOR1AIP2	torsin A interacting protein 2
3.403	B1AU76	NASP	nuclear autoantigenic sperm protein (histone-binding)
3.284	D3Z5G7	Ces1b/Ces1c	carboxylesterase 1C
3.179	P62960	YBX1	Y box binding protein 1
3.014	Q01279	EGFR	epidermal growth factor receptor
2.976	O35350	CAPN1	calpain 1, (mu/I) large subunit
2.835	Q01339	APOH	apolipoprotein H (beta-2-glycoprotein I)
2.735	Q9R0Q6	ARPC1A	actin related protein 2/3 complex, subunit 1A, 41kDa
2.698	A3KGU5	SPTAN1	spectrin, alpha, non-erythrocytic 1
2.548	E9PVM7	GSTM3	glutathione S-transferase mu 3 (brain)
2.537	P01872	IGHM	immunoglobulin heavy constant mu
2.478	Q9CRT8	XPOT	exportin, tRNA
2.467	P23953	Ces1b/Ces1c	carboxylesterase 1C
2.395	P01868	IGHG1	immunoglobulin heavy constant gamma 1 (G1m marker)
2.391	P14901	HMOX1	heme oxygenase 1
2.366	O35857	TIMM44	translocase of inner mitochondrial membrane 44 homolog (yeast)
2.336	Q9JJU9	CRYBB3	crystallin, beta B3
2.316	P01029	C4A/C4B	complement component 4B (Chido blood group)
2.298	Q8K4H1	AFMID	arylformamidase
2.229	Q8BLN5	LSS	lanosterol synthase (2,3-oxidosqualene-lanosterol cyclase)
2.222	Q99LM2	CDK5RAP3	CDK5 regulatory subunit associated protein 3
2.175	Q00898	SERPINA1	serpin peptidase inhibitor, clade A (alpha-1 antiproteinase, antitrypsin), member 1
2.172	Q9JLC3	MSRB1	methionine sulfoxide reductase B1

Table 1 (Continued)

Exp Fold Change	ID	Symbol	Entrez Gene Name
2.172	Q71KU9	FGL1	fibrinogen-like 1
2.133	P04919	SLC4A1	solute carrier family 4 (anion exchanger), member 1 (Diego blood group)
2.085	Q9R1J0	NSDHL	NAD(P) dependent steroid dehydrogenase-like
2.057	K3W4Q8	BSG	basigin (Ok blood group)
2.042	Q9R1Q6	TMEM176B	transmembrane protein 176B
2.001	Q9D6T0	NOSIP	nitric oxide synthase interacting protein
1.981	P06728	APOA4	apolipoprotein A-IV
1.978	Q9DCT8	Crip2	cysteine rich protein 2
1.929	P15327	BPGM	2,3-bisphosphoglycerate mutase
1.925	P04104	KRT1	keratin 1, type II
1.874	D3YUW7	CGN	cingulin
1.857	P08122	COL4A2	collagen, type IV, alpha 2
1.849	Q8VCR2	HSD17B13	hydroxysteroid (17-beta) dehydrogenase 13
1.844	P00920	CA2	carbonic anhydrase II
1.841	Q9QXK7	CPSF3	cleavage and polyadenylation specific factor 3, 73kDa
1.830	J3QMN4	TXNRD2	thioredoxin reductase 2
1.816	P28666	Mug1/Mug2	murinoglobulin 1
1.807	Q00623	APOA1	apolipoprotein A-I
1.805	Q8CIN4	PAK2	p21 protein (Cdc42/Rac)-activated kinase 2
1.803	Q8CHW4	EIF2B5	eukaryotic translation initiation factor 2B, subunit 5 epsilon, 82kDa
1.803	Q9CQ01	RNASET2	ribonuclease T2
1.801	E9PV24	FGA	fibrinogen alpha chain
1.748	Q99K23	UFSP2	UFM1-specific peptidase 2
1.740	P97311	MCM6	minichromosome maintenance complex component 6
1.729	Q6P1D5	SEZ6L	seizure related 6 homolog (mouse)-like
1.728	P13634	CA1	carbonic anhydrase I
1.712	Q8K0E8	FGB	fibrinogen beta chain
1.692	P07759	SERPINA3	serpin peptidase inhibitor, clade A (alpha-1 antiproteinase, antitrypsin), member 3
1.676	Q8K310	MATR3	matrin 3
1.657	Q9DBE0	CSAD	cysteine sulfinic acid decarboxylase
1.647	Q6P2B1	TNPO3	transportin 3
1.640	Q6ZQ58	LARP1	La ribonucleoprotein domain family, member 1
1.639	E9Q509	PKLR	pyruvate kinase, liver and RBC
1.622	P01837	IGKC	immunoglobulin kappa constant

Table 1 (Continued)

Exp Fold Change	ID	Symbol	Entrez Gene Name
1.614	Q9CQC6	BZW1	basic leucine zipper and W2 domains 1
1.601	Q8K1J6	TRNT1	tRNA nucleotidyl transferase, CCA-adding, 1
1.594	Q9JJ28	FLII	flightless I actin binding protein
1.592	P60670	NPLOC4	NPL4 homolog, ubiquitin recognition factor
1.591	Q921M3	SF3B3	splicing factor 3b, subunit 3, 130kDa
1.586	Q9DBM2	EHHADH	enoyl-CoA, hydratase/3-hydroxyacyl CoA dehydrogenase
1.577	Q5SWU9	ACACA	acetyl-CoA carboxylase alpha
1.565	P01867	Ighg2b	immunoglobulin heavy constant gamma 2B
1.562	P20918	PLG	plasminogen
1.561	Q8BJL9	UGT2B7	UDP glucuronosyltransferase 2 family, polypeptide B7
1.556	Q9D379	EPHX1	epoxide hydrolase 1, microsomal (xenobiotic)
1.551	Q91VW5	GOLGA4	golgin A4
1.550	Q8R480	NUP85	nucleoporin 85kDa
1.548	P07309	TTR	transthyretin
1.545	Q8BL66	EEA1	early endosome antigen 1
1.535	P61358	RPL27	ribosomal protein L27
1.528	Q61171	PRDX2	peroxiredoxin 2
1.522	A2A977	CYP4A11	cytochrome P450, family 4, subfamily A, polypeptide 11
1.518	Q99J99	MPST	mercaptopyruvate sulfurtransferase
1.515	Q9CXI3	MOXD1	monooxygenase, DBH-like 1
1.508	Q99PV0	PRPF8	pre-mRNA processing factor 8
1.505	P26883	FKBP1A	FK506 binding protein 1A, 12kDa
1.503	E9QN99	ABHD14B	abhydrolase domain containing 14B
1.503	P29699	AHSG	alpha-2-HS-glycoprotein
1.499	D3Z3S1	PREB	prolactin regulatory element binding
1.492	P43883	PLIN2	perilipin 2
1.489	P23591	TSTA3	tissue specific transplantation antigen P35B
1.486	E9QKL6	IFI16	interferon, gamma-inducible protein 16
1.486	Q8K0U4	HSPA12A	heat shock 70kDa protein 12A
1.485	Q64435	UGT1A6	UDP glucuronosyltransferase 1 family, polypeptide A6
1.484	D3YTY9	KNG1	kininogen 1
1.480	Q8C1A5	THOP1	thimet oligopeptidase 1
1.478	Q91X72	HPX	hemopexin
1.473	E9QA63	Macf1	microtubule-actin crosslinking factor 1
1.470	P09528	FTH1	ferritin, heavy polypeptide 1
1.469	Q9CQW9	IFITM3	interferon induced transmembrane protein 3

Table 1 (Continued)

Exp Fold Change	ID	Symbol	Entrez Gene Name
1.469	Q9DCY0	Keg1	kidney expressed gene 1
1.467	Q5SUH7	CLINT1	clathrin interactor 1
1.465	Q8VCM7	FGG	fibrinogen gamma chain
1.463	Q91XL1	LRG1	leucine-rich alpha-2-glycoprotein 1
1.458	Q9D0E1	HNRNPM	heterogeneous nuclear ribonucleoprotein M
1.455	P19096	FASN	fatty acid synthase
1.446	P24457	Cyp2d9	cytochrome P450, family 2, subfamily d, polypeptide 9
1.437	Q61838	Pzp	pregnancy zone protein
1.430	Q9EP72	EMC7	ER membrane protein complex subunit 7
1.426	A2ALV1	SH3GL2	SH3-domain GRB2-like 2
1.425	Q8BXA1	GOLIM4	golgi integral membrane protein 4
1.423	P48193	EPB41	erythrocyte membrane protein band 4.1
1.422	Q9Z1D1	EIF3G	eukaryotic translation initiation factor 3, subunit G
1.422	P46935	Nedd4	neural precursor cell expressed, developmentally down-regulated 4
1.422	P07724	ALB	albumin
1.422	Q810B6	ANKFY1	ankyrin repeat and FYVE domain containing 1
1.421	Q8VBV7	COPS8	COP9 signalosome subunit 8
1.418	Q5SW19	CLUH	clustered mitochondria (cluA/CLU1) homolog
1.417	Q9QXG4	ACSS2	acyl-CoA synthetase short-chain family member 2
1.410	E9PZJ8	ASCC3	activating signal cointegrator 1 complex subunit 3
1.407	E0CYY1	CIAPIN1	cytokine induced apoptosis inhibitor 1
1.407	Q9D6S7	MRRF	mitochondrial ribosome recycling factor
1.405	Q3UZ39	LRRFIP1	leucine rich repeat (in FLII) interacting protein 1
1.399	Q64505	CYP7A1	cytochrome P450, family 7, subfamily A, polypeptide 1
1.396	P28665	Mug1/Mug2	murinoglobulin 1
1.395	Q9CY64	BLVRA	biliverdin reductase A
-1.356	Q9D1M0	SEC13	SEC13 homolog, nuclear pore and COPII coat complex component
-1.359	Q8VCC1	HPGD	hydroxyprostaglandin dehydrogenase 15-(NAD)
-1.361	P17879	Hspa1b	heat shock protein 1B
-1.367	P26645	Marcks	myristoylated alanine rich protein kinase C substrate
-1.373	Q61735	CD47	CD47 molecule
-1.374	Q9JHJ0	TMOD3	tropomodulin 3 (ubiquitous)

Table 1 (Continued)

Exp Fold Change	ID	Symbol	Entrez Gene Name
-1.383	Q8BK30	NDUFV3	NADH dehydrogenase (ubiquinone) flavoprotein 3, 10kDa
-1.383	Q9ERR7	SEP15	15 kDa selenoprotein
-1.384	Q8BH59	SLC25A12	solute carrier family 25 (aspartate/glutamate carrier), member 12
-1.384	P50516	ATP6V1A	ATPase, H+ transporting, lysosomal 70kDa, V1 subunit A
-1.384	P70671	IRF3	interferon regulatory factor 3
-1.386	Q9D967	MDP1	magnesium-dependent phosphatase 1
-1.394	Q3UID0	SMARCC2	SWI/SNF related, matrix associated, actin dependent regulator of chromatin, subfamily c, member 2
-1.396	P24456	Cyp2d9 (includes others)	cytochrome P450, family 2, subfamily d, polypeptide 9
-1.405	Q8VC97	UPB1	ureidopropionase, beta
-1.408	Q9D517	AGPAT3	1-acylglycerol-3-phosphate O-acyltransferase 3
-1.411	Q9WUM3	CORO1B	coronin, actin binding protein, 1B
-1.415	Q60710	SAMHD1	SAM domain and HD domain 1
-1.416	E9Q557	DSP	desmoplakin
-1.416	P61750	ARF4	ADP-ribosylation factor 4
-1.416	P63321	RALA	v-ral simian leukemia viral oncogene homolog A (ras related)
-1.417	Q9R112	SQRDL	sulfide quinone reductase-like (yeast)
-1.419	F6U2C2	ATXN2	ataxin 2
-1.422	A2AN08	UBR4	ubiquitin protein ligase E3 component n-recognin 4
-1.422	P47754	CAPZA2	capping protein (actin filament) muscle Z-line, alpha 2
-1.430	E9Q4G8	ALCAM	activated leukocyte cell adhesion molecule
-1.433	E9QAS4	CHD4	chromodomain helicase DNA binding protein 4
-1.442	E9Q8N1	TTN	titin
-1.452	Q99KJ8	DCTN2	dynactin 2 (p50)
-1.453	F8WJK8	ST13	suppression of tumorigenicity 13 (colon carcinoma) (Hsp70 interacting protein)
-1.455	Q9JJU8	SH3BGRL	SH3 domain binding glutamate-rich protein like
-1.457	E9PXX7	TXNDC5	thioredoxin domain containing 5 (endoplasmic reticulum)
-1.462	Q2TPA8	Hsd12	hydroxysteroid dehydrogenase like 2
-1.469	Q3TH01	HLA-A	major histocompatibility complex, class I, A
-1.471	Q61879	MYH10	myosin, heavy chain 10, non-muscle

Table 1 (Continued)

Exp Fold Change	ID	Symbol	Entrez Gene Name
-1.487	Q61990	PCBP2	poly(rC) binding protein 2
-1.488	Q9R257	HEBP1	heme binding protein 1
-1.489	Q3U0V1	KHSRP	KH-type splicing regulatory protein
-1.494	P50518	ATP6V1E1	ATPase, H+ transporting, lysosomal 31kDa, V1 subunit E1
-1.495	Q9JLJ5	ELOVL1	ELOVL fatty acid elongase 1
-1.495	Q920A5	SCPEP1	serine carboxypeptidase 1
-1.512	P08752	GNAI2	guanine nucleotide binding protein (G protein), alpha inhibiting activity polypeptide 2
-1.524	Q7TMF3	NDUFA12	NADH dehydrogenase (ubiquinone) 1 alpha subcomplex, 12
-1.537	Q9D1Q6	ERP44	endoplasmic reticulum protein 44
-1.549	P28659	Celf1	CUGBP, Elav-like family member 1
-1.550	Q8VHE0	SEC63	SEC63 homolog, protein translocation regulator
-1.556	Q8VCH6	DHCR24	24-dehydrocholesterol reductase
-1.574	Q924Z4	CERS2	ceramide synthase 2
-1.584	P11930	NUDT19	nudix (nucleoside diphosphate linked moiety X)-type motif 19
-1.589	Q07456	AMBP	alpha-1-microglobulin/bikunin precursor
-1.596	P97855	G3BP1	GTPase activating protein (SH3 domain) binding protein 1
-1.623	A6X935	ITIH4	inter-alpha-trypsin inhibitor heavy chain family, member 4
-1.631	Q921L6	CTTN	cortactin
-1.633	F8VPN4	AGL	amylo-alpha-1, 6-glucosidase, 4-alpha-glucanotransferase
-1.646	Q3B7Z2	OSBP	oxysterol binding protein
-1.647	E9Q8K8	ZC3H4	zinc finger CCCH-type containing 4
-1.650	P45376	AKR1B1	aldo-keto reductase family 1, member B1 (aldose reductase)
-1.651	P50462	CSRP3	cysteine and glycine-rich protein 3 (cardiac LIM protein)
-1.657	E9Q6R7	UTRN	utrophin
-1.668	P14094	ATP1B1	ATPase, Na+/K+ transporting, beta 1 polypeptide
-1.679	Q8VCC2	Ces1g	carboxylesterase 1G
-1.682	Q8BWM0	PTGES2	prostaglandin E synthase 2
-1.690	P97792	CXADR	coxsackie virus and adenovirus receptor
-1.691	Q11136	PEPD	peptidase D
-1.694	P27612	PLAA	phospholipase A2-activating protein
-1.716	A2AJK8	TTC1	tetratricopeptide repeat domain 1
-1.723	P02802	Mt1	metallothionein 1
-1.792	Q8R0W0	EPPK1	epiplakin 1
-1.810	Q8R1S9	SLC38A4	solute carrier family 38, member 4

Table 1 (Continued)

Exp Fold Change	ID	Symbol	Entrez Gene Name
-1.826	H3BJ51	RETSAT	retinol saturase (all-trans-retinol 13,14-reductase)
-1.866	Q9R092	HSD17B6	hydroxysteroid (17-beta) dehydrogenase 6
-1.933	Q9JI75	NQO2	NAD(P)H dehydrogenase, quinone 2
-1.977	Q8JZK9	HMGCS1	3-hydroxy-3-methylglutaryl-CoA synthase 1 (soluble)
-2.006	Q9EP89	LACTB	lactamase, beta
-2.050	Q9JHG7	PIK3CG	phosphatidylinositol-4,5-bisphosphate 3-kinase, catalytic subunit gamma
-2.098	Q9JKB1	UCHL3	ubiquitin carboxyl-terminal esterase L3 (ubiquitin thiolesterase)
-2.127	Q9D5T0	ATAD1	ATPase family, AAA domain containing 1
-2.134	Q5XG73	ACBD5	acyl-CoA binding domain containing 5
-2.163	P16546	SPTAN1	spectrin, alpha, non-erythrocytic 1
-2.362	Q9D8Y0	EFHD2	EF-hand domain family, member D2
-2.385	Q9Z329	ITPR2	inositol 1,4,5-trisphosphate receptor, type 2
-2.391	Q9CQH7	BTF3L4	basic transcription factor 3-like 4
-2.481	Q9JLI6	SCLY	selenocysteine lyase
-2.623	P14115	RPL27A	ribosomal protein L27a
-2.649	Q9CWL8	CTNNBL1	catenin, beta like 1
-2.838	P35278	RAB5C	RAB5C, member RAS oncogene family
-2.888	Q9QYC0	ADD1	adducin 1 (alpha)
-2.897	Q99MR6	SRRT	serrate, RNA effector molecule
-3.083	P02463	COL4A1	collagen, type IV, alpha 1
-3.154	Q8R1J1	TM6SF2	transmembrane 6 superfamily member 2
-3.171	Q8CCJ3	UFL1	UFM1-specific ligase 1
-3.252	P61089	UBE2N	ubiquitin-conjugating enzyme E2N
-3.757	Q9Z2G9	HTATIP2	HIV-1 Tat interactive protein 2, 30kDa
-3.758	D3YVR4	MESDC2	mesoderm development candidate 2
-3.898	Q3THK7	GMPS	guanine monophosphate synthase
-4.233	Q9QYI4	DNAJB12	DnaJ (Hsp40) homolog, subfamily B, member 12
-4.307	O35226	PSMD4	proteasome 26S subunit, non-ATPase 4
-4.407	Q8BH78	RTN4	reticulon 4
-4.492	Q99J77	NANS	N-acetylneuraminic acid synthase
-4.706	P60229	EIF3E	eukaryotic translation initiation factor 3, subunit E
-4.966	Q9EQF5	DPYS	dihydropyrimidinase
-5.054	E9PXN7	UGT1A7 (includes others)	UDP glucuronosyltransferase 1 family, polypeptide A10
-5.710	Q91WC0	SETD3	SET domain containing 3
-6.314	B1AZ15	COBLL1	cordon-bleu WH2 repeat protein-like 1

Table 1 (Continued)

Exp Fold Change	ID	Symbol	Entrez Gene Name
-6.517	P97370	ATP1B3	ATPase, Na+/K+ transporting, beta 3 polypeptide
-7.087	P10922	H1F0	H1 histone family, member 0
-7.152	Q9CZW5	TOMM70A	translocase of outer mitochondrial membrane 70 homolog A (S. cerevisiae)
-7.326	P48024	Eif1	eukaryotic translation initiation factor 1
-9.811	Q91XV3	BASP1	brain abundant, membrane attached signal protein 1
-12.682	Q80W54	ZMPSTE24	zinc metallopeptidase STE24
-19.627	Q8R016	BLMH	bleomycin hydrolase

Table 2: Differentially expressed proteins in the fed state. Differentially expressed proteins (P<0.05 in a Significance A outlier test) in the PANTG liver compared to the wild type (n=3 for each). See methods for metabolic treatment (Pages 62-68).

Exp Fold Change	ID	Symbol	Entrez Gene Name
28.351	Q8R1S9	SLC38A4	solute carrier family 38, member 4
10.609	P62960	YBX1	Y box binding protein 1
9.943	Q61655	DDX19A	DEAD (Asp-Glu-Ala-Asp) box polypeptide 19A
7.023	P58044	IDI1	isopentenyl-diphosphate delta isomerase 1
6.515	Q9ESX5	DKC1	dyskeratosis congenita 1, dyskerin
5.497	Q8BH78	RTN4	reticulon 4
5.266	Q3UJB0	SF3B2	splicing factor 3b, subunit 2, 145kDa
4.886	Q9JKF1	IQGAP1	IQ motif containing GTPase activating protein 1
4.169	Q11136	PEPD	peptidase D
3.783	Q9Z2G9	HTATIP2	HIV-1 Tat interactive protein 2, 30kDa
3.415	Q14DH7	ACSS3	acyl-CoA synthetase short-chain family member 3
3.376	Q8VHE0	SEC63	SEC63 homolog, protein translocation regulator
3.082	Q9DCT8	Crip2	cysteine rich protein 2
2.822	Q9CW03	SMC3	structural maintenance of chromosomes 3
2.629	Q9CZW5	TOMM70A	translocase of outer mitochondrial membrane 70 homolog A (S. cerevisiae)
2.457	Q9CY64	BLVRA	biliverdin reductase A
2.267	Q8R0V5	IDO2	indoleamine 2,3-dioxygenase 2
2.200	Q3TKD0	TNPO1	transportin 1
2.186	Q99J77	NANS	N-acetylneuraminic acid synthase
2.170	Q7TPV4	MYBBP1A	MYB binding protein (P160) 1a
2.158	P43883	PLIN2	perilipin 2
2.156	Q9CQE8	C14orf166	chromosome 14 open reading frame 166
2.143	O08529	CAPN2	calpain 2, (m/II) large subunit
2.061	Q9CQ80	VPS25	vacuolar protein sorting 25 homolog (S. cerevisiae)
2.030	D3YXZ7	SLC35A3	solute carrier family 35 (UDP-N-acetylglucosamine (UDP-GlcNAc) transporter), member A3
1.995	Q8VCH0	Acaa1b	acetyl-Coenzyme A acyltransferase 1B
1.969	Q5FW60	Mup1	major urinary protein 1
1.943	Q9JIK5	DDX21	DEAD (Asp-Glu-Ala-Asp) box helicase 21
1.914	Q921S7	MRPL37	mitochondrial ribosomal protein L37
1.897	Q8BK64	AHSA1	AHA1, activator of heat shock 90kDa protein ATPase homolog 1 (yeast)
1.896	Q9JJU8	SH3BGRL	SH3 domain binding glutamate-rich protein like
1.853	Q8VCI0	PLBD1	phospholipase B domain containing 1
1.845	B7ZDD7	CRAT	carnitine O-acetyltransferase

Table 2 (Continued)

Exp Fold Change	ID	Symbol	Entrez Gene Name
1.827	Q3UZZ6	Sult1d1	sulfotransferase family 1D, member 1
1.824	Q9JLV1	BAG3	BCL2-associated athanogene 3
1.773	Q711T7	NADSYN1	NAD synthetase 1
1.766	Q99JI6	RAP1B	RAP1B, member of RAS oncogene family
1.765	Q8VCC2	Ces1g	carboxylesterase 1G
1.762	Q8R0H9	GGA1	golgi-associated, gamma adaptin ear containing, ARF binding protein 1
1.741	Q8R0J8	IDNK	idnK, gluconokinase homolog (E. coli)
1.720	Q91WG0	Ces2c	carboxylesterase 2C
1.687	Q3TP97	TARS2	threonyl-tRNA synthetase 2, mitochondrial (putative)
1.685	Q5SQB0	NPM1	nucleophosmin (nucleolar phosphoprotein B23, numatrin)
1.684	E9PZJ8	ASCC3	activating signal cointegrator 1 complex subunit 3
1.680	Q61635	Ifi47	interferon gamma inducible protein 47
1.648	F6RWR5	BC021614	cDNA sequence BC021614
1.621	P15208	INSR	insulin receptor
1.614	Q8CEB6	AKR1E2	aldo-keto reductase family 1, member E2
1.612	D3YYD5	VPS29	VPS29 retromer complex component
1.610	G5E8X1	C16orf13	chromosome 16 open reading frame 13
1.603	E9Q8N1	TTN	titin
1.599	E9PVM7	GSTM3	glutathione S-transferase mu 3 (brain)
1.579	P42703	LIFR	leukemia inhibitory factor receptor alpha
1.578	Q8C8T8	TSR2	TSR2, 20S rRNA accumulation, homolog (S. cerevisiae)
1.564	Q8JZK9	HMGCS1	3-hydroxy-3-methylglutaryl-CoA synthase 1 (soluble)
1.554	Q60737	CSNK2A1	casein kinase 2, alpha 1 polypeptide
1.554	Q9D967	MDP1	magnesium-dependent phosphatase 1
1.549	Q8CHW4	EIF2B5	eukaryotic translation initiation factor 2B, subunit 5 epsilon, 82kDa
1.546	Q8BGC4	ZADH2	zinc binding alcohol dehydrogenase domain containing 2
1.530	P19096	FASN	fatty acid synthase
1.528	P54823	DDX6	DEAD (Asp-Glu-Ala-Asp) box helicase 6
1.525	G5E8M7	Gstm6	glutathione S-transferase, mu 6
1.518	Q3V117	ACLY	ATP citrate lyase
1.515	Q8BK30	NDUFV3	NADH dehydrogenase (ubiquinone) flavoprotein 3, 10kDa
1.487	Q8CFB8	PARP3	poly (ADP-ribose) polymerase family, member 3
1.478	F8WIT2	ANXA6	annexin A6
1.477	O08738	CASP6	caspase 6, apoptosis-related cysteine peptidase
1.471	O88325	NAGLU	N-acetylglucosaminidase, alpha

Table 2 (Continued)

Exp Fold Change	ID	Symbol	Entrez Gene Name
1.466	Q5HZI1	MTUS1	microtubule associated tumor suppressor 1
1.457	P63073	EIF4E	eukaryotic translation initiation factor 4E
1.457	Q9D023	MPC2	mitochondrial pyruvate carrier 2
1.447	E9QAA5	SMPD4	sphingomyelin phosphodiesterase 4, neutral membrane (neutral sphingomyelinase-3)
1.431	Q9JI78	NGLY1	N-glycanase 1
1.429	B1AU76	NASP	nuclear autoantigenic sperm protein (histone-binding)
1.426	Q9EQF5	DPYS	dihydropyrimidinase
1.409	P24472	Gsta4	glutathione S-transferase, alpha 4
1.407	Q91WS4	BHMT2	betaine—homocysteine S-methyltransferase 2
1.402	E9Q7G0	NUMA1	nuclear mitotic apparatus protein 1
1.399	F6YBC9	CSNK1A1	casein kinase 1, alpha 1
1.387	Q8C165	PM20D1	peptidase M20 domain containing 1
1.382	Q9R099	TBL2	64ransducing (beta)-like 2
1.378	Q99KR3	LACTB2	lactamase, beta 2
1.377	P28650	ADSSL1	adenylosuccinate synthase like 1
1.377	P01887	B2M	beta-2-microglobulin
1.374	Q9Z1P6	NDUFA7	NADH dehydrogenase (ubiquinone) 1 alpha subcomplex, 7, 14.5kDa
1.373	Q8VE38	OXNAD1	oxidoreductase NAD-binding domain containing 1
1.369	Q08857	CD36	CD36 molecule (thrombospondin receptor)
1.367	Q9Z0M5	LIPA	lipase A, lysosomal acid, cholesterol esterase
1.365	F8WHU9	ZPR1	ZPR1 zinc finger
1.360	P70677	CASP3	caspase 3, apoptosis-related cysteine peptidase
1.359	Q8BJW6	EIF2A	eukaryotic translation initiation factor 2A, 65kDa
1.357	Q8VCZ9	PRODH2	proline dehydrogenase (oxidase) 2
1.357	P06801	ME1	malic enzyme 1, NADP(+)-dependent, cytosolic
1.355	O88736	HSD17B7	hydroxysteroid (17-beta) dehydrogenase 7
1.352	Q6ZQI3	MLEC	malectin
1.350	Q501J6	DDX17	DEAD (Asp-Glu-Ala-Asp) box helicase 17
1.341	Q9QXZ6	Slco1a1	solute carrier organic anion transporter family, member 1a1
1.334	B1AUN3	EIF2B3	eukaryotic translation initiation factor 2B, subunit 3 gamma, 58kDa
1.334	P62342	SELT	selenoprotein T
1.334	P97494	GCLC	glutamate-cysteine ligase, catalytic subunit

Table 2 (Continued)

Exp Fold Change	ID	Symbol	Entrez Gene Name
1.333	Q9D6S7	MRRF	mitochondrial ribosome recycling factor
1.332	Q8R1S0	COQ6	coenzyme Q6 monooxygenase
1.329	Q64514	TPP2	tripeptidyl peptidase II
1.329	O35350	CAPN1	calpain 1, (mu/I) large subunit
1.328	Q78IK2	USMG5	up-regulated during skeletal muscle growth 5 homolog (mouse)
1.322	Q3UIR3	DTX3L	deltex 3 like, E3 ubiquitin ligase
1.321	Q99L20	Gstt3	glutathione S-transferase, theta 3
1.319	Q9DCM2	GSTK1	glutathione S-transferase kappa 1
1.313	F6VK94	TOR1B	torsin family 1, member B (torsin B)
1.311	Q07797	LGALS3BP	lectin, galactoside-binding, soluble, 3 binding protein
1.310	Q9ER72	CARS	cysteinyl-tRNA synthetase
1.309	Q8C1B7	SEPT11	septin 11
1.308	Q9CQ54	NDUFC2	NADH dehydrogenase (ubiquinone) 1, subcomplex unknown, 2, 14.5kDa
1.307	P52792	GCK	glucokinase (hexokinase 4)
1.301	Q8R4H7	NAGS	N-acetylglutamate synthase
1.301	Q8BXA1	GOLIM4	golgi integral membrane protein 4
-1.479	P11276	FN1	fibronectin 1
-1.480	P26638	SARS	seryl-tRNA synthetase
-1.480	P28658	ATXN10	ataxin 10
-1.487	Q64511	TOP2B	topoisomerase (DNA) II beta
-1.488	P42669	PURA	purine-rich element binding protein A
-1.489	P12815	PDCD6	programmed cell death 6
-1.491	Q9WV54	ASAH1	N-acylsphingosine amidohydrolase (acid ceramidase) 1
-1.491	Q8CI94	PYGB	phosphorylase, glycogen; brain
-1.492	Q99MN1	KARS	lysyl-tRNA synthetase
-1.501	Q9WVK4	EHD1	EH-domain containing 1
-1.505	P06683	C9	complement component 9
-1.506	Q99KV1	DNAJB11	DnaJ (Hsp40) homolog, subfamily B, member 11
-1.507	P06728	APOA4	apolipoprotein A-IV
-1.515	E9Q555	RNF213	ring finger protein 213
-1.517	D3YZJ1	SQSTM1	sequestosome 1
-1.525	D3Z0R5	GNPDA1	glucosamine-6-phosphate deaminase 1
-1.525	Q9DBB9	CPN2	carboxypeptidase N, polypeptide 2
-1.527	E9PWQ3	COL6A3	collagen, type VI, alpha 3
-1.529	Q9EP69	SACM1L	SAC1 suppressor of actin mutations 1-like (yeast)
-1.547	P56380	NUDT2	nudix (nucleoside diphosphate linked moiety X)-type motif 2
-1.550	P83940	TCEB1	transcription elongation factor B (SIII), polypeptide 1 (15kDa, elongin C)

Table 2 (Continued)

Exp Fold Change	ID	Symbol	Entrez Gene Name
-1.551	Q8R0J7	VPS37B	vacuolar protein sorting 37 homolog B (S. cerevisiae)
-1.559	Q62165	DAG1	dystroglycan 1 (dystrophin-associated glycoprotein 1)
-1.560	Q8BM72	HSPA13	heat shock protein 70kDa family, member 13
-1.568	Q3UNV4	Cyp2j13	cytochrome P450, family 2, subfamily j, polypeptide 13
-1.574	D6RGA3	LPCAT3	lysophosphatidylcholine acyltransferase 3
-1.577	E9PV24	FGA	fibrinogen alpha chain
-1.581	Q63886	UGT1A1	UDP glucuronosyltransferase 1 family, polypeptide A1
-1.589	Q9JKX3	TFR2	transferrin receptor 2
-1.592	Q9ESP1	SDF2L1	stromal cell-derived factor 2-like 1
-1.600	Q91XL1	LRG1	leucine-rich alpha-2-glycoprotein 1
-1.609	Q8C872	TFRC	transferrin receptor
-1.618	P58389	PPP2R4	protein phosphatase 2A activator, regulatory subunit 4
-1.618	Q99K30	EPS8L2	EPS8-like 2
-1.626	P08032	SPTA1	spectrin, alpha, erythrocytic 1
-1.646	P01029	C4A/C4B	complement component 4B (Chido blood group)
-1.648	Q62313	Tgoln1	trans-golgi network protein
-1.660	Q91W64	Cyp2c70	cytochrome P450, family 2, subfamily c, polypeptide 70
-1.663	Q8CCJ3	UFL1	UFM1-specific ligase 1
-1.669	Q61830	MRC1	mannose receptor, C type 1
-1.670	P01027	C3	complement component 3
-1.674	O54984	ASNA1	arsA arsenite transporter, ATP-binding, homolog 1 (bacterial)
-1.695	P25233	NDN	necdin, melanoma antigen (MAGE) family member
-1.699	P15508	SPTB	spectrin, beta, erythrocytic
-1.725	Q8JZR2	CRK	v-crk avian sarcoma virus CT10 oncogene homolog
-1.726	P04919	SLC4A1	solute carrier family 4 (anion exchanger), member 1 (Diego blood group)
-1.735	P00920	CA2	carbonic anhydrase II
-1.789	Q9R257	HEBP1	heme binding protein 1
-1.802	P70194	CLEC4F	C-type lectin domain family 4, member F
-1.805	Q9CQJ6	DENR	density-regulated protein
-1.806	Q91WT8	RBM47	RNA binding motif protein 47
-1.810	Q8R0X7	SGPL1	sphingosine-1-phosphate lyase 1
-1.831	Q9R1C7	PRPF40A	PRP40 pre-mRNA processing factor 40 homolog A

Table 2 (Continued)

Exp Fold Change	ID	Symbol	Entrez Gene Name
-1.833	Q9QXK7	CPSF3	cleavage and polyadenylation specific factor 3, 73kDa
-1.836	Q9CPX6	ATG3	autophagy related 3
-1.849	E9Q179	GRSF1	G-rich RNA sequence binding factor 1
-1.855	Q9D1M7	FKBP11	FK506 binding protein 11, 19 kDa
-1.856	G5E8J2	ANK1	67nkyrin 1, erythrocytic
-1.858	P43275	Hist1h1a	histone cluster 1, H1a
-1.859	E9QA15	Cald1	caldesmon 1
-1.870	Q8CBM2	ASPH	aspartate beta-hydroxylase
-1.903	D3Z2Y7	GPX3	glutathione peroxidase 3
-1.903	Q99JF5	MVD	mevalonate (diphospho) decarboxylase
-1.911	Q9JLC3	MSRB1	methionine sulfoxide reductase B1
-1.913	E9Q4K7	KIF13B	kinesin family member 13B
-1.924	P48193	EPB41	erythrocyte membrane protein band 4.1
-1.928	Q9DAS9	GNG12	guanine nucleotide binding protein (G protein), gamma 12
-1.930	Q9D8B6	FAM210B	family with sequence similarity 210, member B
-1.940	Q00896	SERPINA1	serpin peptidase inhibitor, clade A (alpha-1 antiproteinase, antitrypsin), member 1
-1.951	Q64282	IFIT1B	interferon-induced protein with tetratricopeptide repeats 1B
-1.953	Q8R1Q9	RBKS	ribokinase
-1.971	E9Q6Z0	CUL5	cullin 5
-1.972	Q80VP1	EPN1	epsin 1
-2.000	E9Q616	AHNAK	AHNAK nucleoprotein
-2.002	P09813	APOA2	apolipoprotein A-II
-2.004	Q6IQY5	CEP70	centrosomal protein 70kDa
-2.010	Q8VCC1	HPGD	hydroxyprostaglandin dehydrogenase 15-(NAD)
-2.067	Q91YR7	PRPF6	pre-mRNA processing factor 6
-2.097	G3UZX6	SUMO3	small ubiquitin-like modifier 3
-2.136	A3KGB4	TBC1D8B	TBC1 domain family, member 8B (with GRAM domain)
-2.143	Q91X72	HPX	hemopexin
-2.143	Q80Y55	BSDC1	BSD domain containing 1
-2.155	B1AZ15	COBLL1	cordon-bleu WH2 repeat protein-like 1
-2.156	Q8K0Z7	TACO1	translational activator of mitochondrially encoded cytochrome c oxidase I
-2.348	P23249	MOV10	Mov10 RISC complex RNA helicase
-2.380	A2A998	C8A	complement component 8, alpha polypeptide
-2.428	Q9CSU0	RPRD1B	regulation of nuclear pre-mRNA domain containing 1B
-2.432	Q7TQD2	TPPP	tubulin polymerization promoting protein

Table 2 (Continued)

Exp Fold Change	ID	Symbol	Entrez Gene Name
-2.484	P58467	SETD4	SET domain containing 4
-2.494	Q8BGS1	EPB41L5	erythrocyte membrane protein band 4.1 like 5
-2.515	O35226	PSMD4	proteasome 26S subunit, non-ATPase 4
-2.696	E9Q415	FCGR2B	Fc fragment of IgG, low affinity IIb, receptor (CD32)
-2.756	Q8K1Z0	COQ9	coenzyme Q9
-2.813	P10107	ANXA1	annexin A1
-2.862	Q64505	CYP7A1	cytochrome P450, family 7, subfamily A, polypeptide 1
-2.994	Q05920	PC	pyruvate carboxylase
-3.063	Q01339	APOH	apolipoprotein H (beta-2-glycoprotein I)
-3.083	Q61646	HP	haptoglobin
-3.094	Q8BM55	TMEM214	transmembrane protein 214
-3.204	A6X935	ITIH4	inter-alpha-trypsin inhibitor heavy chain family, member 4
-3.296	Q9CY02	Ahsp	alpha hemoglobin stabilizing protein
-3.451	P31001	DES	desmin
-3.566	P48024	Eif1	eukaryotic translation initiation factor 1
-3.699	Q3TUE1	FUBP1	far upstream element (FUSE) binding protein 1
-3.729	E9Q852	MLLT4	myeloid/lymphoid or mixed-lineage leukemia; translocated to, 4
-4.531	Q8R1Q8	DYNC1LI1	dynein, cytoplasmic 1, light intermediate chain 1
-4.541	P11031	SUB1	SUB1 homolog, transcriptional regulator
-6.484	Q8CI51	PDLIM5	PDZ and LIM domain 5
-6.690	Q9DBE0	CSAD	cysteine sulfinic acid decarboxylase
-7.503	Q3UFF7	LYPLAL1	lysophospholipase-like 1
-11.102	Q925P2	CEACAM1	carcinoembryonic antigen-related cell adhesion molecule 1 (biliary glycoprotein)
-25.054	P00688	AMY2B	amylase, alpha 2B (pancreatic)

Table 3: Differentially expressed proteins in insulin stimulated state. Proteins (P<0.05 in a Significance A outlier test) in the PANTG liver compared to the wild type (n=3 for each). See methods for metabolic treatment (Pages 69-75).

Exp Fold Change	ID	Symbol	Entrez Gene Name
21.746	Q8BG73	SH3BGRL2	SH3 domain binding glutamate-rich protein like 2
18.470	Q8CI94	PYGB	phosphorylase, glycogen; brain
15.400	Q8BFW7	LPP	LIM domain containing preferred translocation partner in lipoma
12.723	P70227	ITPR3	inositol 1,4,5-trisphosphate receptor, type 3
10.300	P09813	APOA2	apolipoprotein A-II
9.967	P47963	RPL13	ribosomal protein L13
9.156	P43883	PLIN2	perilipin 2
6.153	Q8R1S9	SLC38A4	solute carrier family 38, member 4
5.500	P13516	SCD	stearoyl-CoA desaturase (delta-9-desaturase)
5.322	Q8VCH0	Acaa1b	acetyl-Coenzyme A acyltransferase 1B
5.077	Q64511	TOP2B	topoisomerase (DNA) II beta
4.938	Q91YS7	MAP2K2	mitogen-activated protein kinase kinase 2
4.832	P06801	ME1	malic enzyme 1, NADP(+)-dependent, cytosolic
3.609	J3QML2	ABCC3	ATP-binding cassette, sub-family C (CFTR/MRP), member 3
3.145	P62960	YBX1	Y box binding protein 1
3.072	Q64458	CYP2C8	cytochrome P450, family 2, subfamily C, polypeptide 8
2.917	Q99KR3	LACTB2	lactamase, beta 2
2.897	Q8BJL9	UGT2B7	UDP glucuronosyltransferase 2 family, polypeptide B7
2.894	H3BL34	Ces1e	carboxylesterase 1E
2.856	P47740	ALDH3A2	aldehyde dehydrogenase 3 family, member A2
2.834	Q91X77	Cyp2c54 (includes others)	cytochrome P450, family 2, subfamily c, polypeptide 54
2.765	Q924Y0	BBOX1	butyrobetaine (gamma), 2-oxoglutarate dioxygenase (gamma-butyrobetaine hydroxylase) 1
2.747	Q8VCC2	Ces1g	carboxylesterase 1G
2.698	O54754	AOX1	aldehyde oxidase 1
2.632	Q8VHE0	SEC63	SEC63 homolog, protein translocation regulator
2.624	P26369	U2AF2	U2 small nuclear RNA auxiliary factor 2
2.616	Q9ESX5	DKC1	dyskeratosis congenita 1, dyskerin

Table 3 (Continued)

Exp Fold Change	ID	Symbol	Entrez Gene Name
2.609	Q9DBM2	EHHADH	enoyl-CoA, hydratase/3-hydroxyacyl CoA dehydrogenase
2.607	Q05D44	EIF5B	eukaryotic translation initiation factor 5B
2.561	G3XA17	EIF4G2	eukaryotic translation initiation factor 4 gamma, 2
2.510	Q64459	CYP3A5	cytochrome P450, family 3, subfamily A, polypeptide 5
2.489	P28666	Mug1/Mug2	murinoglobulin 1
2.450	P24472	Gsta4	glutathione S-transferase, alpha 4
2.447	D3Z0Z6	ELOVL5	ELOVL fatty acid elongase 5
2.407	P19096	FASN	fatty acid synthase
2.403	Q91X75	CYP2A6 (includes others)	cytochrome P450, family 2, subfamily A, polypeptide 6
2.387	Q3UP75	UGT3A1	UDP glycosyltransferase 3 family, polypeptide A1
2.362	Q9Z211	PEX11A	peroxisomal biogenesis factor 11 alpha
2.354	E9PZJ8	ASCC3	activating signal cointegrator 1 complex subunit 3
2.336	H7BX26	CEP170	centrosomal protein 170kDa
2.333	P16015	CA3	carbonic anhydrase III
2.318	Q91WG0	Ces2c	carboxylesterase 2C
2.286	Q9D6Y9	GBE1	glucan (1,4-alpha-), branching enzyme 1
2.245	Q8BFZ9	ERLIN2	ER lipid raft associated 2
2.204	P40936	INMT	indolethylamine N-methyltransferase
2.192	Q62417	SORBS1	sorbin and SH3 domain containing 1
2.184	Q6XVG2	Cyp2c54 (includes others)	cytochrome P450, family 2, subfamily c, polypeptide 54
2.172	Q8BK48	Ces2e	carboxylesterase 2E
2.164	Q8BYU6	TOR1AIP2	torsin A interacting protein 2
2.157	J3KMG3	MIA3	melanoma inhibitory activity family, member 3
2.146	Q8R480	NUP85	nucleoporin 85kDa
2.141	P10649	GSTM5	glutathione S-transferase mu 5
2.126	Q9DBE0	CSAD	cysteine sulfinic acid decarboxylase
2.117	A2ATU0	DHTKD1	dehydrogenase E1 and transketolase domain containing 1
2.035	Q8VCT4	CES1	carboxylesterase 1
2.029	Q3V117	ACLY	ATP citrate lyase
2.027	P16045	LGALS1	lectin, galactoside-binding, soluble, 1
2.016	P19639	Gstm3	glutathione S-transferase, mu 3

Table 3 (Continued)

Exp Fold Change	ID	Symbol	Entrez Gene Name
1.997	E9Q509	PKLR	pyruvate kinase, liver and RBC
1.931	P35492	HAL	histidine ammonia-lyase
1.929	Q61133	GSTT2/2B	glutathione S-transferase theta 2 (
1.925	D3YVR4	MESDC2	mesoderm development candidate 2
1.923	Q62048	PEA15	phosphoprotein enriched in astrocytes 15
1.921	D3Z3E6	TMEM56	transmembrane protein 56
1.917	Q9WV68	DECR2	2,4-dienoyl CoA reductase 2, peroxisomal
1.890	P55050	FABP2	fatty acid binding protein 2, intestinal
1.888	Q9WV98	TIMM9	translocase of inner mitochondrial membrane 9 homolog (yeast)
1.884	Q80WJ7	MTDH	metadherin
1.864	P13634	CA1	carbonic anhydrase I
1.856	P54728	RAD23B	RAD23 homolog B, nucleotide excision repair protein
1.852	Q921H8	ACAA1	acetyl-CoA acyltransferase 1
1.839	Q7TSH2	PHKB	phosphorylase kinase, beta
1.829	Q62264	THRSP	thyroid hormone responsive
1.810	Q99L20	Gstt3	glutathione S-transferase, theta 3
1.805	Q91X70	C6	complement component 6
1.797	Q91VF2	HNMT	histamine N-methyltransferase
1.792	O88696	CLPP	caseinolytic mitochondrial matrix peptidase proteolytic subunit
1.792	Q9CXN7	Pbld2	phenazine biosynthesis-like protein domain containing 2
1.788	Q9D379	EPHX1	epoxide hydrolase 1, microsomal (xenobiotic)
1.785	Q9WUZ9	ENTPD5	ectonucleoside triphosphate diphosphohydrolase 5
1.783	G5E8R3	PC	pyruvate carboxylase
1.780	A2AIH8	PIR	pirin (iron-binding nuclear protein)
1.769	Q9CWS0	DDAH1	dimethylarginine dimethylaminohydrolase 1
1.769	F8VPN4	AGL	amylo-alpha-1, 6-glucosidase, 4-alpha-glucanotransferase
1.758	Q5FW57	Gm4952	predicted gene 4952
1.753	P56654	Cyp2c54 (includes others)	cytochrome P450, family 2, subfamily c, polypeptide 54
1.747	P70362	UFD1L	ubiquitin fusion degradation 1 like (yeast)
1.747	P12710	FABP1	fatty acid binding protein 1, liver
1.733	Q61733	MRPS31	mitochondrial ribosomal protein S31

Table 3 (Continued)

Exp Fold Change	ID	Symbol	Entrez Gene Name
1.727	Q91XT4	SEC16B	SEC16 homolog B, endoplasmic reticulum export factor
1.726	Q9CQR4	ACOT13	acyl-CoA thioesterase 13
1.719	Q91WU0	Ces1f	carboxylesterase 1F
1.718	Q8QZR3	Ces2a	carboxylesterase 2A
1.707	Q8VIJ6	SFPQ	splicing factor proline/glutamine-rich
1.706	Q3TI14	MRPS23	mitochondrial ribosomal protein S23
1.683	Q9DB26	PHYHD1	phytanoyl-CoA dioxygenase domain containing 1
1.680	Q9R0H0	ACOX1	acyl-CoA oxidase 1, palmitoyl
1.673	Q8K4H1	AFMID	arylformamidase
1.666	G5E8M7	Gstm6	glutathione S-transferase, mu 6
1.660	P99025	GCHFR	GTP cyclohydrolase I feedback regulator
1.651	P55096	ABCD3	ATP-binding cassette, sub-family D (ALD), member 3
1.643	Q8R0V5	IDO2	indoleamine 2,3-dioxygenase 2
1.642	O70194	EIF3D	eukaryotic translation initiation factor 3, subunit D
1.639	Q9QUH0	GLRX	glutaredoxin (thioltransferase)
1.626	Q91V76	C11orf54	chromosome 11 open reading frame 54
1.616	P16406	ENPEP	glutamyl aminopeptidase (aminopeptidase A)
1.597	G3X982	Aox3	aldehyde oxidase 3
-1.695	P21981	TGM2	transglutaminase 2
-1.696	Q923D5	WBP11	WW domain binding protein 11
-1.698	P97855	G3BP1	GTPase activating protein (SH3 domain) binding protein 1
-1.711	P46638	RAB11B	RAB11B, member RAS oncogene family
-1.713	Q3TML0	PDIA6	protein disulfide isomerase family A, member 6
-1.724	Q61247	SERPINF2	serpin peptidase inhibitor, clade F (alpha-2 antiplasmin, pigment epithelium derived factor), member 2
-1.727	Q9CRD0	OCIAD1	OCIA domain containing 1
-1.738	P09528	FTH1	ferritin, heavy polypeptide 1
-1.739	Q3TDQ1	STT3B	STT3B, subunit of the oligosaccharyltransferase complex (catalytic)
-1.761	E9PYH3	ETNPPL	ethanolamine-phosphate 72hosphor-lyase
-1.762	P08113	HSP90B1	heat shock protein 90kDa beta (Grp94), member 1
-1.765	P51150	RAB7A	RAB7A, member RAS oncogene family
-1.765	Q61699	HSPH1	heat shock 105kDa/110kDa protein 1
-1.781	E9QNH6	MYO1B	myosin IB

Table 3 (Continued)

Exp Fold Change	ID	Symbol	Entrez Gene Name
-1.783	P57716	NCSTN	nicastrin
-1.797	Q9ESP1	SDF2L1	stromal cell-derived factor 2-like 1
-1.799	Q9QZ85	Iigp1	interferon inducible GTPase 1
-1.810	Q99KF1	TMED9	transmembrane p24 trafficking protein 9
-1.813	P04919	SLC4A1	solute carrier family 4 (anion exchanger), member 1 (Diego blood group)
-1.838	P06683	C9	complement component 9
-1.844	O55137	Acot1	acyl-CoA thioesterase 1
-1.853	Q64339	ISG15	ISG15 ubiquitin-like modifier
-1.867	P01867	Ighg2b	immunoglobulin heavy constant gamma 2B
-1.874	Q8CHP5	PYM1	PYM homolog 1, exon junction complex associated factor
-1.878	P14901	HMOX1	heme oxygenase 1
-1.884	P01837	IGKC	immunoglobulin kappa constant
-1.908	P58021	TM9SF2	transmembrane 9 superfamily member 2
-1.933	E9PV24	FGA	fibrinogen alpha chain
-1.940	Q8VC97	UPB1	ureidopropionase, beta
-1.985	Q60991	CYP7B1	cytochrome P450, family 7, subfamily B, polypeptide 1
-2.001	O70400	PDLIM1	PDZ and LIM domain 1
-2.011	Q9DBG7	SRPR	signal recognition particle receptor (docking protein)
-2.015	G3X9T8	CP	ceruloplasmin (ferroxidase)
-2.015	Q9D8B6	FAM210B	family with sequence similarity 210, member B
-2.016	P50462	CSRP3	cysteine and glycine-rich protein 3 (cardiac LIM protein)
-2.020	P53994	RAB2A	RAB2A, member RAS oncogene family
-2.033	P01027	C3	complement component 3
-2.034	O35226	PSMD4	proteasome 26S subunit, non-ATPase 4
-2.047	P70441	SLC9A3R1	solute carrier family 9, subfamily A (NHE3, cation proton antiporter 3), member 3 regulator 1
-2.058	Q80ZP8	MANF	mesencephalic astrocyte-derived neurotrophic factor
-2.063	Q99NB9	SF3B1	splicing factor 3b, subunit 1, 155kDa
-2.066	Q8K0E8	FGB	fibrinogen beta chain
-2.131	P01029	C4A/C4B	complement component 4B (Chido blood group)
-2.165	Q8BLN5	LSS	lanosterol synthase (2,3-oxidosqualene-lanosterol cyclase)
-2.167	Q9CQJ6	DENR	density-regulated protein
-2.179	E9QA15	Cald1	caldesmon 1

Table 3 (Continued)

Exp Fold Change	ID	Symbol	Entrez Gene Name
-2.185	Q8BWN8	ACOT4	acyl-CoA thioesterase 4
-2.229	O35864	COPS5	COP9 signalosome subunit 5
-2.233	Q9EQ32	PIK3AP1	phosphoinositide-3-kinase adaptor protein 1
-2.246	H3BKR2	GNB1	guanine nucleotide binding protein (G protein), beta polypeptide 1
-2.253	Q91V77	S100A1	S100 calcium binding protein A1
-2.275	B1AQR8	LGALS9B	lectin, galactoside-binding, soluble, 9B
-2.276	Q8K0Z7	TACO1	translational activator of mitochondrially encoded cytochrome c oxidase I
-2.278	P62264	RPS14	ribosomal protein S14
-2.330	Q8K2Q0	COMMD9	COMM domain containing 9
-2.352	P58281	OPA1	optic atrophy 1 (autosomal dominant)
-2.352	P11276	FN1	fibronectin 1
-2.359	Q91X72	HPX	hemopexin
-2.361	Q61990	PCBP2	poly(rC) binding protein 2
-2.368	Q8VCM7	FGG	fibrinogen gamma chain
-2.402	Q9D7X3	DUSP3	dual specificity phosphatase 3
-2.423	P17879	Hspa1b	heat shock protein 1B
-2.487	A6X935	ITIH4	inter-alpha-trypsin inhibitor heavy chain family, member 4
-2.516	Q99K30	EPS8L2	EPS8-like 2
-2.520	P97315	CSRP1	cysteine and glycine-rich protein 1
-2.636	Q8CGR7	UPP2	uridine phosphorylase 2
-2.825	E9PUZ8	C4bp	complement component 4 binding protein
-2.834	Q9QXK7	CPSF3	cleavage and polyadenylation specific factor 3, 73kDa
-2.861	P32921	WARS	tryptophanyl-tRNA synthetase
-2.934	Q9D1J3	SARNP	SAP domain containing ribonucleoprotein
-2.949	P01868	IGHG1	immunoglobulin heavy constant gamma 1 (G1m marker)
-3.288	Q923B6	STEAP4	STEAP family member 4
-3.436	E0CYI9	GCC2	GRIP and coiled-coil domain containing 2
-3.825	Q01279	EGFR	epidermal growth factor receptor
-3.944	P47809	MAP2K4	mitogen-activated protein kinase kinase 4
-4.097	Q8BJW6	EIF2A	eukaryotic translation initiation factor 2A, 65kDa
-4.131	D3Z368	CAMK1	calcium/calmodulin-dependent protein kinase I
-5.378	Q61646	HP	haptoglobin

Table 3 (Continued)

Exp Fold Change	ID	Symbol	Entrez Gene Name
-5.563	P62281	RPS11	ribosomal protein S11
-6.881	P60229	EIF3E	eukaryotic translation initiation factor 3, subunit E
-7.557	O55239	NNMT	nicotinamide N-methyltransferase
-13.618	Q9JIK5	DDX21	DEAD (Asp-Glu-Ala-Asp) box helicase 21

Discussion

This proteomic examination of the PANTG provided important mechanistic insight pertaining to the putative mechanism impacting lipid metabolism in the liver of mice with increased circulating PANDER sourced from the endocrine pancreas. Additionally, we demonstrated the strong utility for the implementation of quantitative mass spectrometry based proteomics for the investigation of metabolic disorders or the characterization of novel hormones regulating intracellular signaling.

With the creation of our pancreas-specific overexpressing mouse model, we have recently reported that the PANTG mice display fasting hyperglycemia attributed to impaired hepatic insulin sensitivity when circulating PANDER is overexpressed. A similar proteomic approach in the PANTG revealed upregulation of PEPCK and indicated a mechanism of PANDER-induced gluconeogenesis [21]. This approach was limited though since our previous SILAC analysis employed ethanol treated AML-12 cells (murine hepatic cell line) to serve as the control “spike-in” internal standard for the liver and utilized for protein comparison. In addition, the prior proteomic examination was performed during a random re-fed uncontrolled metabolic state. This experimental design was certainly not ideal for making important comparisons during metabolic states and examining changes in the hepatic proteome.

Therefore, our current approach employed controlled metabolic states (fasting, controlled fed, and insulin-stimulated) with a SILAC-labeled C57BL/6J murine liver (not AML-12 cell line) and evaluated in the established PANTG model. In this current study, we utilized a metabolically labeled "SILAC" mouse liver to provide a superior internal standard enhancing the capability to capture differences in the PANTG liver proteome as compared to the WT control. In all, this is the first dataset to detail global proteome changes in the liver of the PANDER transgenic mouse model, a disease model of selective hepatic insulin resistance and metabolic disease.

Chapter 3 – Investigation of the Pander Transgenic Hepatic Proteome

Introduction

Over the past decade PANcreatic-DERived factor (PANDER or FAM3B) has been investigated with regard to secretion from the endocrine pancreas and biological impact on glycemic regulation both *in-vitro* and *in-vivo* [1, 4, 6, 9-11, 15, 18, 130-135]. Our recently generated pancreas specific overexpressing transgenic mouse model exhibits both fasting and fed glucose intolerance primarily attributed to impaired hepatic insulin signaling concordantly coupled with both increased gluconeogenesis and lipogenesis [21]. This result is consistent with other PANDER animal models that acutely express PANDER within the liver via adenoviral delivery [19]. The mechanism by which PANDER inhibits hepatic insulin signaling has been attributed to suppressed phosphorylation of Akt [16] and AMPK [21] both of which serve as major regulators of gluconeogenesis. However, a major paradox to PANDER signaling has been the documented increase in hepatic lipogenesis despite inhibited insulin signaling [19, 21]. This bifurcation of signaling results in a selective insulin resistant state that mimics what is observed

in T2D animal models and humans [137, 139]. Encompassing prior PANDER research, an emerging hypothesis suggests that the pathophysiological conditions of T2D could potentially induce increased circulating PANDER levels contributing to selective hepatic insulin resistance resulting in increased hepatic glucose output and lipogenesis [59, 60], as precisely observed in our PANTG model. Recent evidence has now indicated that circulating PANDER levels are elevated and associated with metabolic syndrome components in a Chinese population [140]. Plasma PANDER levels significantly correlated with fasting plasma glucose, 2 hour plasma glucose, and triglyceride levels. Between animal model results and recent clinical studies, an emerging theme with PANDER is the role this novel hormone may contribute to in the promotion of hepatic insulin resistance and lipogenesis. Despite this importance, the precise PANDER-induced signaling mechanisms in the liver have yet to be determined.

To elucidate PANDER-induced hepatic molecular mechanisms, we utilized quantitative mass spectrometry based proteomic analysis via stable isotope labeling by amino acids in cell culture (SILAC) as a heuristic tool to characterize hepatic proteomic differences between the PANTG murine liver with that of wild-type mice under three metabolic states: fasting, fed, and insulin-stimulated. To achieve this, SILAC-labeled ($^{13}C_6$-Lys) mouse liver was utilized as an internal standard for relative

quantification of global proteome differences in the liver, a technique rarely used to study metabolic disorders yet previously validated by the examination of insulin signaling and liver proteomic characterization [29]. Differentially expressed proteins using this approach can be analyzed with bioinformatics tools such as Ingenuity Pathway Analysis (IPA) in order to reveal altered molecular networks and their function as well as differences in canonical pathways that can be later validated via additional molecular approaches. This unbiased, global-scale approach has led to novel insight into PANDER-induced hepatic pathway alterations in our PANTG model, in particular, those related to increased lipogenesis.

In all three metabolic states lipid metabolism and fatty acid synthesis were identified as top cellular functions altered in the PANTG mouse. Specific molecules that were differentially expressed include fatty acid synthase (FASN), apolipoprotein A1 (ApoA1) and A4 (ApoA4), acetyl-CoA carboxylase (ACC), stearoyl-CoA desaturase-1 (SCD1), cholesterol 7 alpha-hydroxylase (CYP7A1) and CD36. Furthermore, the activation of the liver X receptor (LXRα) pathway was predicted which is a central modulator to these differentially expressed proteins. Taken together, this data suggest a high level of correlation with the available literature on the effects of PANDER overexpression on the liver. Our study also revealed numerous unidentified

differentially expressed proteins and pathways due to PANDER overexpression from the pancreas, many of which are involved in hepatic lipogenesis and lipid transport. Apart from these pathways, our proteomic approach revealed a number of molecules related to glycogen metabolism. Initial proteomic characterization of the PANTG mouse revealed glycogen phosphorylase to have a marked increase in mice treated with insulin. Additionally, our phosphoproteomic approach revealed an increase in an uncharacterized phosphorylation site on glycogen synthase (GSK), concordant with prior evidence of our PANTG mouse demonstrating decreased hepatic glycogen content.

Materials and Methods

Statistics And Pathway Analysis

Raw files from LC-MS/MS (Orbitrap XL) were processed in MaxQuant 1.2.2.5 employing the Andromeda search algorithm and searched against the UniprotKB reference database for *Mus musculus*, concatenated with reversed protein sequences. A second database of known contaminants provided with the MaxQuant suite was also employed. All fractions for each biological sample were combined for analysis. Constant modification of carbamidomethylation of cysteine and variable modifications of oxidized methionine and acetylated protein N-termini were used. Additionally, Lys-6 for the spike-in internal standard was set as a label in the group-

specific parameter section. A false discovery rate of 1% was used for peptides and proteins. A minimum peptide length of 6 amino acids was used. Razor and unique peptides were used for identification and quantification. Protein ratio values were reconstructed using median peptide ratio values across all three biological replicates for each experimental group where the final ratio for each protein was calculated by determining the ratio-of-ratio (PANTG/Internal Standard / (WT/Internal Standard)). Final ratios were input into the Perseus processing suite (Perseus version 1.2.0.13). Statistical analysis was performed using the Significance A outlier test where statistical significance based on magnitude fold-change was established at $P<0.05$. Ratio values and Uniprot Protein identification numbers of differentially expressed proteins were uploaded to Ingenuity Pathway Analysis (IPA) to determine canonical pathways, networks and upstream regulators in the liver affected by increased pancreas-secreted PANDER. We note that the outlier test based on the ratio distribution of the combined replicates was performed to increase coverage depth of differentially expressed proteins. The limitation of this approach is the increased false discovery rate of differentially expressed proteins as variance within groups is not specifically considered in the statistical filtering. Given only lysine-terminated tryptic peptides were used for relative quantitation,

coverage of quantifiable proteins was limited (more so for lower abundance proteins) and therefore the Significance A filtering approach was utilized in order to enhance bioinformatic analysis. Additionally, we have generated a modified proteinGroups file generated by MaxQuant that lists relative expression ratios for each biological replicate, showing all proteins with measurable relative standard deviation (RSD) values. In order to achieve statistical significance based on 1.5-fold change in expression (relative to wild-type, which is a value close to the Significance A test cut-off for significance at $P<0.05$ for the three metabolic conditions) using the Student's t-test (with the assumption that variance is the same at higher expression), approximately 30% RSD (after error propagation from ratio-of-ratio calculation) or less would be needed. For higher fold-change values (>2-fold), statistical significance using the Student's t-test could be achieved at RSD values measured for most proteins in the modified proteinGroups file. The modified protein list represents all hepatic proteins that are quantifiable with the methodology and instrumentation used in this study. This file as well as all mass spectrometric data has been deposited to the ProteomeXchange Consortium via the PRIDE partner repository with the dataset identifier PXD004171 and 10.6019/PXD004171. In addition, further raw data and a detailed description of the proteomic analysis can be

found in the *Data in Brief* manuscript associated with this study including Venn-Diagrams of unique proteins across metabolic states (Figure 12) and complete listing of all differentially expressed proteins [35].

Hepatic Phosphoproteomic Analysis of The Insulin Stimulated PANTG Mouse

For the analysis of phosphoproteomic changes in the liver of the PANTG mouse, the same lysate was used from the insulin stimulated condition. Protein concentration was quantified using the Peirce 660 nm protein assay kit supplemented with the provided ionic detergent compatibility reagent (IDCR). Equal mass of labeled and unlabeled protein (~1.2mg per sample) or "light" and "heavy" protein respectively, were combined and digested using the filter aided spin procedure (FASP) method (Expedeon). Briefly, 30 µL of the protein mixture (~12.5mg/ml) was added to the spin column and lysate buffer exchanged to 8M urea using centrifugation prior to iodoacetamide alkylation and then exchanged to 50 mM ammonium bicarbonate for trypsin/Lys-C digestion at a ratio of 1:40 (w/w). Digestion was carried out overnight in a humidified incubator at 37°C. Protein was eluted off the column by addition of 0.5M NaCl followed by centrifugation. Samples were desalted using solid phase enrichment C18 columns (The Nest Group, Inc.). Briefly, columns were activated using 100% acetonitrile followed by equilibration

with 0.1% formic acid in water. Samples were loaded onto the columns and washed three times using equal volumes of 0.1% formic acid in water. Samples were eluted using 90% acetonitrile / 0.1% formic acid in water. Prior to strong cation exchange fractionation samples were concentrated in a vacuum concentrator (Thermo) prior to resuspension with 5 mM ammonium formate and 25% acetonitrile.

Fractionated "spiked-in" peptides were enriched for phosphopeptides using the PolyMAC-Ti magnetic bead phosphopeptide enrichment kit (Expedeon). Samples were handled following kit guidelines. Briefly, samples are re-suspended and incubated with magnetic capture beads. Using a magnetic test tube rack, beads are captured to allow for the exchange of buffers for several wash steps. Beads are then re-suspended in elution buffer. The eluted peptides were concentrated in a vacuum concentrator (Thermo) and re-suspended in 0.1% formic acid in water prior to liquid chromatography tandem mass spectrometry (LC-MS/MS) using the same method as previously mentioned.

Raw files were processed in MaxQuant 1.2.2.5 as previously outlined, with the additional parameter of the variable modification phospho STY selected. For statistical analysis, the average intensity of each representational peptide for

phosphorylated proteins in each biological replicate was used to determine a ratio average (PANTG average / WT average) for the determination of increased or decreased modification. To test for significance, a Welch's two-tailed t-test was carried out using the same intensity values.

Immunoblotting

Approximately 100 mg of tissue was excised from a lobe of mouse liver for tissue lysis. Liver samples were identical from those obtained during the SILAC analysis as detailed earlier. In brief, following isolation the liver was submerged in cold T-PER lysis buffer (Thermo) supplemented with 1X HALT protease inhibitor and lysed using a Qiagen TissueRupter until tissue debris was no longer visible. Cellular lysate was then heated at 95 °C for five minutes followed by brief sonication. The tissue lysate was cleared by centrifugation at 16,000× *g* for 5 min and the supernatant was collected and stored at −80 °C prior to further analysis. Protein concentration was quantified using the Pierce BCA Protein assay following the manufacturer's protocol. Fifty µg was separated by SDS-PAGE (Mini-PROTEAN TGX Pre-Cast gels, 4–20%) and electro-transferred to a PVDF membrane using the iBlot semi-dry transfer apparatus (Invitrogen). PVDF membranes were then probed with primary antibodies against FAS, (C20G5, Cell Signaling Technology), LXRα (P-20, Santa Cruz), and CYP7A1 (ab65596, Abcam). All primary antibodies were diluted

1:500 in StartBlock Blocking Buffer (Thermo). Detection was achieved utilizing horseradish-peroxidase-conjugated goat secondary antibody (Bio-Rad) diluted 1:10,000 in StartBlock followed by chemiluminescence detection using Pierce ECL Western Blotting Substrate (Thermo). Emitted signal was detected using the Amersham™ Imager 600 (GE Healthcare Life Sciences). Relative protein levels were normalized to GAPDH (2118, Cell Signaling) and expression levels and densitometry analysis were quantified with ImageQuantTL (GE Healthcare Life Sciences).

Cell Culture and Transient Transfection

BNL-CL2 (BALB/c embryonic normal liver) cells were cultured until passage five in standard DMEM (4.5 g/L glucose, L-glutamine and sodium pyruvate) supplemented with 10% FBS and 1% PenStrep (Thermo) at 37 °C, 5% CO_2. Approximately 2×10^5 cells per well were plated in a tissue culture treated 24-well dish (Becton-Dickinson). After 24 h, media was replaced with DMEM without glucose, L-glutamine and sodium pyruvate supplemented with 1% FBS for 4 h prior to transfection. LXRα signaling plasmids and control plasmids (Cignal Reporter Assay Kit, Qiagen) were transfected using Lipofectamine 2000 (Invitrogen, Carlsbad, CA). Transfection of each plasmid was performed in triplicate in two independent experiments. Two hours post transfection, media was replaced with DMEM supplemented with 1% FBS and 1% PenStrep with the addition of PANDER (0.25 nM, 0.5 nM

and 1 nM) for 18 h. Cells were washed with PBS and lysed in 100 µl of 1X Glo Lysis Buffer (Promega), utilizing the Dual-Luciferase Reporter Assay System (Promega) for luciferase activation. Signal emission was detected with a Monolight 3010 luminometer (Analytical Luminescence Laboratory, San Diego, CA).

In a similar experiment, 1.1B4 cells (hybrid cell line formed by the electrofusion of a primary culture of human pancreatic islets with PANC-1, a human pancreatic ductal carcinoma cell line) cultured identically as previously mentioned were transfected as previously described with the same LXRα signaling plasmid. This cell type was chosen because LXRα is described to be active in the Islets of Langerhans [45, 141, 142] and displayed higher transfection efficiency. As a positive control the known non-steroidal agonist of LXRα (T0901317, SigmaAldrich, 20 nm) and antagonist (GSK 2033, AxonMedChem, 20 nm) were used in addition to treatment with exogenous PANDER (0.25 nm, 0.5 nm, 1 nm, 2nm, 4nm, 8nm) for analysis of synergistic effects. Significance in all experiments was determined by a student's two-tailed t-test.

Results

Network and Pathway Analysis

Of the 228, 239 and 189 significantly differentially expressed and quantifiable proteins in the fasted, fed, and insulin-

stimulated conditions within the PANTG liver as compared to WT, respectively (Figure 12), IPA analysis revealed the top predicted primary molecular and cellular functions altered in the PANTG for all metabolic states was lipid metabolism based on −log(p-value) score (Figure 13). Within the fasting, fed and insulin-stimulated conditions, 51, 42 and 50 differentially expressed proteins, respectively, with lipogenic associated functions were identified. The most significant metabolic changes in the predicted activation state were found during insulin stimulation with numerous functions having a significant predicted activation as determined by z-score in IPA (z-score values >2 or <−2 indicate activation or inhibition, respectively) (Figure 15). These functions included fatty acid synthesis, concentration of lipid, concentration of fatty acid, and oxidation of lipid and conversion of lipid (Table 4). The most significantly activated lipogenic that were identified included fatty acid synthesis and concentration of lipid with 27 proteins converging on these predicted activated networks (Figure 14).

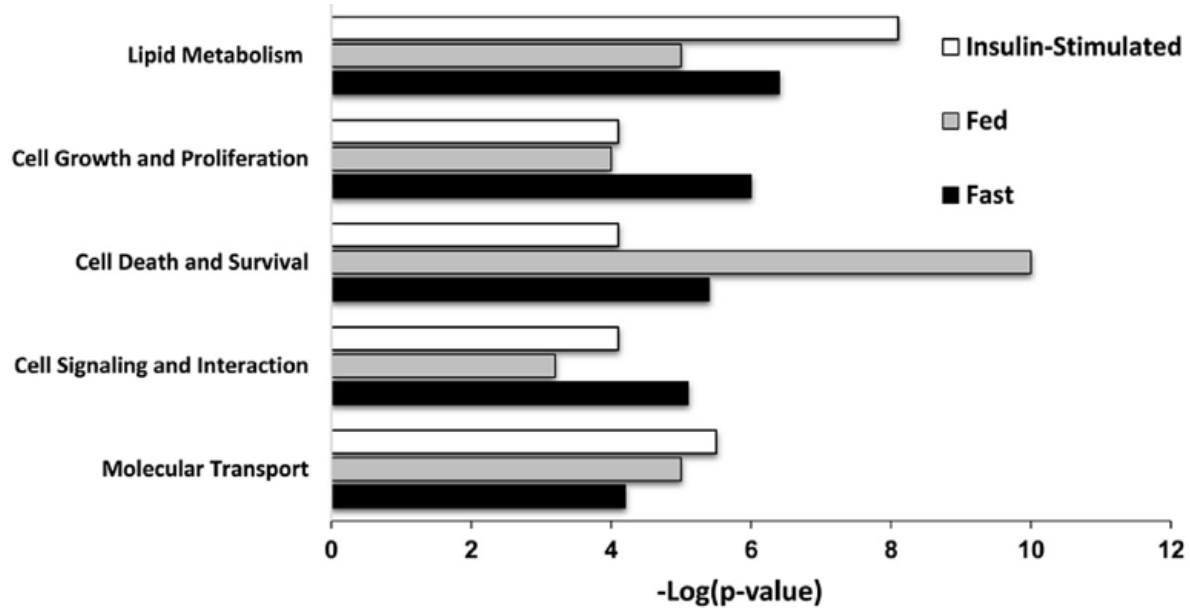

Figure 13: IPA determination of altered molecular and cellular functions with the PANTG liver. Molecular and cellular function analysis was determined based on the identified differentially expressed proteins of the PANTG and WT liver expression Only functions that were identified in all metabolic states of insulin stimulated (top bar, white fill), fed (middle bar, grey fill), and fasting (bottom bar, black fill) conditions with a score cutoff of –log(p-value) greater than two are shown as determined by Fisher's Exact test.

Table 4: List of metabolic functions with significantly predicted increased activation state based on activation z-score identified during insulin conditions within PANTG liver as compared to WT.

Biological function	**Activation z-score**	**Molecules involved**
Fatty-acid metabolism	2.751	ABCC3, ABCD3, ACAA1, ACLY , Acot1, ACOT4, ACOX1, APOA2, Ces1d, CYP2C18, CYP2C8, DECR2, EGFR, EHHADH, ELOVL5, EPHX1, FABP1, FABP2, FASN, HMOX1, MAP2K4, ME1, PLIN2, SCD, SLC9A3R1
Conversion of fatty acid	2.219	ACLY, ACOX1, CYP2C8, DECR2, FASN
Concentration of triacylglycerol	2.019	ACLY ,ACOT13, APOA2 ,C3, CES1, Ces1d, LOVL5, ENTPD5, FABP1, FASN, PEX11A, PLIN2, SCD, SORBS1, STEAP4, THRSP
Concentration of acylglycerol	2.008	FABP1, SORBS1, SCD, STEAP4, PLIN2, C3, APOA2, THRSP, ACOT13, ENTPD5, CES1, PEX11A, ELOVL5, ACLY, EGFR, FASN
Concentration of fatty acid	2.543	ACLY, ACOT13, APOA2, C3, Ces1d, EGFR, EHHADH, ELOVL5, FABP1, HMOX1, PEX11A, PLIN2, SCD
Concentration of lipid	1.945	ABCC3, ACLY ,ACOT13, APOA2, C3, CES1, Ces1d, CYP3A5, EGFR, EHHADH, ELOVL5, ENTPD5, FABP1, FABP2, FASN, HMOX1, HP, PEX11A, PLIN2, RAB7A, SCD, SORBS1, STEAP4, TGM2, THRSP
Concentration of cholesterol	0.686	ACOT13, APOA2, CES1, Ces1d, CYP3A5, ENTPD5, FABP1, FABP2, HP, RAB7A, SCD, STEAP4, TGM2
Oxidation of lipids	2.224	ABCD3, ACAA1, ACOX1, AOX1, Aox3, APOA2, C3, CYP2C8, CYP3A5, EHHADH, FABP1, FABP2, SCD
Beta-oxidation of fatty acid	2.418	ABCD3,ACAA1,ACOX1,EHHADH,FABP1,FABP2,SCD

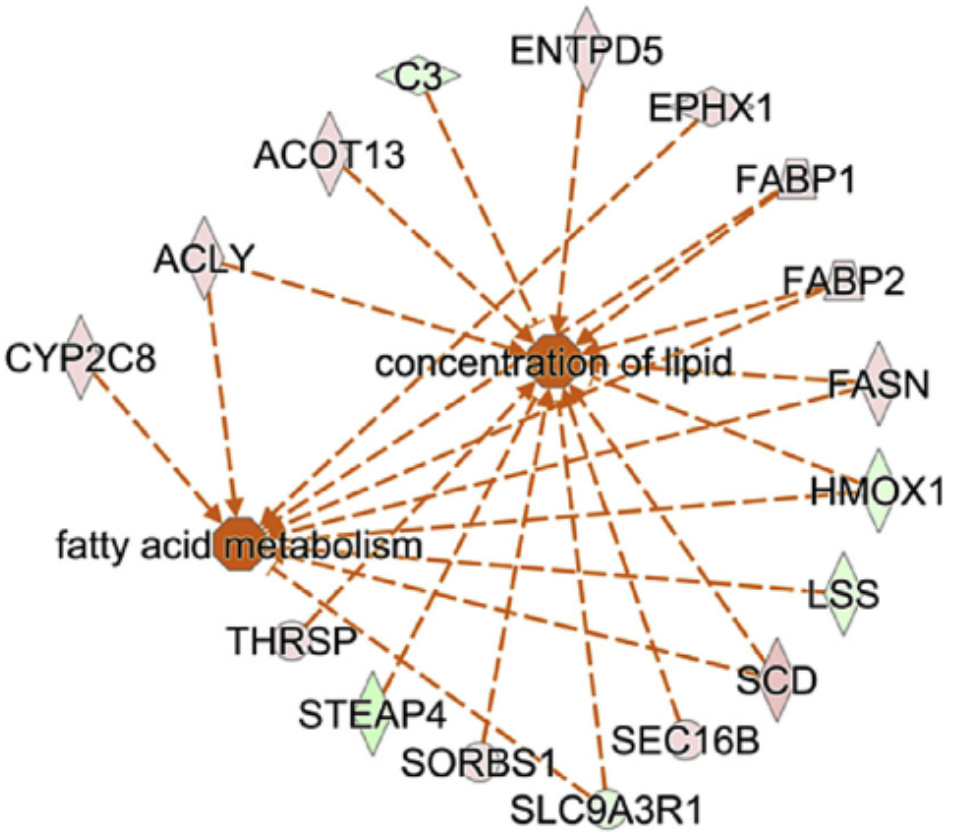

Figure 14: Network analysis of significantly differentially expressed lipogenic associated proteins during insulin stimulatory conditions in PANTG liver. Proteins with a positive association with increased lipogenic states of both fatty acid metabolism and concentration of lipid are shown. Orange dotted lines indicated strong direct association between shown proteins and the predicted activation of fatty acid metabolism and concentration of lipid. The outer nodes represent differentially expressed proteins where red and green represent up and down regulation, respectively. Protein names are as follows: CYP2C8- cytochrome P450, family 2, subfamily C, polypeptide 8, ACLY- ATP citrate lyase, ACOT13-acyl-CoA thioesterase 13, C3-complement component 3, ENTPD5-ectonucleoside triphosphate diphosphohydrolase 5, EPHX1-epoxide hydrolase 1, FABP1 fatty acid binding protein 1, FABP2- fatty acid binding protein 2, FASN- fatty acid synthase, HMOX1-heme oxygenase 1, LSS-lanosterol synthase, SCD-stearoyl-CoA desaturase, SEC16B- SEC16 homolog B, endoplasmic reticulum export factor, SLC9A3R1-solute carrier family 9, subfamily A (NHE3, cation proton antiporter 3), member 3 regulator 1, SORBS1- sorbin and SH3 domain containing 1, STEAP4- STEAP family member 4, and THRSP- thyroid hormone responsive.

Proteomic Identification of Pander-Induced Hepatic LXR Pathway

Due to the significant change in hepatic lipogenesis as determined by our proteomic approach, a mechanism or canonical pathway was then evaluated to potentially identify the etiology supporting this phenotype. Therefore, IPA was used to identify putative canonical pathways in all metabolic states that could potentially regulate the observed lipogenic pathways. Network analysis revealed that Liver X Receptor activation was identified as the most significantly predicted overall affected pathway across metabolic states (Figure 15). In addition, acute phase response signaling was also revealed as a significant canonical pathway.

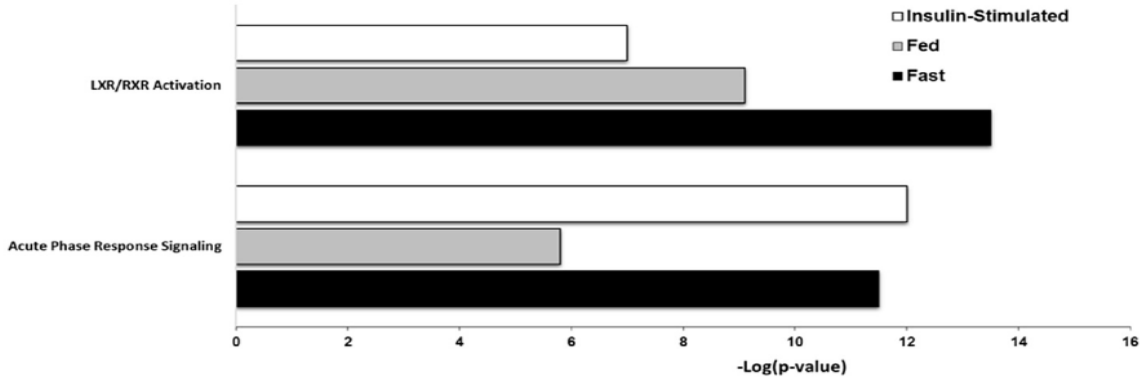

Figure 15: Canonical pathway analysis of significantly differentially expressed proteins during all metabolic conditions in PANTG liver. Canonical pathways with a score cutoff of –log(p-value) greater than 4 as determined by Fisher's Exact test and z-score greater than 2 are shown in metabolic states of insulin-stimulated (top bar, white fill, fed (middle bar, grey fill), and fasting (bottom bar, black fill).

Validation of Pander-Induced Hepatic LXR Pathway and Fatty Acid Synthase Expression

Liver X receptors (LXR) are transcription factors belonging to the class II nuclear receptor superfamily and are composed of 2 isoforms [37-39]. LXRα is highly expressed in the liver, intestine, and adipose tissues whereas LXRβ is ubiquitously expressed. Upon activation, LXRs form a heterodimer with the retinoid X receptor α, which binds to LXR response elements and enhances targeted gene expression in a functional-dependent manner. LXRs appear to regulate overall glucose, cholesterol, bile acid, and triglyceride homeostasis [45]. One of the most critical gene targets governed by LXR involved in lipogenesis is FasN, which was shown by our proteomic analysis to be significantly increased in PANTG livers in all metabolic states [53, 54]. Several LXR targets including FasN and SCD1 not only pass the Significance A outlier test based on the ratio distribution of the combined biological replicates but also demonstrate statistical significance using the *t*-test ($p < 0.05$) in the insulin-stimulated group. Other targets such as Cyp7A1 and CD36 are lower abundance proteins with limited peptide coverage, which affect quantitation accuracy. Therefore, these proteins require further validation by a targeted approach such as western blot analysis. We then sought to precisely examine expression of LXR and dominant targets of LXR such as FasN and

Cyp7A1 in the PANTG liver. Livers obtained during the proteomic investigation of PANTG were also examined for levels of LXRα expression. In brief, PANTG and WT livers obtained and snap-frozen as previously detailed for the proteomic analysis were probed for LXRα, FasN and Cyp7A1 expression by western analysis. Samples from the insulin-stimulated conditions were examined since this metabolic condition demonstrated the most significant differentially expressed lipid metabolism network (Figure 16). During insulin-stimulated conditions, LXRα was significantly increased (*Image J*, $P < 0.05$) as compared to WT liver expression (Figure 16). In addition, hepatic expression of FasN and Cyp7A1 were increased during insulin-stimulated conditions (*Image J*, $P < 0.05$). In summary, LXRα and critical LXRα targets such as FasN and Cyp7A1 were increased in PANTG model and indicates this pathway may potentially be activated during conditions of high circulating PANDER.

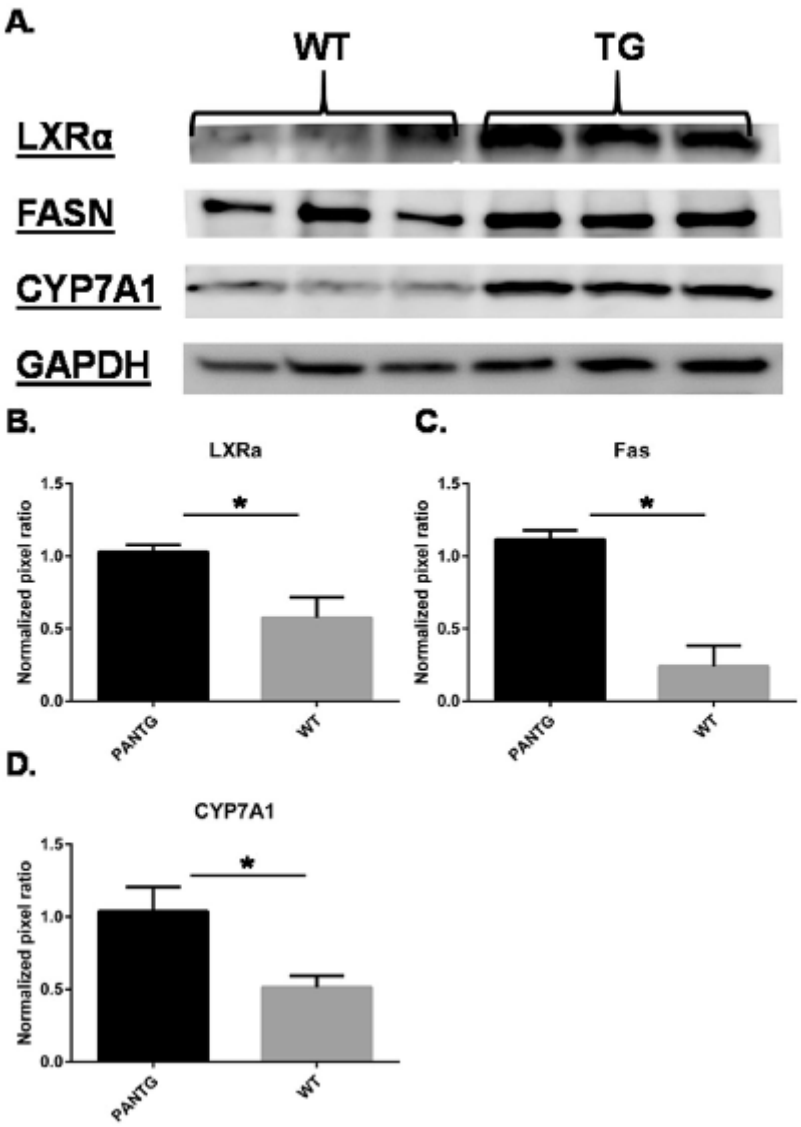

Figure 16: Western blotting and validation of LXRα and LXR targets (FASN and CYP7A1) in insulin stimulated PANTG mice. (A) Liver lysate (40 µg) from age and gender matched PANTG mice during overnight fasting and insulin-stimulated conditions (n = 3). Immunoblotting was performed to measure expression of LXRα, FASN, CYP7A1 and loading control of GAPDH. Lanes: 1–3 and 4–6 are WT and TG liver lysate, respectively. Densitometry analysis on (B) LXRα expression; (C) FASN and (D) CYP7A1. (P<0.05, ImageJ) for both conditions.

Pander Stimulates LXR Transcriptional Activity In-Vitro

The above studies examined the abundance of LXR and targets of LXR in the PANTG liver. However, we also wanted to determine if PANDER may govern or induce LXR transcriptional activity. To examine this, reporter gene analysis was performed using a commercially available LXR response element (LXRE) mediated luciferase assay (Qiagen, Cignal LXR Reporter Kit). This LXRα reporter assay measures the transcriptional activity of liver X receptor (LXR) and this was determined in the context of exogenous PANDER application. A liver derived cell line, BNL-CL2, was exposed to increasing concentrations of purified secreted PANDER (AstraZeneca) and LXR-directed transcriptional activity was measured. PANDER can significantly increase LXRE directed luciferase expression at a range of concentrations from 0.25 to 1 nM in a dose-dependent manner (Figure 17).

Due to limitations of transfection efficiency in the BNL-CL2 cell line, 1.1B4 cells were used to test the effects of the non-steroidal agonist and antagonist T0901317 and GSK 2033, respectively, as well as in the presence of exogenous PANDER. At various concentrations of exogenous PANDER, LXRE directed luciferase expression was increased in a dose-dependent manner (Figure 18). The average fold change between 0 nm PANDER treatment and 1 nm PANDER treatment is 1.7 (N=6, P=1.5986E-06) and 1.96 between 0 nm and 8 nm PANDER treatment (N=6,

P=8.83022E-08) (Figure 19). The agonist T0901317 promoted LXRE directed luciferase expression 3.6 fold on average (N=6, P=1.6538E-06) at a concentration of 20 nm and 4.8 fold increase on average in the presence of 8 nm PANDER (N=6, P=2.88502E-07) (Figures 21 and 22). Between the agonist and agonist + PANDER treatment, a significant 1.3 fold increase was observed (P=0.00012) (Figure 21). In the presence of the antagonist GSK 2033, LXRE directed luciferase expression was decreased 0.31 fold on average (P=1.01421E-05) (Figures 23 and 24). The presence of 8 nm PANDER was able to attenuate the effects of GSK 2033 by increasing luciferase expression 1.19 fold (P=0.008) (Figure 23). Taken together, as matched with increased LXR expression in the liver of the PANTG, PANDER is also capable of directly stimulating LXR-directed transcriptional activity *in-vitro* and synergizes or attenuates the effects of the agonist and antagonist, respectively.

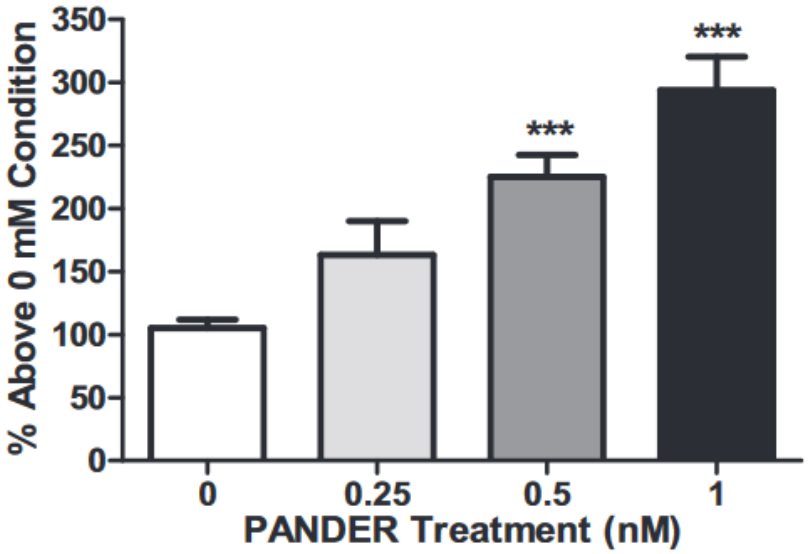

Figure 17: PANDER increased LXRE transcriptional activity in BNL-CL2 cells. Reporter gene analysis was performed on BNL-CL2 liver-derived cells transfected with LXRE-luciferase plasmids exposed to increasing concentrations of purified secreted PANDER (AstraZeneca) followed by measurement of luciferase activity. Treatments performed in triplicate in duplicate biological experiments. *** denotes $P < 0.001$ as determined by Student's *t*-test from 0 nM PANDER condition.

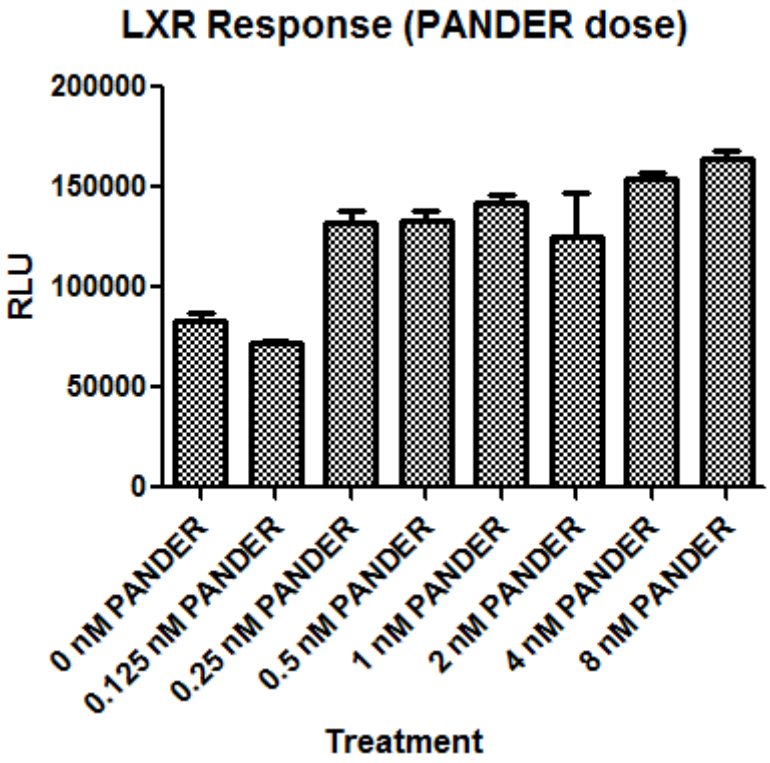

Figure 18: PANDER increased LXRE transcriptional activity in 1.1B4 cells. Reporter gene analysis was performed on 1.1B4 human islet-like cells transfected with LXRE-luciferase plasmids exposed to increasing concentrations of purified secreted PANDER (AstraZeneca) followed by measurement of luciferase activity. Treatments performed in sextuplicate in one experiment.

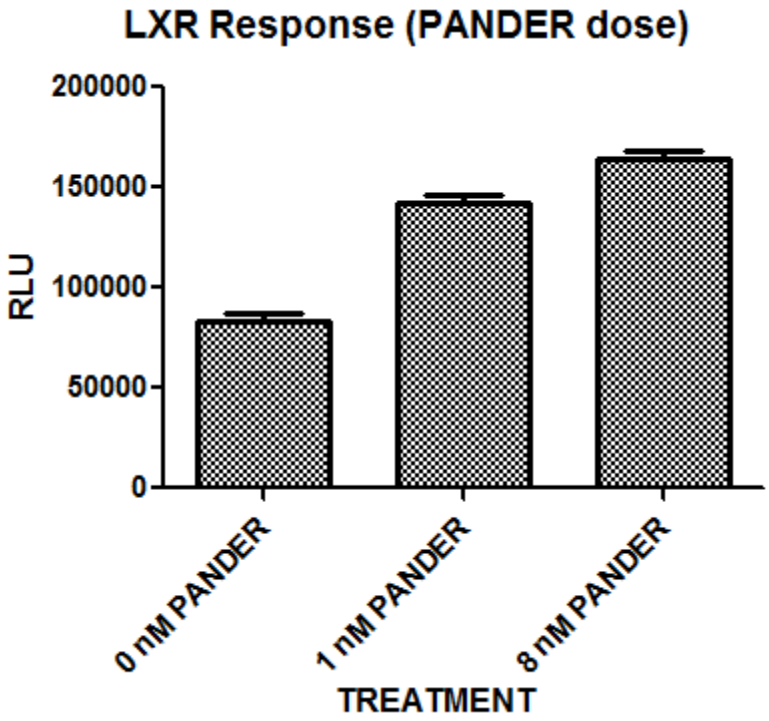

Figure 19: PANDER increased LXRE transcriptional activity in 1.1B4 cells. Reporter gene analysis was performed on 1.1B4 human islet-like cells transfected with LXRE-luciferase plasmids exposed to increasing concentrations of purified secreted PANDER (AstraZeneca) followed by measurement of luciferase activity. Treatments performed in sextuplicate in one experiment. The average fold change between 0 nm PANDER treatment and 1 nm PANDER treatment is 1.7 (N=6, P=1.5986E-06) and 1.96 between 0 nm and 8 nm PANDER treatment (N=6, P=8.83022E-08)

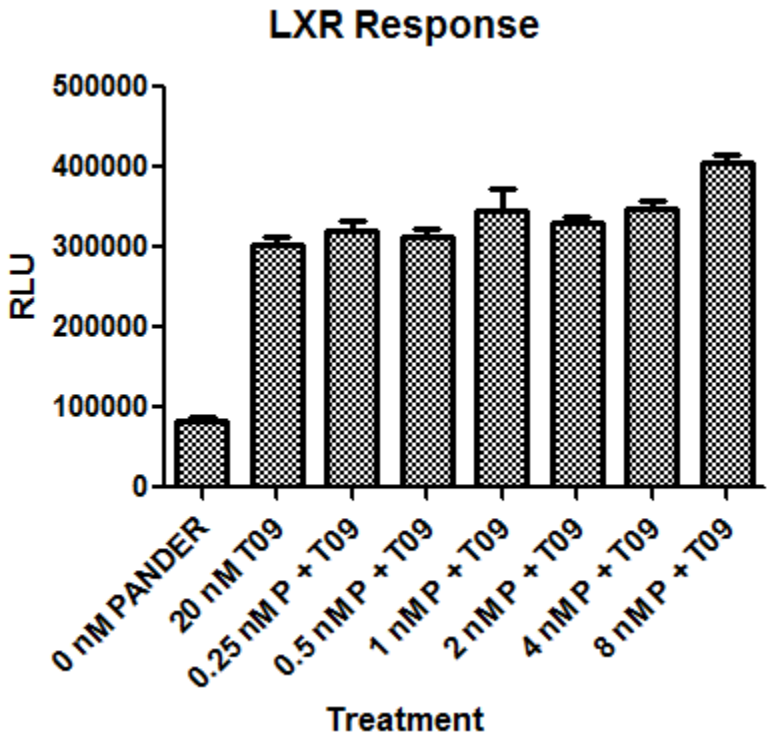

Figure 20: T0901317 and/with PANDER increased LXRE transcriptional activity in 1.1B4 cells. Reporter gene analysis was performed on 1.1B4 human islet-like cells transfected with LXRE-luciferase plasmids exposed to increasing concentrations of purified secreted PANDER (AstraZeneca) followed by measurement of luciferase activity. Treatments performed in sextuplicate in one experiment.

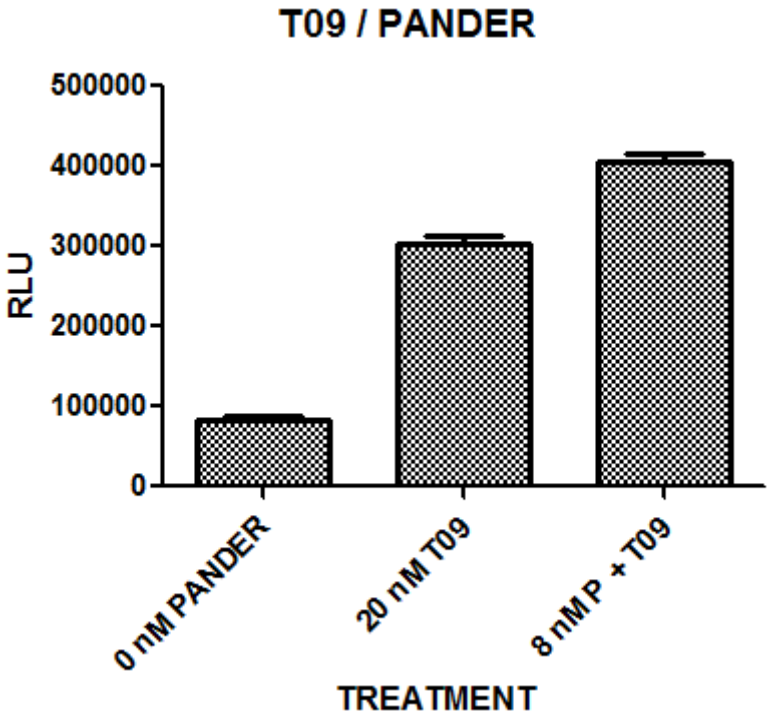

Figure 21: T0901317 and/with PANDER increased LXRE transcriptional activity in 1.1B4 cells. Reporter gene analysis was performed on 1.1B4 human islet-like cells transfected with LXRE-luciferase plasmids exposed to increasing concentrations of purified secreted PANDER (AstraZeneca) followed by measurement of luciferase activity. Treatments performed in sextuplicate in one experiment. The agonist T0901317 promoted LXRE directed luciferase expression 3.6 fold on average (N=6, P=1.6538E-06) at a concentration of 20 nm and 4.8 fold increase on average in the presence of 8 nm PANDER (N=6, P=2.88502E-07). Between the agonist and agonist + PANDER treatment, a significant 1.3 fold increase was observed on average (P=0.00012).

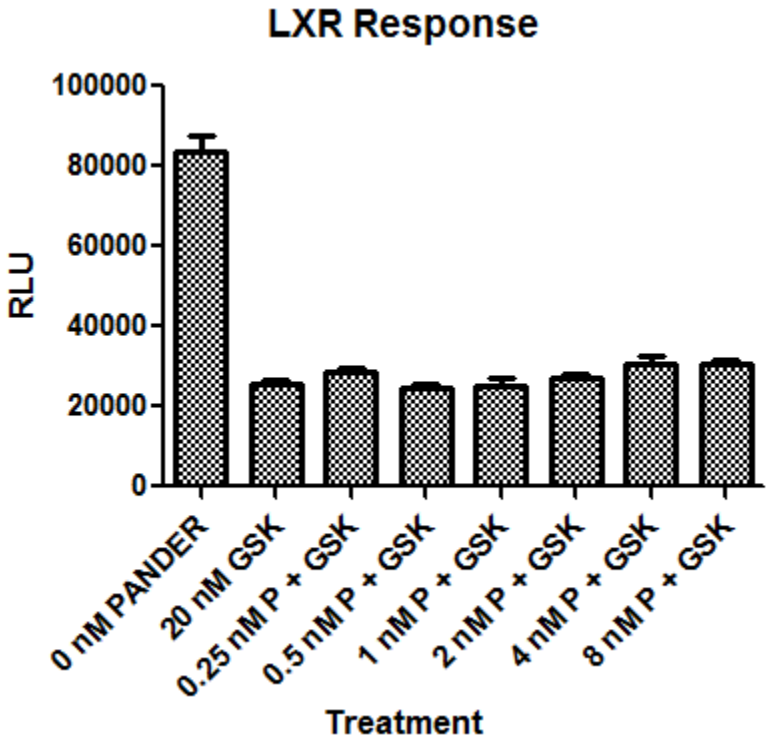

Figure 22: GSK 2033 and/with PANDER increased LXRE transcriptional activity in 1.1B4 cells. Reporter gene analysis was performed on 1.1B4 human islet-like cells transfected with LXRE-luciferase plasmids exposed to increasing concentrations of purified secreted PANDER (AstraZeneca) followed by measurement of luciferase activity. Treatments performed in sextuplicate in one experiment.

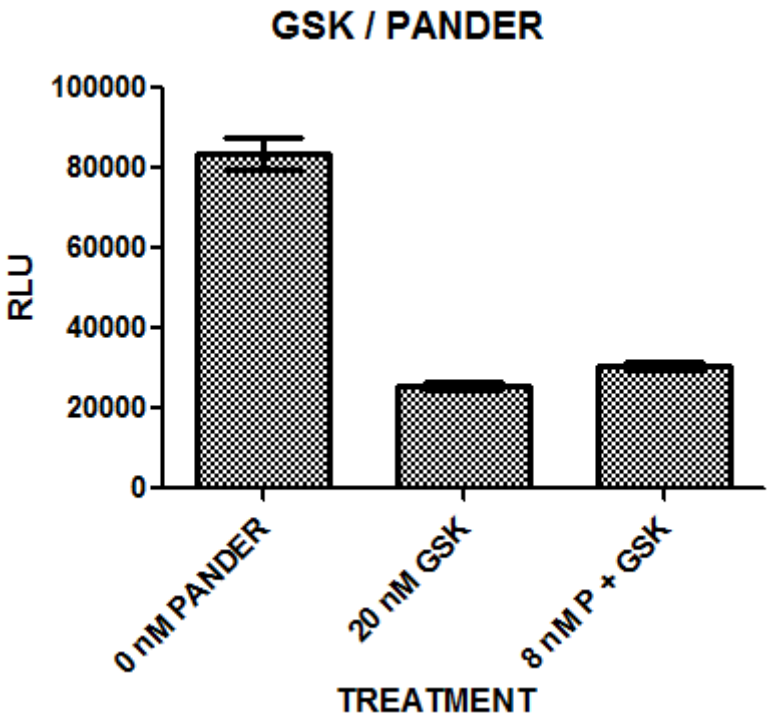

Figure 23: GSK 2033 and/with PANDER increased LXRE transcriptional activity in 1.1B4 cells. Reporter gene analysis was performed on 1.1B4 human islet-like cells transfected with LXRE-luciferase plasmids exposed to increasing concentrations of purified secreted PANDER (AstraZeneca) followed by measurement of luciferase activity. Treatments performed in sextuplicate in one experiment. In the presence of the antagonist GSK 2033, LXRE directed luciferase expression was decreased 0.31 fold on average (P=1.01421E-05). The presence of 8 nm PANDER was able to attenuate the effects of GSK 2033 by increasing luciferase expression 1.19 fold (P=0.008)

Phosphoproteomic Analysis Reveals Increased Phosphorylation of Glycogen Synthase

In order to reveal altered signaling events in the PANTG liver, a similar proteomic profiling approach was employed with the addition of a phosphopeptide enrichment step. 1,142 phosphosites were identified in the PANTG mouse under insulin stimulated condition as predicted by MaxQuant. Of those, 198 peptides were quantifiable and 20 peptides significantly differentially expressed (Table 20). Most notably a recently identified but uncharacterized phosphosite was identified on serine 627 on GSK with a confidence of 98.7% as predicted by MaxQuant [143] (Figure 24.

Apart from altered biochemical pathways pertaining to lipid metabolism and fatty acid synthesis, our initial proteomic analysis revealed several proteins responsible for the phosphorylation of glycogen synthase (GSK), most notably in the insulin stimulated condition. Glycogen phosphorylase kinase (PHK) was increased 1.84 as well as Glycogen phosphorylase increased 18.5 fold in the PANTG mouse under insulin stimulation (Table 3), evidence that further suggests increased phosphorylation of glycogen synthase.

Table 5: List of significantly differentially modified (phosphorylated) proteins in the PANTG mouse. For statistical analysis, the average intensity of each representational peptide for phosphorylated proteins in each biological replicate was used to determine a ratio average (PANTG average / WT average) for the determination of increased or decreased modification where a value over 1 is increased and below 1 is decreased. To test for significance, a student's two-tailed t-test was carried out using the same intensity values. The probability from MaxQuant is shown, where a value closer to one correlates to stronger confidence. Here a probability cut-off was set to 0.90, with the exception of the proteins displayed in the first two rows.

Protein name	Phospho (STY) Probabilities	RATIO AVERAGE	T TEST
General transcription factor IIIC, polypeptide 3	S(0.5)S(0.5)PKENPDDSEVPSSSGIDSAK	0.904	0.005
General transcription factor IIIC, polypeptide 3	S(0.5)S(0.5)PKENPDDSEVPSSSGIDSAK	0.904	0.005
Acyl-CoA dehydrogenase family member 11	METDVT(0.034)S(0.909)DT(0.058)VEVIPQHK	1.735	0.007
Glycogen [starch] synthase, liver OS=Mus musculus	FHIEPT(0.012)S(0.987)PPT(0.001)TDGFK	1.625	0.007
40S ribosomal protein S3 OS=Mus musculus	DEIIPT(0.005)T(0.993)PIS(0.002)EQK	0.554	0.010
Nucleolar protein 58 OS=Mus musculus	EEPIS(1)EEEPCTSTAVPS(1)PEK	1.242	0.020
Serine/arginine repetitive matrix protein 2	SEQPISQVIPS(0.015)IS(0.985)PEHK	0.842	0.025
Thyroid hormone receptor-associated protein 3	FSGEEGEIEDDES(0.997)GT(0.003)ENREEK	1.208	0.026
Ribonuclease H2 subunit A	EAEDVIWEDS(1)EAEEDPERPGK	1.251	0.030
Pinin	SIS(1)PGKENINSQEVEK	1.240	0.031
Gephyrin	EVHDEIEDIPS(1)PPPPIS(0.989)PPPT(0.008)T(0.002)S(0.001)PHK	1.662	0.032
Eukaryotic translation initiation factor 3 subunit G	GIPIPT(0.003)GDT(0.172)S(0.825)PEPEIIPGDPIPPPK	0.863	0.036
2-hydroxyacyl-CoA lyase A lyase 1	PES(1)NSAEGSDRSEEQVSGAK	1.756	0.039
Trans-Golgi network integral membrane protein 1	GDKS(0.993)S(0.007)EPTEDVETK	1.209	0.039
GMP synthase [glutamine-hydrolyzing]	TINMT(0.002)T(0.043)S(0.955)PEEK	1.676	0.040
Serine/threonine-protein kinase PAK 2	YIS(1)FTPPEK	0.946	0.042
Myosin-9 OS=Mus musculus	GTGDCS(1)DEEVDGK	0.808	0.053
Synaptosomal-associated protein (Fragment)	ATWGDGGDNS(1)PSNVVSK	1.131	0.058
Nuclear ubiquitous casein and cyclin-dependent kinase substrate 1	TPSPKEEDEEAES(1)PPEKK	1.232	0.058

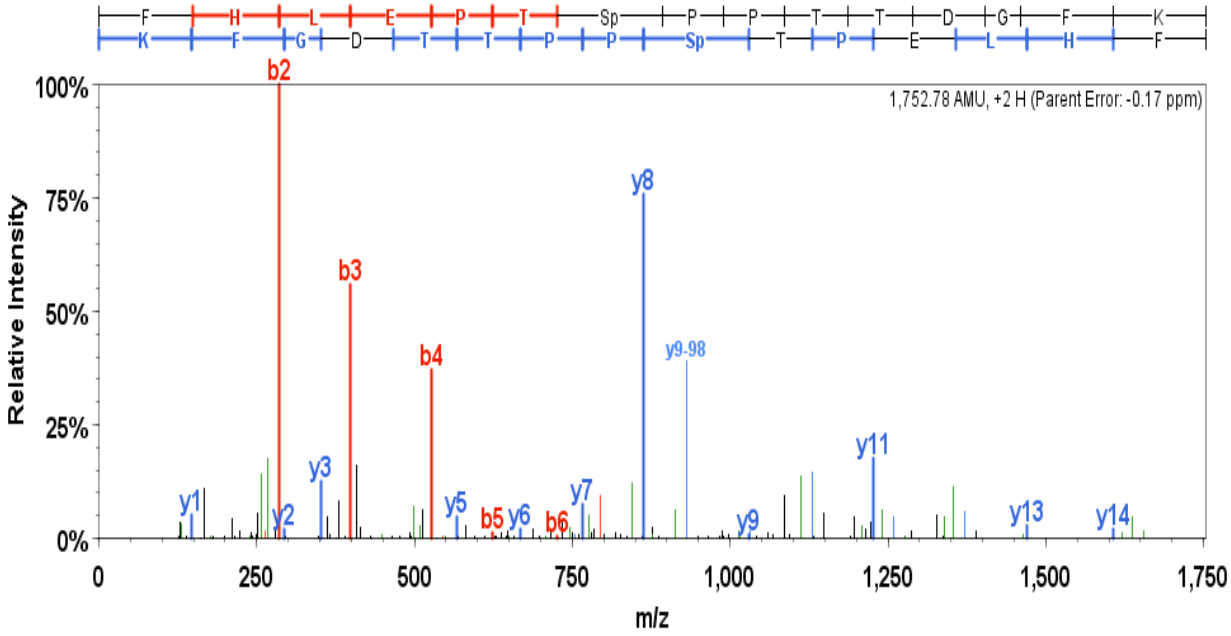

Figure 24: Increased phosphorylation of glycogen synthase at Ser627. Annotated MS/MS spectra of glycogen synthase peptide showing phosphorylation detection at Serine 627.

Discussion

This proteomic examination of the PANTG provided important mechanistic insight pertaining to the putative mechanism impacting lipid metabolism in the liver of mice with increased circulating PANDER sourced from the endocrine pancreas. Additionally, we demonstrated the strong utility for the implementation of quantitative mass spectrometry based proteomics for the investigation of metabolic disorders or the characterization of novel hormones regulating intracellular signaling. Evidence to date has demonstrated that PANDER can promote a selective hepatic insulin resistant (SHIR) phenotype whereby insulin signaling is partially inhibited and therefore hepatic glucose production and lipogenesis is increased [21], phenomena observed in T2D animal models and clinical human observations [137]. Earlier studies demonstrated that PANDER overexpression induces fasting hyperglycemia by upregulating gluconeogenic gene pathways and subsequently increasing hepatic glucose output in mice [17, 19, 21]. These effects were attributed to the presence of increased transcript levels of PEPCK and Glucose 6 phosphatase (G6Pase) due to inhibited phosphorylation of critical insulin signaling molecules such as Akt and AMPK. However, these similar studies revealed increased hepatic lipogenesis despite suppressed insulin signaling. Therefore, due to the complex nature of this metabolic process,

we employed a comprehensive proteomic approach to identify putative novel mechanisms of this process. Our MS based methods demonstrated a proteomic profile similar to the observed lipogenic phenotype and supports the utility of using this tool to unravel complex signaling mechanisms.

Our proteomic data strongly complements the described published studies on PANDER's role in the mouse liver with regard to inducing increased hepatic lipogenesis which has long been attributed to hyperinsulinemia [144], a hallmark of T2D and non-alcoholic fatty liver disease [145, 146]. However, pertaining to lipid metabolism in the PANTG liver, little is known of the biochemistry generating the increase of lipid production, especially fatty acid synthesis and lipogenesis. In our study we have provided data indicating that PANDER overexpression acts to increase gene expression modulated by a similar nuclear binding protein: the liver X receptor (LXR). Insulin mediated activation of lipogenic pathways has been described extensively. LXR has been shown to drive overexpression of lipogenic genes in hyperinsulinemia conditions [51, 147]. Since the most significant effects of PANDER were observed during insulin-stimulatory conditions, our data suggests that PANDER acts in concert with insulin to potentially promote hepatic lipid production and fatty acid synthesis. Given the fact that PANDER does appear to be located within pancreatic β-cell insulin

granules [4, 7], this co-packaging may indicate complementary functionality in terms of distal biological effects on target tissues such as the liver. Increased hepatic lipid metabolism was also observed by proteomic analysis during fasting and fed conditions but not to the same level of statistical significance as insulin-stimulated. There are several potential putative mechanisms describing this effect. As mentioned previously, increased lipogenic gene regulation by PPARγ regulation has been described by blunted FOXO1 signaling [19]. Interestingly, our network analysis also indicated that PPARγ was a significantly predicted upstream regulator of the observed lipogenic effect in our PANTG model (data not shown). Alternatively, recent studies have indicated that Carbohydrate-Responsive Element Binding Protein (ChREBP) binds directly to the PANDER promoter [5]. This gene plays a key role in the control of lipogenesis through the regulation of lipogenic genes [148, 149]. PANDER may be acting in concert with ChREBP enhancing PANDER-induced lipogenesis [5]. Our current data suggests a novel putative mechanism that implicates LXR as a key modulator of genes driving a hepatic steatotic phenotype in the PANTG mice. In the insulin-stimulated condition we saw this effect exaggerated where downstream targets of LXR such as FASN, ApoA1, ApoA4, ACC, SCD1, CYP7A1 and CD36 are all upregulated. Additionally, vLDL was increased in the PANTG liver suggesting an increase of intercellular

oxysterols. Oxysterol is the main activating ligand required for LXR-RXR dimerization [41]. LDL influx is mediated by certain cell membrane transporters, CD36 being one of them [150], leading to an increase in intracellular cholesterol content that can be subsequently oxidized [151]. Taken together, we have demonstrated and validated that the LXR signaling pathway may be involved in PANDER-induced hepatic lipogenesis.

As detailed in prior review articles, PANDER has widespread interactions with both the liver and the endocrine pancreas [59-61]. Pancreatic islets obtained from the PANDER knockout mouse (PANDER KO) displayed an impaired glucose stimulated insulin secretion (GSIS) [18]. The mechanism for this decreased biological function has yet to be determined precisely, although the observed inhibited intracellular Ca^{2+} response is believed to have a role in the impaired GSIS of the PANKO model. Importantly, LXR activation has been demonstrated to stimulate insulin secretion upon T0901317 (agonist of LXR) activation and promoting expression of FASN and ACC (also increased in our PANTG) in pancreatic islets [152, 153]. Concordantly, pancreatic islets from LXR knockout mice have disrupted GSIS with increased lipid deposition [154]. Although not experimentally confirmed in the PANKO model, the absence of PANDER may have inhibited pancreatic LXR expression resulting in the observed impaired GSIS. Another highly relevant finding is that chronic LXR

activation particularly under high glucose conditions promotes pancreatic β-cells apoptosis [155]. An identical biological effect was initially reported for PANDER overexpression [7]. Some of the earliest investigations demonstrated that PANDER could induce apoptosis of pancreatic β-cells and cell lines in a time and dose dependent manner [7, 9]. Taken together, PANDER induced LXR activation may provide a central rationale for the observed pleiotropic actions of this novel hormone in both the liver and pancreas.

Previously described glycogen content is decreased in the PANTG mouse liver [21]. In our current study, we demonstrated proteomic evidence supporting this phenotype. In the insulin stimulated condition, glycogen phosphorylase kinase (PHK) and glycogen phosphorylase was significantly upregulated compared to the wild-type control. Additionally our phosphoproteomic experiment revealed an increase of the phosphorylation site serine 627 on glycogen synthase which has been characterized but its biological role is unknown, although thought to be active [156-159]. This phosphorylation site may present a novel role in signaling events regulating glycogenolysis. Taken together, this data suggest an increase in the phosphorylation of glycogen synthase which is known to inactivate the protein leading to decreased glycogen content [160].

Cao *et al.* revealed systemic PANDER levels are significantly correlated with increased fasting blood glucose (FBG), triglycerides, and high-density lipoprotein cholesterol in an Asian population (N=212, aged40-65) with varying degrees of glucose intolerance and T2D. Furthermore, logistic regression analysis showed circulating PANDER was associated with increased risk of IGT or T2D following cofounder adjustment. In general, they found that elevated plasma PANDER was significantly associated with numerous metabolic syndrome components, which is certainly consistent with our proteomic investigation and other animal model studies revealing increased lipogenesis or hepatic steatosis during conditions of increased PANDER expression [161]. Further studies are needed and the almost near absence of human clinical and physiological *in-vivo* data presents a major limitation in the understanding of PANDER and etiological role within T2D. However, our proteomic investigation certainly supports the findings of this initial clinical study in that increased PANDER levels are associated with both increased hepatic lipogenesis and its potential consequences in humans such as promoting or initiating T2D or Metabolic Syndrome. Given that LXR is an important gene in the regulation and homeostasis of cholesterol [162], PANDER-induced effects on cholesterol may also be mediated by the LXR pathway. LXR also regulates the transcription of CYP7A1, the rate limiting step of

converting cholesterol to bile acid as to effectively rid the cell of cholesterol [163]. LXR activation also promotes the generation of other lipogenic genes increasing lipid accumulation and fatty acid synthesis. Accompanying this is the evidence of increased triglycerides seen phenotypically in the PANTG mouse in previous studies [19, 21]. Additional studies are needed to precisely address both the molecular mechanism of PANDER-induced lipogenesis and the potential detrimental consequences when circulating levels are increased in humans in terms of the role in both initiation and onset of T2D or hepatic steatosis.

Chapter 4 – Exploring Proteomic Changes in the Fatty Liver

Abstract

Fatty liver disease is a looming problem, especially in the United States where an estimated 30% of obese individuals manifest signs of non-alcoholic fatty liver disease (NAFLD). NAFLD can progress into more sever disease, such as non-alcoholic steatohepatitis (NASH) and cirrhosis, and even provoke hepatic tumorigenesis. In an effort to outline mechanistic features of fatty liver pathophysiology, stable isotope labeling of amino acids in cell culture was used as a quantitative proteomic approach to compare mice on a longitudinal high fat diet (HFD) to those on a normal diet. In all, there were 224, 234, 189, and 179 differentially expressed proteins at the 1, 2, 5, and 9 week time points, respectively. Several of these proteins were predicted to be involved in lipid metabolism, autophagy, and phagocytosis. LXR was identified as a predicted canonical pathway active after two weeks HFD exposure. The suggested biomarker, FABP5, was downregulated ~2 fold in 3 of the 4 proteomic time points. In an effort to outline mechanistic details in parallel to gross metabolic phenotype, glucose intolerance and insulin resistance were measured by GTT and ITT,

respectively, resulting in insignificant results. In all, the dataset provides a general proteomic overview of critical proteins altered due to high fat diet induced liver disease.

Introduction

With the worsening global obesity epidemic, recognition of non-alcoholic fatty liver disease (NAFLD) and its significance in metabolic disease has been increasing in recent years [164]. The prevalence of NAFLD is weakly estimated in the general population ranging from 5 to 30% and in 75% of patients with obesity and T2D [164-166]. Although usually those with NAFLD are obese [167, 168], not all obese individuals develop the disease and the reason why, even when the severity of obesity is the same, is poorly understood [169].

NAFLD is used to describe several liver diseases such as steatosis, and can develop into more sever diseases such as non-alcoholic steatohepatitis (NASH), cirrhosis, and hepatocellular carcinoma [170]. It is generally accepted that once the liver is fatty, it becomes insulin resistant [171, 172], whereby the overproduction of glucose and fatty acids lead to the dangerous combination of hyperglycemia and hypertriglyceridemia [172, 173]. Much is known about the gross metabolic phenotype of obesity and fatty liver disease, but precisely how the liver becomes fatty is weakly understood. Peripheral insulin

resistance has been thought to contribute to the disease by increasing plasma concentrations of glucose and fatty acids, known to promote hepatic fatty acid synthesis while impairing β-oxidation [75, 174]. On the contrary, *Kraegen* et al. reported that the liver in rodents was insulin resistant even before muscle became insulin resistant when on a high fat diet [175]. Taken together, the mechanism by which hepatic fat accumulation occurs and how it leads to hepatic insulin resistance is still undetermined. Regardless, rodents fed a high fat diet, particularly C57/BL6 mice (that can spontaneously develop impaired insulin secretion and glucose intolerance), are prone to global insulin resistance and obesity [176-179], due to a high availability of free fatty acids (FFAs) relative to peripheral requirements. One consequence of elevated FFAs in the serum is decreased β-oxidation in the liver resulting in hepatic triglyceride accumulation [137, 169, 180, 181].

Proteomic analyses offer unparalleled utility when studying the molecular changes of a biological system in a heuristic manner, allowing for the elucidation of underlying mechanisms of disease. The use of proteomics has been employed in a number of ways to investigate fatty liver and hepatitis, identifying protein markers of disease and the effects of diet/obesity and insulin resistance [76, 182-188]. Although the information gained from these studies is valuable, recent technological

advances in mass spectrometry have allowed for improved protein identification and quantification by eliminating issues associated with 2DE coupled with mass spectrometry. Mass spectrometry based proteomics has been on the rise in the study of metabolic disease (see review in Chapter 1), as well as in the study of NAFLD. iTRAQ has been used to identify non-invasive markers of NAFLD [189] and to study the effects of drugs against the disease [190]. Here we used spike-in SILAC in this longitudinal study for the identification of protein profile changes in the liver of C57/BL6 mice on a high fat diet (HFD). Metabolic phenotyping, including glucose and insulin tolerance testing (GTT and ITT, respectively) was performed in order to demonstrate glucose intolerance and insulin resistance due to a high fat diet over the course of nine weeks. High fat fed and control mice were sacrificed to determine hepatic proteomic changes during the time course. This unique experimental design allows for the determination of differentially expressed proteins involved in hepatic insulin signaling and altered mechanisms of lipid and glucose metabolism during global insulin resistance due to a high fat diet.

Materials and Methods

Animals and Diet

Normal, young C57BL/6 mice were obtained from the Jackson Laboratory (Bar Harbor, Maine). The mice were provided food and water *ad libitum* (unless otherwise specified) and at six weeks of age began the nine week trial of either receiving normal chow (NC) or high fat diet (HFD) food. Mice were randomly separated into two major groups, either for metabolic testing or proteomic analysis, and caged individually. Testing was performed at five time points (T0, week 1, 2, 5, and 9) in which mice.

Glucose and Insulin Tolerance Testing

In an effort to test for insulin resistance, the same group of ten mice (5 NC, 5 HFD) was used in both GTTs and ITTs. Prior to each test, mice were fasted for 18 hours. All mice were either dosed dextrose (2g/kg) or insulin (1u/kg, Humulin) by an intraperitoneal (IP) injection for glucose or insulin tolerance testing. Blood glucose levels were recorded using a TrueTrack blood glucose monitor on blood obtained from the tail vein at each time point (T0, 15, 30, 60, 120 minute). Mice were allowed to return to resting metabolic conditions for at least two days between GTT and ITT. Data was recorded and statistical analysis performed (student's two tailed t-test of average values) in GraphPad version 5 and Microsoft Excel.

Proteomic Experimental Design

At each time point, mice (N=3, either normal chow or HFD fed mice) were humanly euthanized and livers snap frozen in liquid nitrogen as previously described and stored at -80°C. All sample preparations for mass spectrometry analysis, including protein extraction, FASP digestion, desalt, SCX chromatography, and LC-MS/MS was performed as previously described (see Chapter 2).

Statistical and Pathway Analysis

Statistical analysis comparing the hepatic proteome between the control and HFD fed mice was performed as previously described (see Chapter 2). Briefly, normalized intensity values selected by a significance outlier test (SigA) were tested for significance using the Welch's 2-tailed t-test. Median ratio values of time-lapse matched mice (i.e. week 2 HFD vs week 2 NC mice) were used for calculated protein fold change (median HFD / median NC) and Uniprot Protein identification numbers of differentially expressed proteins were uploaded to Ingenuity Pathway Analysis (IPA) to determine canonical pathways, networks, and predicted disease states in the liver affected by a high fat diet.

Results

Metabolic Phenotyping

During the first three weeks, mice on a HFD did not display a significant difference in body mass compared to NC control mice (Figure 25). After nine weeks on a high fat diet, the liver of those mice exhibited characteristics of a fatty liver disease; physical increase in size and the appearance of lipid accumulation (Figure 26). Although insignificant, those mice on a HFD trend towards peripheral glucose intolerance during a GTT after 1 week, as made apparent at the 30 minute time point (P=0.08, HFD 502.6±76.1 vs NC 396±94.4) (Figure 27). Peripheral glucose tolerance was unremarkable in mice after two weeks on a HDF (Figure 28).

Mice on a HFD were able to manifest an insulin resistant phenotype as demonstrated by ITT. After injection with a bolus of insulin, mice on the NC diet maintained lower blood glucose levels with significance at the 60 minute time point (P=0.008, HFD 391.7±41.8 vs NC 223.33±20.6) (Figure 29). After two weeks on a HFD, blood glucose levels of the HFD fed mice, in response to a bolus of insulin, was similar to that of the NC control mice (Figure 30).

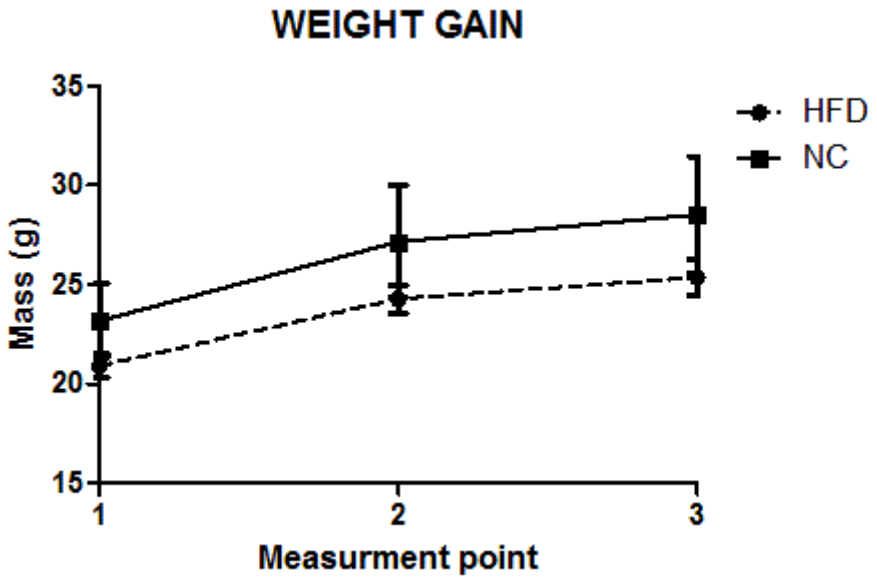

Figure 25: Weight gain of HFD or NC fed mice. Prior to metabolic testing, mice were weighed. Values are expressed as means plus standard deviation (N=10, 5 HFD vs 5 NC fed mice, no significance by student's two-tailed t-test).

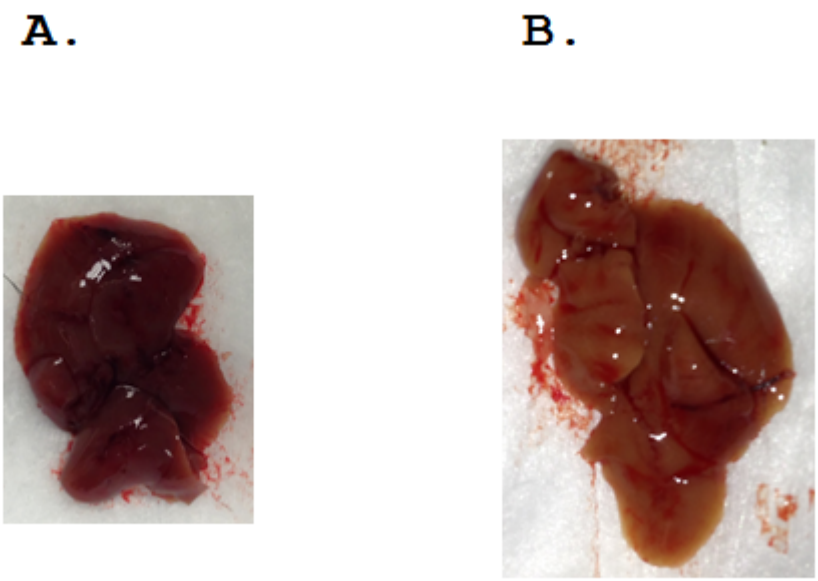

Figure 26: Physical signs of fatty liver. Shown in **A** is a representation of the liver of mice on a NC diet. **B** represents a liver of mice on a HFD, where the physical appearance of increased size (images are to scale) and lipid accumulation is apparent.

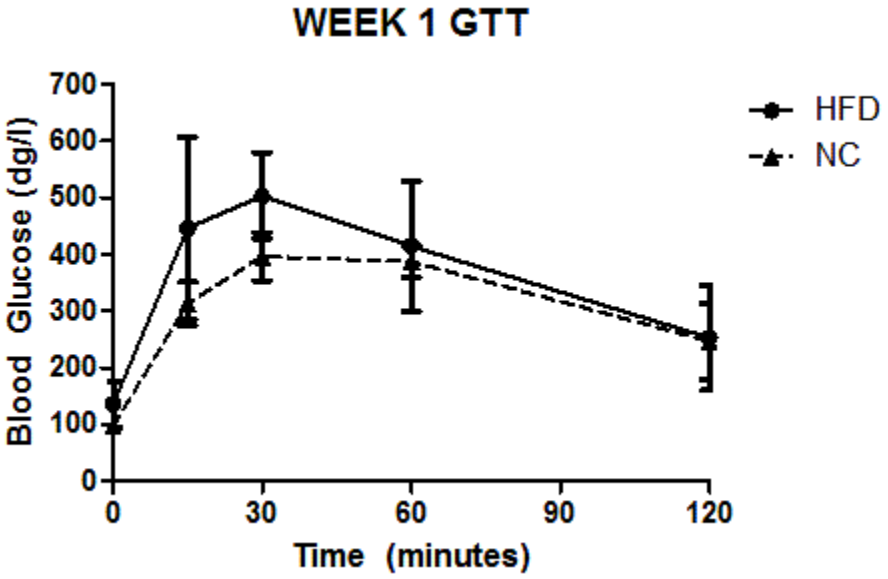

Figure 27: GTT after one week on high fat chow. Glucose tolerance testing was performed after an 18 hour fast followed by IP injection of dextrose at 2g/kg and blood glucose readings measured at the times indicated. Values are expressed as means plus standard deviation. (P=0.08, HFD 502.6±76.1 vs NC 396±94.4 at 30 minutes).

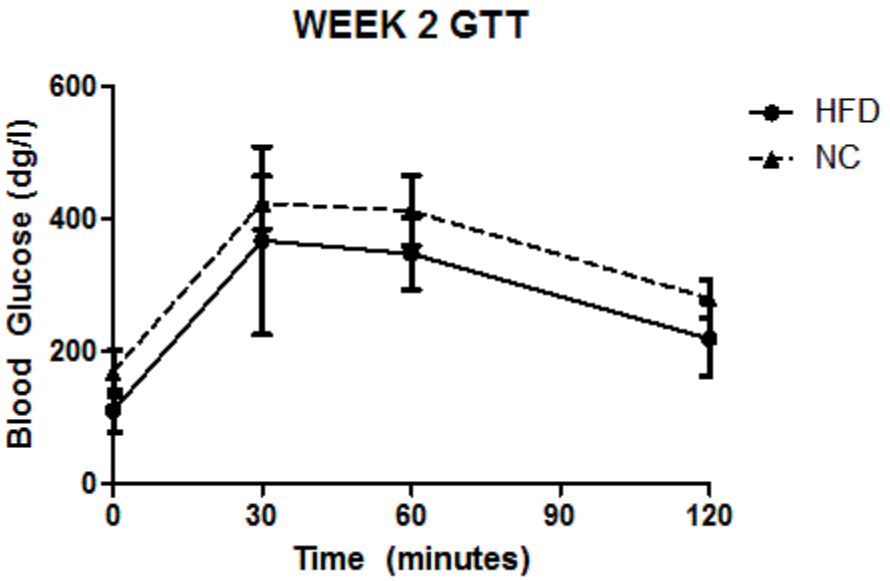

Figure 28: GTT after two weeks on high fat chow. Glucose tolerance testing was performed after an 18 hour fast followed by IP injection of dextrose at 2g/kg and blood glucose readings measured at the times indicated. Values are expressed as means plus standard deviation.

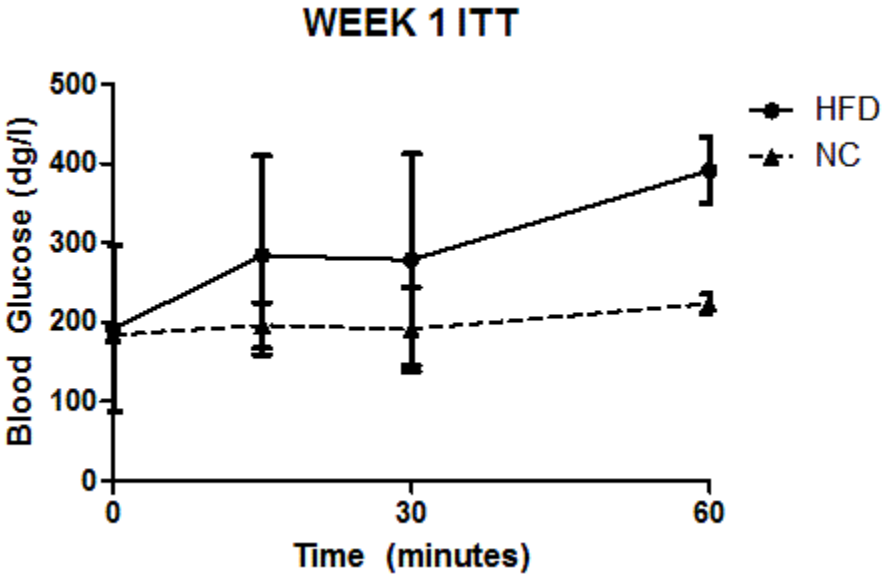

Figure 29: ITT after one week on high fat chow. Insulin tolerance testing was performed after an 18 hour fast followed by IP injection of insulin (Humulin) at 1u/kg and blood glucose readings measured at the times indicated. Values are expressed as means plus standard deviation (P=0.008, HFD 391.7±41.8 vs NC 223.33±20.6 at 60 minutes).

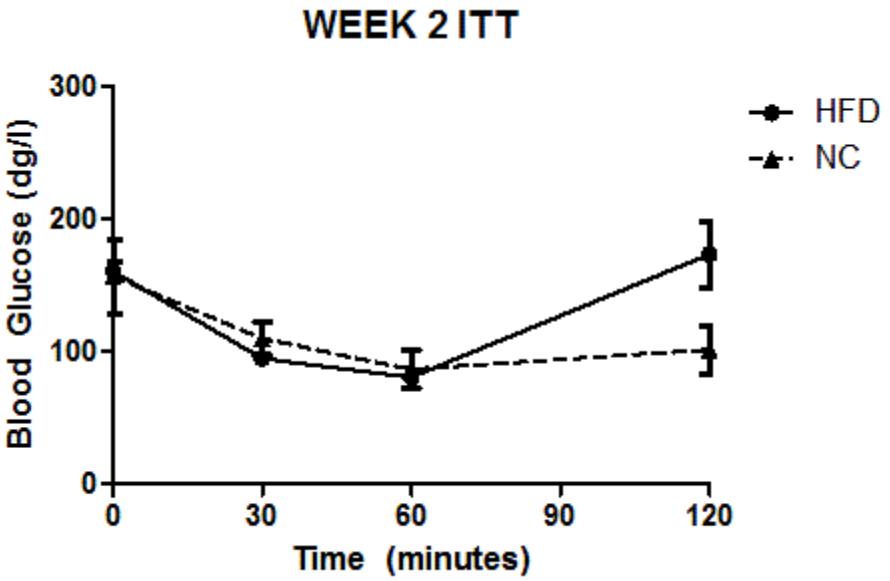

Figure 30: ITT after two weeks on high fat chow. Insulin tolerance testing was performed after an 18 hour fast followed by IP injection of insulin (Humulin) at 1u/kg and blood glucose readings measured at the times indicated. Values are expressed as means plus standard deviation.

Proteomic Characterization of the HFD Liver and Network Analysis

In order to comprehensively dissect the global hepatic proteome changes as a result of longitudinal high fat diet, spike-in SILAC was performed on mice fed a HFD and compared to mice on a normal diet. Diet induced obesity in C57/BL6 mice have demonstrated remarkable ability to act as a model of insulin resistance and fatty liver disease [191]. The quantitative proteomic approach compared mice on a HFD and NC diet over the time-span of 9 weeks at 4 intervals (1, 2, 5, and 9 weeks). Metabolic testing, including GTTs and ITTs were performed in parallel to identify incidence of insulin resistance. Following dietary exposure, livers were extracted and processed by tryptic digestion, desalting, SCX chromatography, and finally analyzed by LC-MS/MS. Across all dietary conditions, there were 18,058 unique peptides correlating to 3,310 quantifiable proteins. Of those, there were 224, 234, 189, and 179 differentially expressed proteins at the 1, 2, 5, and 9 week time points, respectively (listed in Appendix II).

Proteomic Analysis: Effects After 2 Weeks HFD

Proteomic examination of the differentially expressed proteins using IPA revealed the most significant changes existing at the two week time point. Several hepatic cellular functions were altered in HFD fed mice having a predicted activation or inactivation by z-score in IPA (z-score <2 or >2 indicating

activation or inhibition, respectively). Increased functions included engulfment and phagocytosis of cells, autophagy, and quantity of carbohydrate (Figure 30). A major decrease in cell death was predicted with a z-score<-3 (Figure 30). At two weeks, several disease functions were identified to be altered, including damage and necrosis of liver tissue, apoptosis of hepatocytes, and increased indication of NAFLD and hepatic steatosis (Figure 31). The canonical pathway involving the DNA binding protein, LXR, a known modulator of lipid metabolism, is predicted active based on activation z-score (z-score>2.646 P=6.14E6).

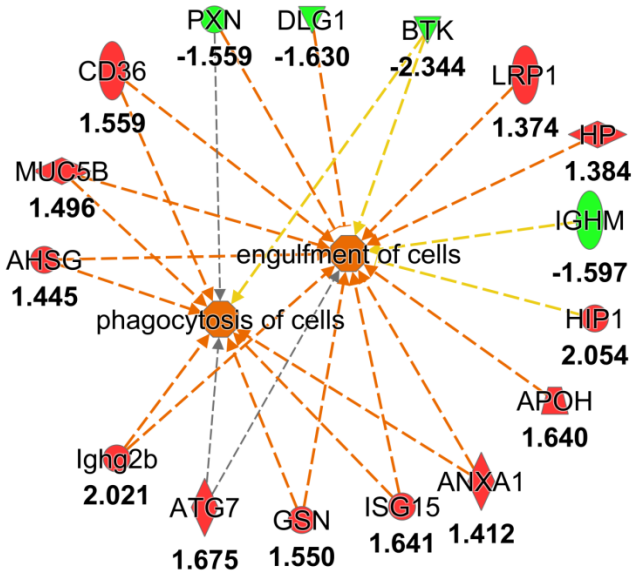

Figure 31: Cellular functions altered after 2 week HFD exposure. Proteins with a positive association with increased phagocytosis of cells and engulfment of cells are shown. Orange dotted lines indicated strong direct association between shown proteins and the predicted activation of phagocytosis of cells and engulfment of cells are shown. The outer nodes represent differentially expressed proteins where red and green represent up and down regulation, respectively.

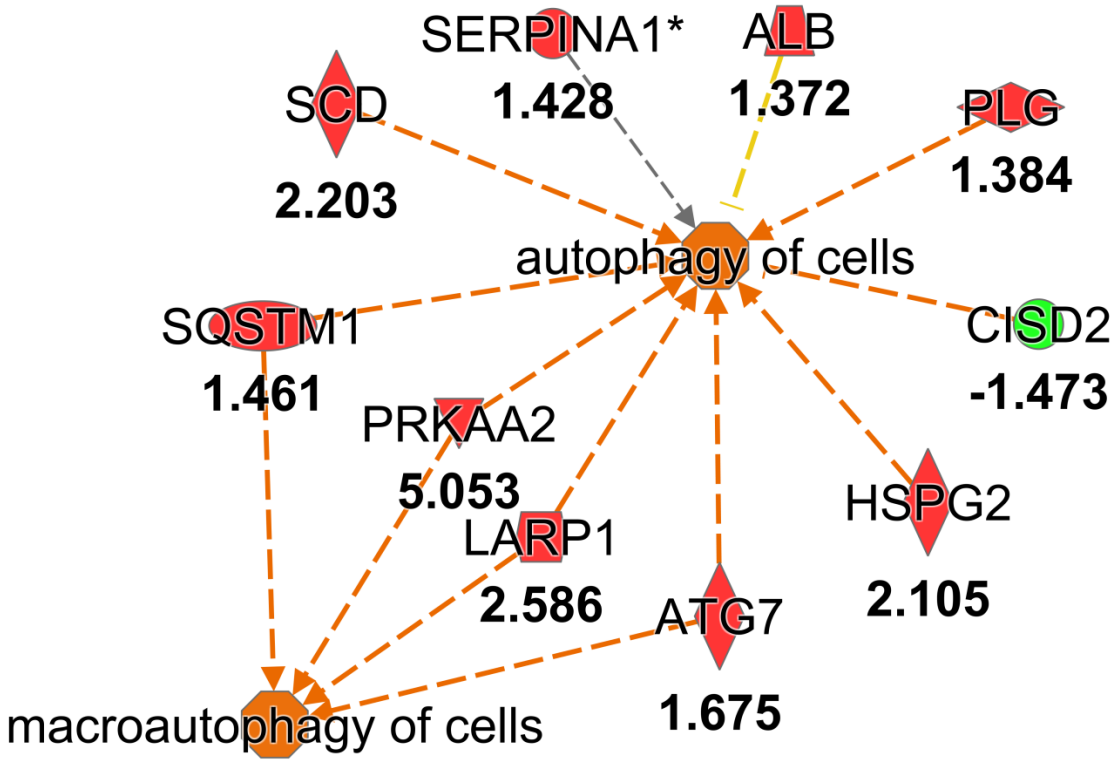

Figure 31: Continued. Proteins with a positive association with increased macroautophagy and autophagy of cells are shown. Orange dotted lines indicated strong direct association between shown proteins and the predicted activation of macroautophagy and autophagy of cells. The outer nodes represent differentially expressed proteins where red and green represent up and down regulation, respectively.

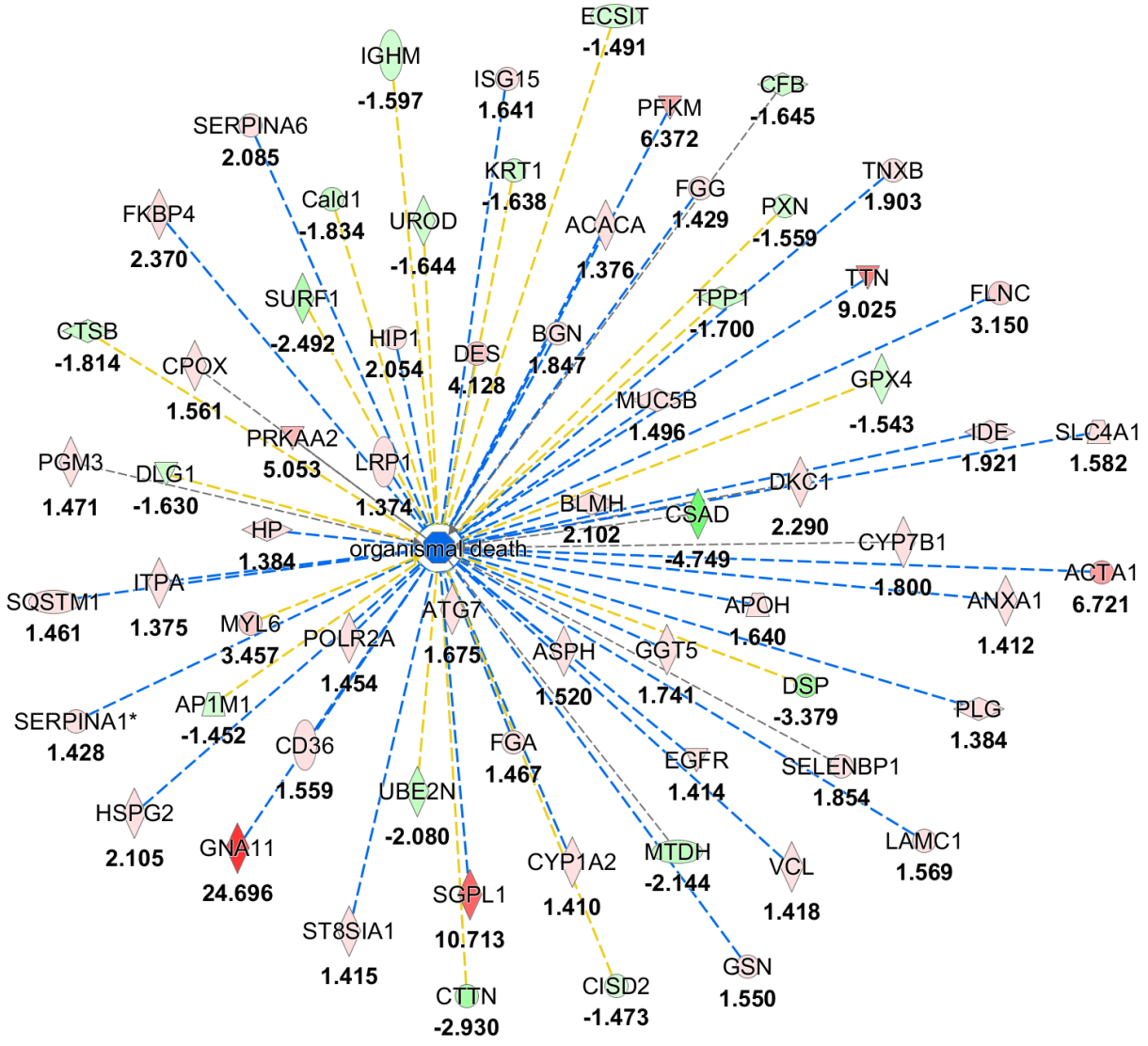

Figure 31: Continued. Proteins with a positive association with increased organism death are shown. Orange dotted lines indicated strong direct association between shown proteins and the predicted activation of organism death. The outer nodes represent differentially expressed proteins where red and green represent up and down regulation, respectively.

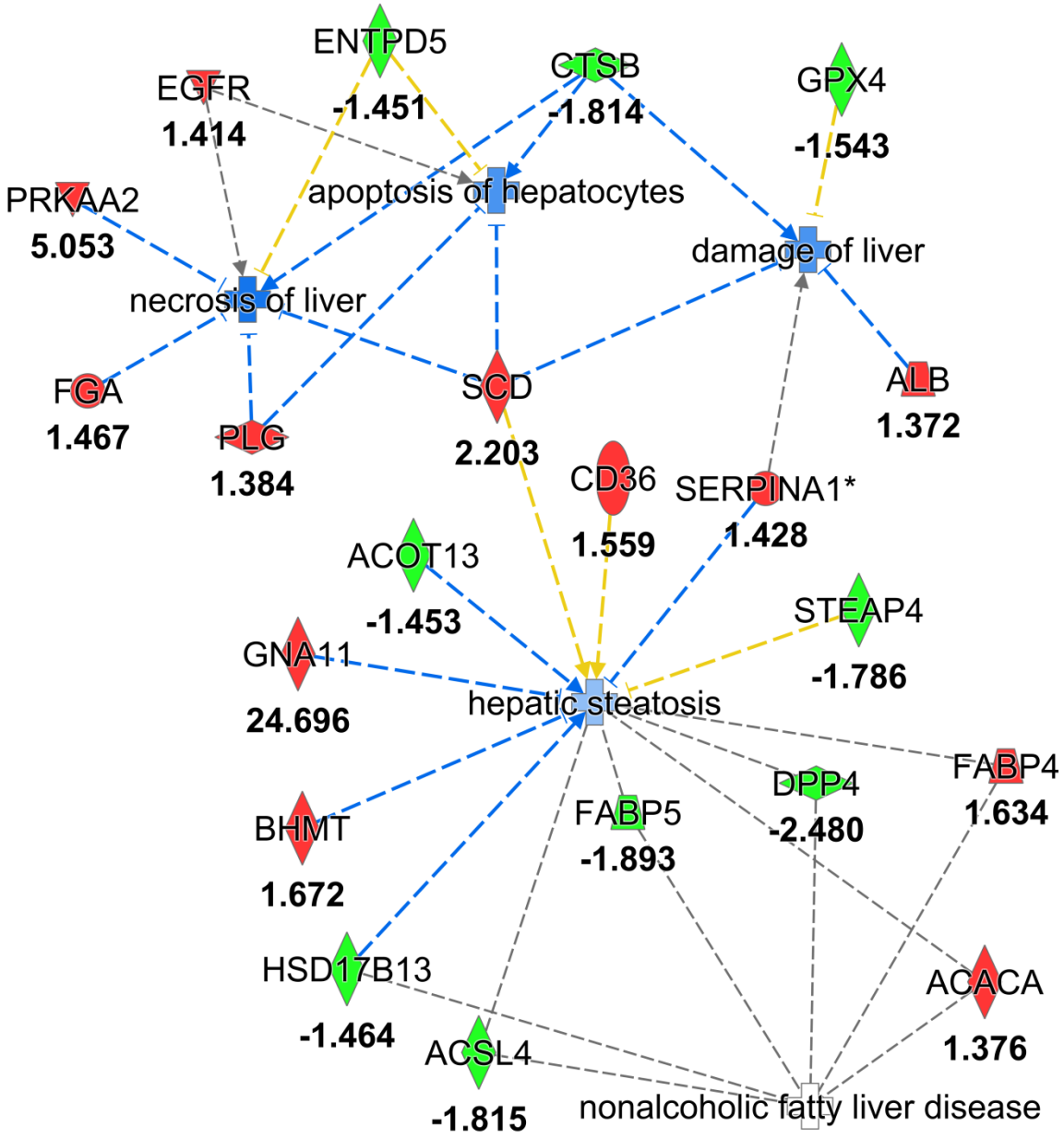

Figure 32: Disease functions altered after 2 weeks HFD. Proteins with an association with necrosis of liver, apoptosis of hepatocytes, damage of liver, and hepatic steatosis are shown. Orange dotted lines indicated strong direct association between shown proteins and the predicted activation of macroautophagy and autophagy of cells. The outer nodes represent differentially expressed proteins where red and green represent up and down regulation, respectively.

Table 6: Proteins modulated by LXR activation after 2 weeks HFD.

Protein Name	Fold Change
acetyl-CoA carboxylase alpha	1.376
alpha 2-HS glycoprotein	1.445
albumin	1.372
apolipoprotein H	1.64
CD36 molecule	1.559
fibrinogen alpha chain	1.467
paraoxonase 3	1.365
stearoyl-CoA desaturase	2.203
serpin family A member 1	1.428

Proteomic Analysis: Effects After 9 Weeks HFD

High fat diet induced insulin resistance is expected to be in full swing after 9 weeks. 5 proteins, including fatty acid amide hydrolase (FAAH), fatty acid synthase (FasN), 1-acly-sn-glycerol-3-phosphate acyltransferase beta (AGPAT), glycerol-3-phosphate acyltransferase 1 (GPAM), and low density lipoprotein receptor (LDLR) were involved in cellular functions related to the metabolism and synthesis of triacylglycerol, as well as the synthesis and deposition of lipids (Figure 32). Perhaps outlining an imperfection of IPA, apparent in the two week analysis, too, is the predicted "protection" of inflammation and necrosis of the liver and hepatic steatosis, when the opposite is beyond doubt the case (Figure 33).

Interestingly, FABP5, a protein known to be involved in NAFLD and thought to perhaps represent a novel biomarker of the disease [192-194], is markedly downregulated (~-2 fold on average) in 3 of the 4 time points (Figure 34).

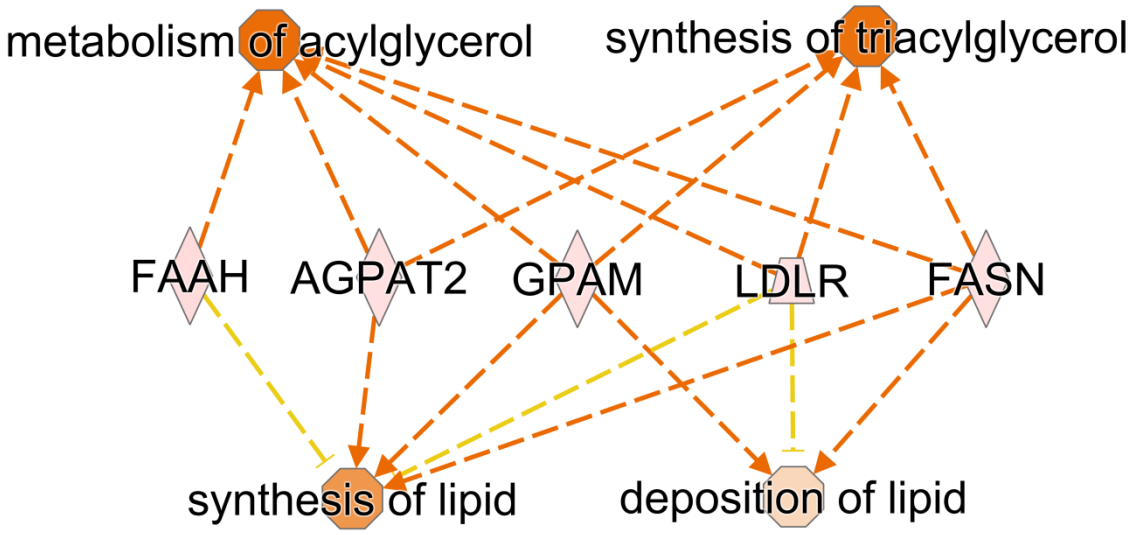

Figure 33: Proteins involved in the synthesis and metabolism of triacylglycerol and lipids after 9 weeks on HFD. Proteins with a positive association with increased metabolism of acylglycerol, synthesis of triacylglycerol, synthesis of lipid, deposition of lipid are shown. Orange dotted lines indicated strong direct association between shown proteins and the predicted activation of aforementioned functions. The outer nodes represent differentially expressed proteins where red and green represent up and down regulation, respectively.

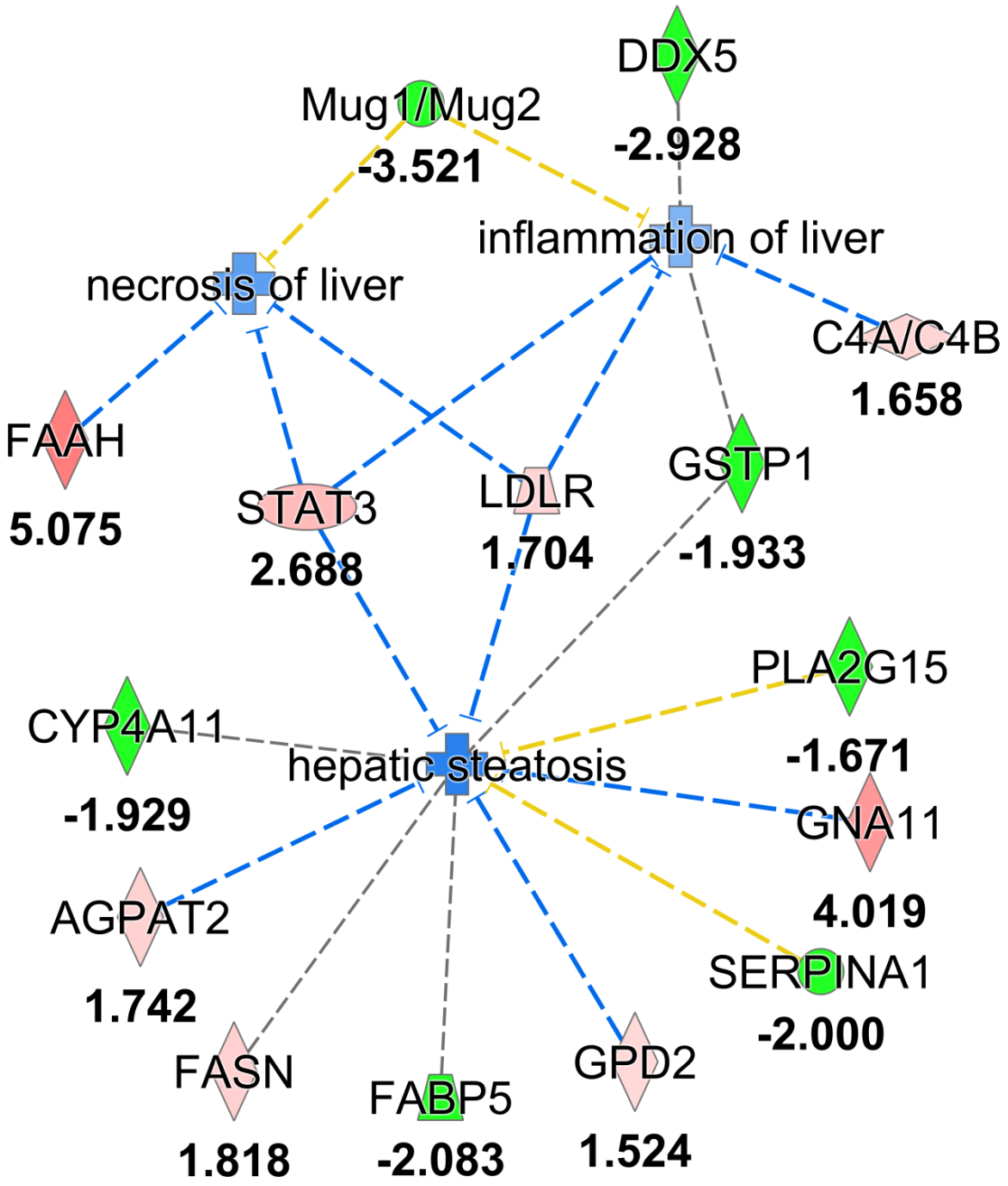

Figure 34: Disease functions altered after 9 weeks HFD. Proteins with an association with necrosis of liver, inflammation of liver, and hepatic steatosis are shown. Orange dotted lines indicated strong direct association between shown proteins and the predicted activation of necrosis of liver, inflammation of liver, and hepatic steatosis. The outer nodes represent differentially expressed proteins where red and green represent up and down regulation, respectively.

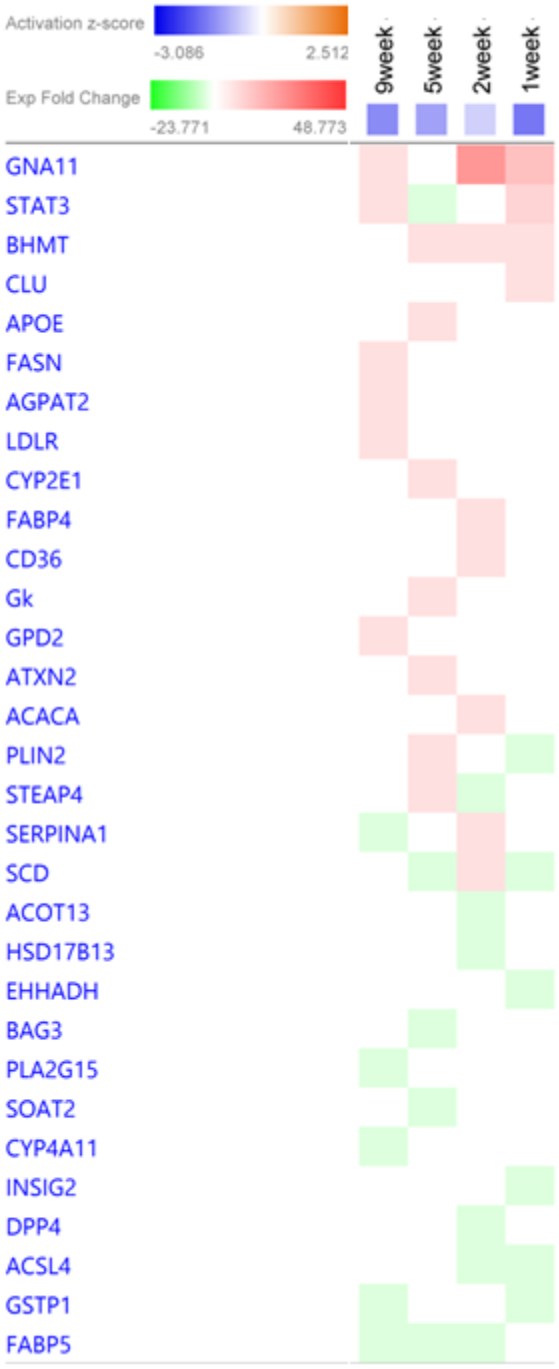

Figure 35: Heat-map of proteins involved in NAFLD. Blue suggested inactivation based on prediction on z-score. Red indicates proteins that are upregulated and green indicating proteins that are down regulated.

Discussion

To the best of my knowledge, this is the first experiment of its kind to employ quantitative mass spectrometry based proteomics in parallel with metabolic testing in an effort to outline mechanistic features of the onset and progression of fatty liver disease. The information gained from this study was not ideal for unraveling or providing major mechanistic insight in the pathogenesis or pathological progression of NAFLD, however did provide a languid proteomic overview of the pathophysiology of fatty liver disease. Regardless, such analyses can certainly provide a strong foundation for the understanding of the disease and the potential for novel drug targets [195-197]. This could be highly useful since the options are limited, medication wise, for the treatment of NAFLD. Most treatment options are insulin sensitizing agents, such as the biguanide metformin and thiozoladinediones (TZDs). Since insulin resistance is commonly associated in patients with NAFLD and is involved in hepatic lipid accumulation [75, 198], insulin sensitizing agents demonstrate better efficacy compared to insulin injections, since hyperinsulinemia is most likely present and increasing insulin action by flooding the system with more insulin becomes redundant [199]. Metformin is an interesting drug being that its mechanism of action is weakly understood [200]. Even still, metformin is considered the "go to" drug for decades now, since

its ability to improves global insulin sensitivity also extends to the benefit of the liver by decreasing hepatic steatosis by downregulating TNFα and lipid associated transcription factors [201]. Activation of PPARγ has been shown to improve insulin sensitivity, and agonist, such as those belonging to the TZD drug class [202], have been demonstrated clinically to protect against liver inflammation and fibrosis by inhibiting activation of hepatic stellate cells [203, 204]. A better understanding of pathways promoting NAFLD could potentially allow for the development of novel therapeutics. An initial hypothesis proposed by Christopher Day and Oliver James proposed the "two-hit" explanation of the pathogenesis of NASH. The accumulation of lipids in the form of triglycerides in the liver is required for the onset of NASH and constitutes the first "hit". Subsequently this would cause injury to the fatty hepatocytes in the form of oxidative stress and would trigger the second "hit", where inflammation and necrosis, the histopathological hallmarks of NASH, become apparent [205, 206]. Decades have passed since this proposal has been made popular and yet the story of how NASH occurs is still not well established. More recent data suggests that the accumulation of triglycerides in the form of lipid droplets does not directly play a role in inflammation and cellular injury [207, 208], but instead lipid peroxidation causing steatohepatitis. A parallel hypothesis is certain

metabolites of fatty acids causing damage to the liver and promoting NASH. Recent data suggests that metabolites of free fatty acids can cause lipotoxic effects in the liver by means of endoplasmic reticulum (ER) stress, inflammation, apoptosis, necrosis, and dysmorphic features including ballooning and Mallory-Denk body formations (aggregates in the cytoplasm of liver cells) [209-213]. Because of this, metabolomics, or the large scale study of biochemical intermediates, may offer unique insight in the pathophysiology of NAFLD and NASH.

To begin the discussion of the proteomic data, proteins that are known to be involved in major pathways implicated in fatty liver disease, such as fatty acid uptake, *de novo* lipogenesis, and fatty acid oxidative pathways, will be analyzed.

FFA absorption into the liver is mediated by plasma membrane transporters, namely fatty acid translocase (FAT or CD36), fatty acid binding proteins (FABPs), and fatty acid transporter proteins (FATP). Although we did not detect levels of FATPs directly, at nine weeks a suggested increase in cellular functions was detected by IPA: metabolism of acylglycerol and synthesis of triacylglycerol mediated by fatty acid amide hydrolase (FAAH) and FasN (see Figure 32). FATBs are known to contain motifs for fatty acyl-CoA synthetase function [214, 215] similar to long-chain fatty acid CoA ligase 4 (Acsl4), shown to

be significantly downregulated at the first two proteomic time points. CD36 is a transmembrane protein that promotes fatty acid uptake [216] and its expression is known to be upregulated in response to diet-induced obesity [217] and was observed by our proteomic approach after two weeks of HFD exposure. FABPs have demonstrated a crucial role regarding intracellular transport of FFAs [218]. In animal models, knocking out FABP1 protects the animal from diet-induced obesity [219]. FAB4 and FAB5 expression has been correlated with hepatic fatty acid uptake in those with NAFLD [192], and could potentially serve as novel biomarkers of disease. The expression patterns of FAPBs are unclear under normal or pathophysiological conditions. Here, FABP4 was down regulated at the two week time point and FABP5 downregulated at the 2^{nd}, 5^{th}, and 9^{th} week proteomic time points.

De novo lipogenesis is characterized by the integration triglyceride synthesis, saturated fatty acid synthesis, and glycolysis. In this proteomic analysis, several key rate limiting enzymes were upregulated in the HFD mice (Figures 33 and 34), including acetyl-CoA carboxylase alpha (ACACA), fatty acid synthase (FasN), and stearoyl-CoA desaturase (SCD), suggesting increased lipogenesis during disease state. ACACA catalyzes the rate limiting step in fatty acid biosynthesis converting acetyl-CoA to malonyl-CoA [220], two metabolites utilized by FasN in the last step of fatty acid biosynthesis

synthesizing long-chain saturated fatty acids [221]. SCD is responsible for the formation of monounsaturated fatty acids from saturated fatty acyl-CoAs [222], and suppression resulted in the amelioration of hepatic steatosis in mice by decreased lipogenesis and increased fatty acid beta oxidation [223]. These molecules share strong implications in the pathophysiology of fatty liver disease as TG synthesis is known to be active during disease conditions [224].

In the proteomic analysis, LXRα was identified as a canonical pathway predicted to be upregulated in IPA after 2 weeks HFD. As discussed previously, LXRα regulate overall glucose, cholesterol, bile acid, and triglyceride homeostasis (Figure 8) [45]. LXRα can directly activate critical genes necessary for hepatic *de novo* lipogenesis which serves as a contributor to triglyceride accumulation in non-alcoholic fatty liver disease (NAFLD) [48, 49] either indirectly by increasing expression of SREBP-1c [50] and ChREBP [51], and directly by promoting transcription of SCD1 [52], FasN [53], and ACC [54].

Recent studies suggest that Kupffer cells (KCs), stellate macrophages in the liver, play an important role in the pathophysiology of NAFLD. It has been characterized that defective phagocytic function may impede the clearance of substances that can lead to the destruction of hepatocytes,

leading to inflammation and hepatic steatosis [225-234]. After a two week HFD exposure, IPA predicted phagocytosis and engulfment of cells as two activated cellular functions in the liver. The literature is sparse on the topic, but KP cell phagocytic ability can be exploited to detect early and late stages of NASH by magnetic resonance imaging [235, 236]. Carbamazepine, an anticonvulsant, has been shown to stimulate autophagic functions, decreasing fibrosis in an animal model [237]. It is unknown whether agents that can enhance autophagic function can induce the removal of hepatic lipids and treat/prevent cellular damage.

Autophagy has recently been characterized as an important function in hepatic lipid metabolism [238] as the lysosome can contain lipases that degrade exogenous lipoproteins and intracellular lipids. This suggests that the regulation of the breakdown of lipids, or lipolysis, is related to macroautophagy [239]. The proteomic evaluation predicted autophagy and macroautophagy as cellular functions upregulated after 2 weeks of HFD exposure (Figure 30), perhaps defining a compensatory function in order to decrease intracellular lipid accumulation.

Liver disease has been directly correlated to hepatocellular carcinoma (HCC) [240]. Once the liver is in crisis due to oxidative stress and cirrhosis, hepatocellular carcinoma is a

common cancer that can develop from cirrhosis [241]. The factors leading to HCC are poorly defined [242]. In terms of autophagy, it may promote cancer cell survival or serve as a tumor suppressor [243], and in HCC impairment is not characterized. After 2 weeks HFD exposure, a major downregulation of organism death was predicted by IPA with a z-score < -3 including 66 proteins (Figure 30). Taken all together, the proteomic data suggests that the liver is in state of distress.

Limitations of this study are most likely related to the uncontrolled metabolic states that the mice were in. As previously mentioned, C57/BL6 mice are known to spontaneously develop impaired insulin signaling and glucose intolerance [176-179]. Additionally, a HFD affects the mice's metabolism dramatically; after a short span of even days, mice can develop insulin resistance in several tissues, including the muscle, adipose, pancreases, and liver [244], making precise measurements at critical instances and occurrences of disease convoluted and difficult. At the time this dissertation was drafted, the approach taken for the comparison effects of a HFD could perhaps be improved on. HFD fed mice were compared to mice on a normal diet that were the same age. Given the physiology of the C57/BL6 mice, the design compared a diseased mouse to a more diseased mouse. To circumvent this, perhaps the median fold change of HFD fed mice to the youngest mice on a NC diet would

provide clearer data, as the younger mouse is less diseased at that point. Another approach is to reduce hepatic lipid accumulation by use of certain drugs. One such drug, 2, 4-dinitrophenol (2,4-DNP), a mitochondrial uncoupler, was used by *Samuel* et al. to increase energy expenditure and prevent hepatic accumulation. HFD fed mice proteomes were then compared to 2,4-DNP treated control mice on a normal diet by 2DE [170]. Nevertheless, the proteomic analysis at hand provides an expansive dataset comprising of hepatic proteins involved in early and late stages of disease due to dietary induced metabolic disease. Additionally, the study at hand demonstrates the utility of mass spectrometry based proteomics in elucidating important molecular characteristics of disease.

Chapter 5 – Conclusions and Future Directions

Overview and Summary of Major Findings

Metabolic disease and type 2 diabetes are characterized by insulin resistance and generally glucose intolerance, resulting in the overall conditions of hyperglycemia, hyperinsulinemia, and hyperlipidemia [68]. In this dissertation, quantitative mass spectrometry based proteomics was used as a heuristic tool for the discovery of disease mechanisms driving these conditions in two proven animal models representing insulin resistance.

Hepatic Proteome Characterization of the PANTG Mouse

Inflammatory cytokines and similar signaling molecules have long been implicated in the onset and progression of T2D [245]. Pancreatic-derived factor is one such protein that elicits a pleiotropic affect promoting the pathophysiological conditions of T2D, such as promoting ß-cell destruction and impacting hepatic insulin signaling. The major focus of this dissertation was to analyze the hepatic proteome changes under elevated circulating levels of PANDER in the PANTG mouse model under controlled metabolic states. The spike-in SILAC method was able to produce a dataset of over 3,000 quantifiable proteins and

revealed that increased endocrine signaling of PANDER from the pancreases acts on the liver to promote hepatic lipogenesis (Tables 1, 2, and 3). Most marked differences were seen in the insulin stimulatory conditions, where important molecules involved in lipid biogenesis, such as ACC, FasN, SCD1, and CD36, were significantly upregulated (Figure 15). Additionally, IPA analysis revealed several cellular functions pertaining to lipid metabolism to be significantly up-regulated by predicted z-score activation, including fatty-acid metabolism, conversion of fatty acid, concentration of acylglycerol, concentration of triacylglycerol, concentration of fatty acid, concentration of lipid, oxidation of lipids, and concentration of cholesterol (Table 4). Also revealed by IPA analysis was the predicted canonical pathway activation of the liver X receptor (LXR). LXR is responsible for the expression of several genes related to lipid metabolism, and many of them were identified to be upregulated in the PANTG mice (Figure 15). In addition to lipogenic genes modulated by LXR, Cyp7A1, an important transport molecule for the export of cholesterol as bile acid, displayed increased expression in the PANTG mouse liver. FasN and Cyp7A1 were used as targets for validation by Western blotting (Figure 16). In relation to the known phenotype of the PANTG mouse, whereby increased circulating levels of PANDER seems to promote a selective hepatic insulin resistant state [21, 138], the study

at hand shed light on specific proteins and biochemical pathways driving it, providing valuable information for the elucidation of the mechanisms driving PANDER induced disease.

Pander Affects LXR Promoter Activity

In addition to lipogenic protein targets and suggested LXR canonical pathway activation by IPA, LXRα expression was up-regulated in the PANTG mouse liver during the insulin stimulated condition as shown by Western blotting, demonstrating its self-promoting regulation. To characterize this interesting finding further, luciferase assays using LXR signaling constructs were used to investigate PANDER induced LXR activation. In BNL-CL2 cells, a mouse liver cell line, exogenous PANDER treatment increased LXR promoter activity in a dose-wise dependent manner (Figure 17). The effects of the potent non-steroidal agonist and antagonist, T090137 and GSK 2033, respectively, were used as positive and negative controls for LXR promoter activity. In addition, the synergistic effects of the compounds were investigated by dually treating cells *in vitro* with various concentrations of exogenous PANDER. Initially this was carried out in the BNL-CL2 cell line, but due to technical limitations, a cell line that displayed higher transfection efficiency, 1.1B4 cells (fusion between human islet cells and PANC-1 cells), was used. In this model, LXR promoter activity was increased in response to exogenous PANDER treatment in a dose-dependent

manner (Figure 18 and 20). Although the agonist and antagonist affected LXR promoter activity as expected, a marked synergistic affect was observed when 1.1B4 cells were dually treated with PANDER and the drugs. PANDER treatment increased LXR promoter expression 1.3 fold in 1.1B4 cells when also treated with the agonist T0901317, suggesting that PANDER directly or indirectly increases LXR promoter activity (Figure 20 and 22). GSK 2033 markedly lowered LXR promoter activity by 70% in 1.1B4 cells (Figure 22 and 24), however dual PANDER treatment, although slight, attenuated the effects of the antagonist 1.2 fold (Figure 23).

Hepatic Phosphoproteome Analysis of the PANTG Mouse Liver

Phosphoproteomic analysis allows for the unique large-scale observation of the assemblage of phosphorylated proteins. Protein phosphorylation is a reversible post-translational modification and is and is thought of as a molecular switch; these "switching" events are critical in several intercellular signaling pathways. Having the ability to observe whole systems and their relative phosphorylation state can provide even more in-depth knowledge of intercellular biochemical pathways altered by disease. This is because several protein pathways rely on changes in phosphorylation state, not exclusively changes in protein expression. Cellular events triggered by insulin signaling, by way of interaction with membrane proteins, are

almost entirely reliant on changes in phosphorylation state [246]. Because PANDER displays a profound pleiotropic effect due to altered hepatic insulin signaling, a phosphoproteomic analysis would allow for an enhance understanding of mechanistic abnormalities due to increased circulating levels of PANDER. In the PANTG mouse, hepatic glycogen content is markedly reduced compared to wild-type mice [21]. In another animal model, acute hepatic overexpression of PANDER elevated the gluconeogenic genes PEPCK and G6Pase in the liver due to increased phosphorylated cAMP-binding protein levels. Here, SILAC spiked-in protein lysate from the same mice used for the proteomic analysis was enriched for phosphoproteins using a titanium-based nanopolymer in combination with SCX chromatography. The enriched phosphoproteome was analyzed by LC-MS/MS for the identification and relative quantitation of phosphorylated peptides. 1,157 phosphorylated peptides were identified using this method. However, due to technical limitations, many were not quantifiable, and will be discussed shortly. Of the quantifiable proteins, only 20 were considered statistically significant. The most notable protein was the increased phosphorylation of glycogen synthase (Table 5, Figure 24). Although the information about the particular phosphosites (Ser627 on glycogen synthase) it is hypothesized to be active. Phosphorylation of glycogen synthase inactivates the proteins anabolic ability to synthesize

glycogen. Further evidence to support elevated phosphorylation of GSK was the observation of glycogen phosphorylase kinase (PHK) being increased 1.84 as well as glycogen phosphorylase increased 18.5 fold in the PANTG liver during insulin stimulation. Both of these molecules are responsible for promoting the phosphorylation state of GSK. Taken together, combining the proteomic and phosphoproteomic analysis revealed a functional pathway driving the decrease of glycogen content seen in the PANTG liver and provided evidence of a novel active phosphorylation site on glycogen synthase

LIMITATIONS OF THE STUDY

The expected cause of the low number of quantifiable phosphopeptides during this experiment was due to the fact that the SILAC labeled mouse liver used for spike-in only produces peptides labeled with the heavy lysine isotope; even though arginine is considered an essential amino acid, the mouse is able to produce it on its own [247], hence why only lysine is used for metabolic labeling in the animal. Digestion with trypsin and LysC produce peptides terminated on the carboxyl end with both lysine and arginine, convoluting the mixture with peptides that cannot be relatively quantified. In the proteomic study, this was not an issue because the magnitude of proteins that can be confidently identified and quantified by using heavy labeled mouse lysate is much higher, simply because compared to

the available peptides post phospho-enrichment are much lower. On the contrary, the amount of protein needed suitable for phosphoproteomic analysis is high; in the case of this experiment, 1.2 mg of protein (spike-in + lysate) was used for phosphoproteome analysis as compared to 0.4 mg (spike-in + lysate) for the proteome analysis of the PANTG mouse. Achieving this amount of protein by tissue procurement can be challenging; combined with the high cost of isotopes used in the culture media makes typical phosphoproteomic analyses costly and difficult. Albeit the price of SILAC labeled mouse livers are high, the protein yield obtainable from these tissues decreases experimental error and heterogeneity between individual protein lysate samples compared to lysates obtained from tissue procurement. A potential renovation to circumvent this problem could be combining tissue lysate from heavy arginine labeled tissue from procurement with heavy lysine labeled tissue from mice. Theoretically, the method would work, as one would want the spike-in lysate to be as complex as possible; as in having a high degree of peptide overlap with the lysate under investigation. SILAC relies on relative peptide abundance for quantitation; therefore large differences in peptide abundance would not hinder the comparison as long as peptide abundance exists in a measurable amount.

Metabolic and Proteomic Evaluation of High Fat Diet Fed Mice

High fat diet induced insulin resistance and fatty liver are well characterized abnormalities in mice. In this study, gross metabolic phenotyping was performed in an effort to outline critical instances of fatty liver onset in parallel to hepatic proteomic analysis for the identification of key proteins involved in non-alcoholic fatty liver disease. Unfortunately, due to a low N size and technical limitations, the metabolic studies were terminated pre-maturely and the data acquired from them was largely insignificant. However, several studies have previously outlined the toxic effect a high fat diet has on the murine liver. The major goal and focus of this study was to identify differentially expressed proteins to characterize early and late stages of disease onset by means of SILAC based proteomics, an experimental approach non-existent in the literature. In all, out of 18,058 peptides correlating to 3,310 quantifiable proteins, 224, 234, 189, and 179 differentially expressed proteins where characterized in the HFD mouse liver as compared to their respective control (Appendix II). The data suggest that lipid metabolism, including free fatty acid absorption and *de novo* lipogenesis is highly altered at the two week time-point; LXR activation was a predicted canonical function by use of IPA. The predicted activation of LXR was due to increased expression of CD36, SCD, and FasN (FasN at the 9

week time-point) (Table 6). Fatty acid binding proteins 4 and 5 were downregulated in the HFD mouse (Figure 34). FABPs have been suggested as novel biomarkers of NAFLD progression, and their expression during the diseased state is poorly characterized. Here, FABP5 demonstrated marked downregulation at the 2, 5, and 9 week time-points (~-2 fold). This data suggests that downregulation of certain FABPs can be used to predict NAFLD and similar disease's progression. Autophagic cellular functions were predicted to be active in the HFD liver, suggesting an important role in lipid metabolism. Recent studies have shown that lysosomes contain lipases for the degradation of excess intercellular lipid content and relates lipolysis and macroautophagy [238]. Here, it is suggested that macroautophagy is a critical cellular function for lipid homeostasis (Figures 32 and 33). Autophagy has also been implicated in hepatocellular carcinoma (HCC), but its role is poorly defined [243].

LIMITATIONS OF THE STUDY

For the metabolic assays, simply increasing the N size and performing the analysis over a longer time-span would undoubtedly produce significant results. As previously mentioned, it is well accepted that glucose intolerance develops rapidly in mice on a high fat diet. Tissue sections from the HFD mouse liver can be compared to those mice on a normal diet, most likely displaying increased lipid accumulation.

As for the proteomic analysis, there were several limitations. With so much data, analyzing it can become extremely challenging, especially when time-point analyses are accounted for. Less time points and shorter time in between them could give rise to clearer global hepatic proteomic changes. The comparison strategy could be optimized; as previously discussed, the low confidence when discerning proteomic differences between the NC fed mice from their matched HFD fed mice was due to the ability of C57/BL6 mice to develop metabolic syndrome spontaneously. The analysis could be performed again, this time comparing the HFD time points to a single group of NC fed mice. Additionally, the use of 2, 4-DNP could further reduce the onset of spontaneous disease in the black mouse.

Certainly hepatic steatosis and other related inflammatory disease are expected to be increased in HFD fed mice, however IPA predicted the opposite. Here, it is difficult to tell where lays the issue. Certain predictions made by IPA are based on limited information, sometimes backed by a single experiment reporting changes in mRNA expression instead of actual protein expression; therefore one must be cautious when using IPA to draw relevant conclusions. Contrary, perhaps more suitable controls could circumvent this problem, as well.

Future Directions

In this dissertation, the major studies were focused on the proteomic characterization of the PANDER transgenic mouse liver. Due to the pleiotropic nature of the molecule, the PANTG mouse is a unique model due to its inherent ability to simulate selective hepatic insulin resistance, a poorly understood metabolic phenomenon. The proteomic dataset obtained during this investigation shed light on key features driving lipogenesis in the PANTG liver; yet there is still a wealth of information to be analyzed within it. This information could be valuable for the future research of pancreatic derived-factor, as there are many facets to the PANDER story still undetermined. The major studies also demonstrated the strong utility of the use of proteomics in the field of endocrinology, as displayed in the high fat diet induced fatty liver analysis.

Unexplored Information In The PANTG Proteomic Dataset

The overall phenotype of the PANTG mouse led to focused and logical attention on proteins involved in lipid metabolism. Regardless of such molecules being identified as the most profound metabolic targets, the proteomic dataset also contains information regarding the transport of cholesterol and various other molecules, a topic so far only under brief investigation. Several differentially expressed proteins included those in the ATP-binding cassette (ABC) transporter families. These molecules

are responsible for transporting several small biological molecules, namely cholesterols, across cell membranes [248]. Closely related to these transport molecules were the identification of several proteins in the incredibly diverse cytochrome p450 (CYPs) super-family. CYPs in general are involved in enzymatic reactions and their levels of expression can have considerably metabolic consequences [249]. In our study one such molecule, Cyp7A1, was of focus due to its important role in bile acid synthesis [250]. There are several other important CYP proteins differentially expressed under the various metabolic conditions which could potentially hold information relating to the hepatic metabolome, a topic that will be disused in greater length shortly. A hypothesis could be drawn from this information alone relating the influx or creation of oxysterols necessary for LXR activation. Apart from these metabolic proteins, the focus of the dataset presented in this thesis was a figurative handful of molecules, not a reason for scientific discontent. As with any –omic study, researchers are using the technique to a fraction of its potential; the field is still in its infancy. Put simply, more information is obtained than one research knows what to do with. Here, the dataset can serve as a bench mark for decades of PANDER research if one was so inclined.

Improvement of the Experimental Design

Technology

Technology is something that is ever improving, and that extends to mass spectrometry. During the course of this investigation, there have been several recent developments in mass analyzers. Not long after the dataset was acquired using an Orbitrap XL, the core facility which housed the instrumentation for this study obtained the more recent Q Exactive. This mass analyzer features a hybrid quadrupole-orbitrap allowing for much higher resolution when compared to the Orbitrap XL, increasing the potential for more protein IDs and more sensitive quantitative analysis. Improvements have not only been made for mass spectrometers, but also during the separation of the sample during high-performance liquid chromatography. Temperature enclosed housing of the RP column inline to mass spectrometry greatly increases the reproducibility of respective retention times between HPLC runs, another technology obtained, unfortunately, too late. An interesting direction the PANTG proteomic experiment could take is simply repeating it this enhanced technology, producing a refined dataset.

Creating a Better Mouse

Performing a backcross of the PANTG mouse onto a strain with pure genetics, such as the C57/BL6 mouse, would produce a mouse

with less genetic variability. This would undoubtedly translate to an enhanced phenotype as it did for the PANDER knockout (PANKO) mouse [18, 20]. Phenotypic analysis, including hyperinsulinemic-euglycemic clamp assays, glucose tolerance testing, fasting glycemia, and insulin tolerance testing could be performed, as well as measurements of important dietary hormones, or metabolic biomolecules such as hepatic glycogen and lipid content. Such an animal model would most likely decrease proteome variability between individual experimental groups, allowing for a higher number of confident quantifiable proteins.

METABOLOMICS

The study or large scale analysis of biological intermediates, metabolites, in a biological system is referred to as metabolomics. This research field allows for the indirect view of cellular function, allowing for a unique and informative look into functional genomics by determining phenotypes caused by differences in gene expression. The metabolome has more traditionally been analyzed using nuclear magnetic resonance (NMR) spectroscopy [251, 252], however mass spectrometry has entered the field, offering more robust capabilities [253]. Metabolomics offers, reasonably, enhance insight into T2D research, due to the ability to detect long and short term physiological changes by more stable patterns of metabolite expression, as well as a tool for biomarker discovery [254].

Proteomic Evaluation of Other Tissues in the PANTG Mouse

Much of the focus regarding PANDER's biological role has been in the pancreas. Various models have demonstrated the ability for PANDER to induce β-cell destruction via apoptosis, impaired insulin secretion, and impaired response to insulin stimulating secretagogues (see Chapter 1). Evaluating functional changes in these models using proteomics could offer insight into mechanisms driving the PANDER induced physiological response.

Proteomic Evaluation of the PANKO Mouse

A logical next step for the heuristic elucidation of mechanisms altered due to PANDER signaling would be the proteomic evaluation of the PANKO mouse liver. This analysis would have a multifaceted function. One would be to further detail mechanistic changes due to circulating PANDER levels, as the PANKO model displays protective traits in relation to glucose homeostasis and insulin sensitivity [20]. Another would be the ability to compare proteomic datasets for the determination of synergistic or deleterious effects of PANDER singling.

Pander as a Therapeutic Target For T2D

Type 2 diabetes is characterized by the metabolic triad of hyperglycemia, hyperinsulinemia, and hypertriglyceridemia. Patients with T2D do have higher circulating levels of PANDER, suggesting the possibility of PANDER serving as a potential

therapeutic target for the treatment of the disease. One study showed that siRNA mediated PANDER knockdown ameliorating hepatic steatosis, fasting hyperglycemia, and insulin resistance [255]. This finding suggests that a specific PANDER antagonist could be developed thereby decreasing hepatic glucose production and importing insulin sensitivity in those with T2D.

References

1. Zhu, Y., et al., *Cloning, expression, and initial characterization of a novel cytokine-like gene family.* Genomics, 2002. **80**(2): p. 144-50.
2. Abdel-Meguid, S.S., et al., *Three-dimensional structure of a genetically engineered variant of porcine growth hormone.* Proceedings of the National Academy of Sciences, 1987. **84**(18): p. 6434-6437.
3. Burkhardt, B.R., et al., *Tissue-specific and glucose-responsive expression of the pancreatic derived factor (PANDER) promoter.* Biochim Biophys Acta, 2005. **1730**(3): p. 215-25.
4. Xu, W., et al., *Interferon-gamma-induced regulation of the pancreatic derived cytokine FAM3B in islets and insulin-secreting betatc3 cells.* Mol Cell Endocrinol, 2005. **240**(1-2): p. 74-81.
5. Ratliff, W.A., et al., *Hepatic nutrient and hormonal regulation of the pancreatic-derived factor (PANDER) promoter.* Molecular and Cellular Endocrinology, 2015. **413**: p. 101-112.
6. Burkhardt, B.R., et al., *PDX-1 interaction and regulation of the Pancreatic Derived Factor (PANDER, FAM3B) promoter.* Biochim Biophys Acta, 2008. **1779**(10): p. 645-51.
7. Cao, X., et al., *Pancreatic-derived factor (FAM3B), a novel islet cytokine, induces apoptosis of insulin-secreting beta-cells.* Diabetes, 2003. **52**(9): p. 2296-303.
8. Johansson, P., et al., *FAM3B PANDER and FAM3C ILEI represent a distinct class of signaling molecules with a non-cytokine-like fold.* Structure, 2013. **21**(2): p. 306-13.
9. Cao, X., et al., *Effects of overexpression of pancreatic derived factor (FAM3B) in isolated mouse islets and insulin-secreting betatc3 cells.* Am J Physiol Endocrinol Metab, 2005. **289**(4): p. E543-50.
10. Yang, J., et al., *Mechanisms of glucose-induced secretion of pancreatic-derived factor (PANDER or FAM3B) in pancreatic beta-cells.* Diabetes, 2005. **54**(11): p. 3217-28.
11. Burkhardt, B.R., et al., *PANDER-induced cell-death genetic networks in islets reveal central role for caspase-3 and cyclin-dependent kinase inhibitor 1A (p21).* Gene, 2006. **369**: p. 134-41.

12. Detjen, K.M., et al., *Downregulation of p21waf/cip-1 mediates apoptosis of human hepatocellular carcinoma cells in response to interferon-γ.* Experimental Cell Research, 2003. **282**(2): p. 78-89.
13. Liadis, N., et al., *Caspase-3-Dependent β-Cell Apoptosis in the Initiation of Autoimmune Diabetes Mellitus.* Molecular and Cellular Biology, 2005. **25**(9): p. 3620-3629.
14. Jin, Y.H., et al., *Caspase 3-mediated Cleavage of p21 WAF1/CIP1 Associated with the Cyclin A-Cyclin-dependent Kinase 2 Complex Is a Prerequisite for Apoptosis in SK-HEP-1 Cells.* Journal of Biological Chemistry, 2000. **275**(39): p. 30256-30263.
15. Wang, O., et al., *Mechanisms of glucose-induced expression of pancreatic-derived factor in pancreatic beta-cells.* Endocrinology, 2008. **149**(2): p. 672-80.
16. Yang, J., et al., *PANDER binds to the liver cell membrane and inhibits insulin signaling in hepg2 cells.* FEBS Lett, 2009. **583**(18): p. 3009-15.
17. Wilson, C.G., et al., *Liver-specific overexpression of pancreatic-derived factor (PANDER) induces fasting hyperglycemia in mice.* Endocrinology, 2010. **151**(11): p. 5174-84.
18. Robert-Cooperman, C.E., et al., *Targeted disruption of pancreatic-derived factor (PANDER, FAM3B) impairs pancreatic beta-cell function.* Diabetes, 2010. **59**(9): p. 2209-18.
19. Li, J., et al., *Pancreatic-derived factor promotes lipogenesis in the mouse liver: role of the Forkhead box 1 signaling pathway.* Hepatology, 2011. **53**(6): p. 1906-16.
20. Moak, S.L., et al., *Enhanced glucose tolerance in pancreatic-derived factor (PANDER) knockout C57BL/6 mice.* Dis Model Mech, 2014. **7**(11): p. 1307-15.
21. Robert-Cooperman, C.E., et al., *PANDER transgenic mice display fasting hyperglycemia and hepatic insulin resistance.* J Endocrinol, 2014. **220**(3): p. 219-31.
22. Athanason, M.G., et al., *Quantitative proteomic profiling reveals hepatic lipogenesis and liver X receptor activation in the PANDER transgenic model.* Mol Cell Endocrinol, 2016. **436**: p. 41-49.
23. Saad, M.J., et al., *Regulation of insulin receptor substrate-1 in liver and muscle of animal models of insulin resistance.* J Clin Invest, 1992. **90**(5): p. 1839-49.
24. Kerouz, N.J., et al., *Differential regulation of insulin receptor substrates-1 and -2 (IRS-1 and IRS-2) and phosphatidylinositol 3-kinase isoforms in liver and muscle of the obese diabetic (ob/ob) mouse.* J Clin Invest, 1997. **100**(12): p. 3164-72.

25. Taniguchi, C.M., B. Emanuelli, and C.R. Kahn, *Critical nodes in signalling pathways: insights into insulin action.* Nat Rev Mol Cell Biol, 2006. **7**(2): p. 85-96.
26. O'Brien, R.M. and D.K. Granner, *Regulation of gene expression by insulin.* Physiol Rev, 1996. **76**(4): p. 1109-61.
27. Krüger, M., et al., *Dissection of the insulin signaling pathway via quantitative phosphoproteomics.* Proceedings of the National Academy of Sciences, 2008. **105**(7): p. 2451-2456.
28. Kruger, M., et al., *SILAC mouse for quantitative proteomics uncovers kindlin-3 as an essential factor for red blood cell function.* Cell, 2008. **134**(2): p. 353-64.
29. Kruger, M., et al., *Dissection of the insulin signaling pathway via quantitative phosphoproteomics.* Proc Natl Acad Sci U S A, 2008. **105**(7): p. 2451-6.
30. Monetti, M., et al., *Large-scale phosphosite quantification in tissues by a spike-in SILAC method.* Nat Methods, 2011. **8**(8): p. 655-8.
31. Krämer, A., et al., *Causal Analysis Approaches in Ingenuity Pathway Analysis (IPA).* Bioinformatics, 2013.
32. Ning, J., et al., *Insulin and insulin signaling play a critical role in fat induction of insulin resistance in mouse.* Am J Physiol Endocrinol Metab, 2011. **301**(2): p. E391-401.
33. Amigo, L., et al., *Hepatic overexpression of sterol carrier protein-2 inhibits VLDL production and reciprocally enhances biliary lipid secretion.* J Lipid Res, 2003. **44**(2): p. 399-407.
34. Hanson, R.W. and L. Reshef, *Regulation of phosphoenolpyruvate carboxykinase (GTP) gene expression.* Annu Rev Biochem, 1997. **66**: p. 581-611.
35. Athanason, M.G., Stevens, S. M., Burkhardt, B.R., *Hepatic SILAC Proteomic Data from PANDER Transgenic Model* Data in Brief, 2016. ***Submitted***.
36. Robert-Cooperman, C.E., et al., *PANDER transgenic mice display fasting hyperglycemia and hepatic insulin resistance.* Journal of Endocrinology, 2014. **220**(3): p. 219-231.
37. Edwards, P.A., M.A. Kennedy, and P.A. Mak, *lxrs; oxysterol-activated nuclear receptors that regulate genes controlling lipid homeostasis.* Vascul Pharmacol, 2002. **38**(4): p. 249-56.
38. Steffensen, K.R. and J.A. Gustafsson, *Putative metabolic effects of the liver X receptor (LXR).* Diabetes, 2004. **53 Suppl 1**: p. S36-42.
39. Ducheix, S., et al., *The liver X receptor: a master regulator of the gut-liver axis and a target for non*

alcoholic fatty liver disease. Biochem Pharmacol, 2013. **86**(1): p. 96-105.
40. Lehmann, J.M., et al., *Activation of the nuclear receptor LXR by oxysterols defines a new hormone response pathway.* J Biol Chem, 1997. **272**(6): p. 3137-40.
41. Janowski, B.A., et al., *An oxysterol signalling pathway mediated by the nuclear receptor lxrα.* 1996.
42. Janowski, B.A., et al., *Structural requirements of ligands for the oxysterol liver X receptors lxrα and lxrβ.* Proceedings of the National Academy of Sciences, 1999. **96**(1): p. 266-271.
43. Björkhem, I., S. Meaney, and U. Diczfalusy, *Oxysterols in human circulation: which role do they have?* Current opinion in lipidology, 2002. **13**(3): p. 247-253.
44. Li, Y., et al., *Induction of human liver X receptor α gene expression via an autoregulatory loop mechanism.* Molecular endocrinology, 2002. **16**(3): p. 506-514.
45. Baranowski, M., *Biological role of liver X receptors.* J Physiol Pharmacol, 2008. **59 Suppl 7**: p. 31-55.
46. Chisholm, J.W., et al., *The LXR ligand T0901317 induces severe lipogenesis in the db/db diabetic mouse.* J Lipid Res, 2003. **44**(11): p. 2039-48.
47. Gao, M., et al., *Concurrent activation of liver X receptor and peroxisome proliferator-activated receptor alpha exacerbates hepatic steatosis in high fat diet-induced obese mice.* Plos One, 2013. **8**(6): p. E65641.
48. Repa, J.J., et al., *Regulation of mouse sterol regulatory element-binding protein-1c gene (SREBP-1c) by oxysterol receptors, lxralpha and lxrbeta.* Genes Dev, 2000. **14**(22): p. 2819-30.
49. Postic, C. And J. Girard, *Contribution of de novo fatty acid synthesis to hepatic steatosis and insulin resistance: lessons from genetically engineered mice.* J Clin Invest, 2008. **118**(3): p. 829-38.
50. Cha, J.Y. and J.J. Repa, *The liver X receptor (LXR) and hepatic lipogenesis - The carbohydrate-response element-binding protein is a target gene of LXR.* Journal of Biological Chemistry, 2007. **282**(1): p. 743-751.
51. Chen, G., et al., *Central role for liver X receptor in insulin-mediated activation of Srebp-1c transcription and stimulation of fatty acid synthesis in liver.* Proc Natl Acad Sci U S A, 2004. **101**(31): p. 11245-50.
52. Chu, K., et al., *Stearoyl-coenzyme A desaturase 1 deficiency protects against hypertriglyceridemia and increases plasma high-density lipoprotein cholesterol induced by liver X receptor activation.* Mol Cell Biol, 2006. **26**(18): p. 6786-98.

53. Joseph, S.B., et al., *Direct and indirect mechanisms for regulation of fatty acid synthase gene expression by liver X receptors.* J Biol Chem, 2002. **277**(13): p. 11019-25.
54. Talukdar, S. And F.B. Hillgartner, *The mechanism mediating the activation of acetyl-coenzyme A carboxylase-alpha gene transcription by the liver X receptor agonist T0-901317.* J Lipid Res, 2006. **47**(11): p. 2451-61.
55. Repa, J.J., J.M. Dietschy, and S.D. Turley, *Inhibition of cholesterol absorption by SCH 58053 in the mouse is not mediated via changes in the expression of mrna for ABCA1, ABCG5, or ABCG8 in the enterocyte.* J Lipid Res, 2002. **43**(11): p. 1864-74.
56. Kennedy, M.A., et al., *ABCG1 has a critical role in mediating cholesterol efflux to HDL and preventing cellular lipid accumulation.* Cell Metab, 2005. **1**(2): p. 121-31.
57. Repa, J.J., et al., *Regulation of ATP-binding cassette sterol transporters ABCG5 and ABCG8 by the liver X receptors alpha and beta.* J Biol Chem, 2002. **277**(21): p. 18793-800.
58. Peet, D.J., et al., *Cholesterol and bile acid metabolism are impaired in mice lacking the nuclear oxysterol receptor LXR alpha.* Cell, 1998. **93**(5): p. 693-704.
59. Wilson, C.G., C.E. Robert-Cooperman, and B.R. Burkhardt, *pancreatic-derived factor: Novel hormone pandering to glucose regulation.* FEBS Lett, 2011.
60. Wang, C., et al., *Role of pancreatic-derived factor in type 2 diabetes: evidence from pancreatic beta cells and liver.* Nutr Rev, 2012. **70**(2): p. 100-6.
61. Yang, J. And Y. Guan, *Family with sequence similarity 3 gene family and nonalcoholic fatty liver disease.* J Gastroenterol Hepatol, 2013. **28 Suppl 1**: p. 105-11.
62. Zimmet, P., *Globalization, coca-colonization and the chronic disease epidemic: can the Doomsday scenario be averted?* Journal of internal medicine, 2000. **247**(3): p. 301-310.
63. Amos, A.F., D.J. mccarty, and P. Zimmet, *The rising global burden of diabetes and its complications: estimates and projections to the year 2010.* Diabetic medicine, 1997. **14**(S5): p. S7-S85.
64. King, H., R.E. Aubert, and W.H. Herman, *Global burden of diabetes, 1995-2025: prevalence, numerical estimates, and projections.* Diabetes care, 1998. **21**(9): p. 1414-1431.
65. Guariguata, L., et al., *Global estimates of diabetes prevalence for 2013 and projections for 2035.* Diabetes Res Clin Pract, 2014. **103**(2): p. 137-49.
66. Astrup, A. And N. Finer, *Redefining type 2 diabetes:'diabesity'or 'obesity dependent diabetes mellitus'?* Obesity Reviews, 2000. **1**(2): p. 57-59.

67. Defronzo, R.A., R.C. Bonadonna, and E. Ferrannini, *Pathogenesis of NIDDM: a balanced overview.* Diabetes care, 1992. **15**(3): p. 318-368.
68. Lin, Y. And Z. Sun, *Current views on type 2 diabetes.* Journal of Endocrinology, 2010. **204**(1): p. 1-11.
69. Das, S.K. and S.C. Elbein, *The genetic basis of type 2 diabetes.* Cellscience, 2006. **2**(4): p. 100.
70. Choi, S.M., et al., *Insulin regulates adipocyte lipolysis via an Akt-independent signaling pathway.* Molecular and cellular biology, 2010. **30**(21): p. 5009-5020.
71. Stumvoll, M., B.J. Goldstein, and T.W. van Haeften, *Type 2 diabetes: principles of pathogenesis and therapy.* Lancet, 2005. **365**(9467): p. 1333-46.
72. Van Schaftingen, E. And I. Gerin, *The glucose-6-phosphatase system.* Biochemical Journal, 2002. **362**(3): p. 513-532.
73. Young, J., *Gluconeogenesis in cattle: significance and methodology.* Journal of dairy science, 1977. **60**(1): p. 1-15.
74. Duncan, R.E., et al., *Regulation of lipolysis in adipocytes.* Annual review of nutrition, 2007. **27**: p. 79.
75. Marchesini, G., et al., *Association of nonalcoholic fatty liver disease with insulin resistance.* The American journal of medicine, 1999. **107**(5): p. 450-455.
76. Kirpich, I.A., et al., *Integrated hepatic transcriptome and proteome analysis of mice with high-fat diet-induced nonalcoholic fatty liver disease.* The Journal of nutritional biochemistry, 2011. **22**(1): p. 38-45.
77. Matsumoto, M., et al., *Dual role of transcription factor foxo1 in controlling hepatic insulin sensitivity and lipid metabolism.* The Journal of clinical investigation, 2006. **116**(9): p. 2464-2472.
78. Brown, M.S. and J.L. Goldstein, *The SREBP pathway: regulation of cholesterol metabolism by proteolysis of a membrane-bound transcription factor.* Cell, 1997. **89**(3): p. 331-340.
79. Horton, J.D., J.L. Goldstein, and M.S. Brown, *srebps: activators of the complete program of cholesterol and fatty acid synthesis in the liver.* The Journal of clinical investigation, 2002. **109**(9): p. 1125-1131.
80. Shimomura, I., et al., *Decreased IRS-2 and increased SREBP-1c lead to mixed insulin resistance and sensitivity in livers of lipodystrophic and ob/ob mice.* Mol Cell, 2000. **6**(1): p. 77-86.
81. Stumvoll, M., B.J. Goldstein, and T.W. van Haeften, *Type 2 diabetes: principles of pathogenesis and therapy.* The Lancet, 2005. **365**(9467): p. 1333-1346.
82. Wilkins, M., *Proteomics data mining.* Expert review of proteomics, 2009. **6**(6): p. 599-603.

83. Lopez, J., *Two-dimensional electrophoresis in proteome expression analysis.* Journal of chromatography B, 2007. **849**(1): p. 190-202.
84. Ünlü, M., M.E. Morgan, and J.S. Minden, *Difference gel electrophoresis. A single gel method for detecting changes in protein extracts.* Electrophoresis, 1997. **18**(11): p. 2071-2077.
85. Patton, W.F. and J.M. Beechem, *Rainbow's end: the quest for multiplexed fluorescence quantitative analysis in proteomics.* Current opinion in chemical biology, 2002. **6**(1): p. 63-69.
86. Cellulaire, B., *Two-dimensional gel electrophoresis in proteomics: old, old fashioned, but it still climbs up the mountains.* Proteomics, 2002. **2**: p. 3-10.
87. Gygi, S.P., et al., *Correlation between protein and mrna abundance in yeast.* Molecular and cellular biology, 1999. **19**(3): p. 1720-1730.
88. Sanchez, J.C., et al., *The mouse SWISS-2D PAGE database: a tool for proteomics study of diabetes and obesity.* Proteomics, 2001. **1**(1): p. 136-163.
89. Ahmed, M., J. Forsberg, and P. Bergsten, *Protein Profiling of Human Pancreatic Islets by Two-Dimensional Gel Electrophoresis and Mass Spectrometry.* Journal of Proteome Research, 2005. **4**(3): p. 931-940.
90. Ahmed, M. And P. Bergsten, *Glucose-induced changes of multiple mouse islet proteins analysed by two-dimensional gel electrophoresis and mass spectrometry.* Diabetologia, 2005. **48**(3): p. 477-485.
91. Sparre, T., et al., *IL-1β induced protein changes in diabetes prone BB rat islets of Langerhans identified by proteome analysis.* Diabetologia, 2002. **45**(11): p. 1550-1561.
92. Tilton, R.G., et al., *Diabetes-induced changes in the renal cortical proteome assessed with two-dimensional gel electrophoresis and mass spectrometry.* Proteomics, 2007. **7**(10): p. 1729-1742.
93. Douette, P., et al., *Steatosis-Induced Proteomic Changes in Liver Mitochondria Evidenced by Two-Dimensional Differential In-Gel Electrophoresis.* Journal of Proteome Research, 2005. **4**(6): p. 2024-2031.
94. Lee, S., et al., *Targeted disruption of the alpha isoform of the peroxisome proliferator-activated receptor gene in mice results in abolishment of the pleiotropic effects of peroxisome proliferators.* Molecular and cellular biology, 1995. **15**(6): p. 3012-3022.
95. Aoyama, T., et al., *Altered constitutive expression of fatty acid-metabolizing enzymes in mice lacking the*

peroxisome proliferator-activated receptor α (pparα). Journal of Biological Chemistry, 1998. **273**(10): p. 5678-5684.
96. Leone, T.C., C.J. Weinheimer, and D.P. Kelly, *A critical role for the peroxisome proliferator-activated receptor α (pparα) in the cellular fasting response: the pparα-null mouse as a model of fatty acid oxidation disorders.* Proceedings of the National Academy of Sciences, 1999. **96**(13): p. 7473-7478.
97. Vamecq, J. And N. Latruffe, *Medical significance of peroxisome proliferator-activated receptors.* The Lancet, 1999. **354**(9173): p. 141-148.
98. Tontonoz, P., E. Hu, and B.M. Spiegelman, *Stimulation of adipogenesis in fibroblasts by pparγ2, a lipid-activated transcription factor.* Cell, 1994. **79**(7): p. 1147-1156.
99. Edvardsson, U., et al., *Hepatic protein expression of lean mice and obese diabetic mice treated with peroxisome proliferator-activated receptor activators.* Proteomics, 2003. **3**(4): p. 468-478.
100. Højlund, K., et al., *Proteome analysis reveals phosphorylation of ATP synthase β-subunit in human skeletal muscle and proteins with potential roles in type 2 diabetes.* Journal of Biological Chemistry, 2003. **278**(12): p. 10436-10442.
101. Hu, Q., et al., *The Orbitrap: a new mass spectrometer.* Journal of mass spectrometry, 2005. **40**(4): p. 430-443.
102. Makarov, A., et al., *Dynamic range of mass accuracy in LTQ Orbitrap hybrid mass spectrometer.* Journal of the American Society for Mass Spectrometry, 2006. **17**(7): p. 977-982.
103. Gygi, S.P., et al., *Quantitative analysis of complex protein mixtures using isotope-coded affinity tags.* Nature biotechnology, 1999. **17**(10): p. 994-999.
104. Kippen, A.D., et al., *Development of an Isotope Dilution Assay for Precise Determination of Insulin, C-peptide, and Proinsulin Levels in Non-diabetic and Type II Diabetic Individuals with Comparison to Immunoassay.* Journal of Biological Chemistry, 1997. **272**(19): p. 12513-12522.
105. Ong, S.-E., et al., *Stable isotope labeling by amino acids in cell culture, SILAC, as a simple and accurate approach to expression proteomics.* Molecular & cellular proteomics, 2002. **1**(5): p. 376-386.
106. Oda, Y., et al., *Accurate quantitation of protein expression and site-specific phosphorylation.* Proceedings of the National Academy of Sciences, 1999. **96**(12): p. 6591-6596.
107. Geiger, T., et al., *Use of stable isotope labeling by amino acids in cell culture as a spike-in standard in*

quantitative proteomics. Nature protocols, 2011. **6**(2): p. 147-157.
108. Monetti, M., et al., *Large-scale phosphosite quantification in tissues by a spike-in SILAC method.* Nature methods, 2011. **8**(8): p. 655-658.
109. Zanivan, S., M. Krueger, and M. Mann, *In vivo quantitative proteomics: the SILAC mouse.* Integrin and Cell Adhesion Molecules: Methods and Protocols, 2012: p. 435-450.
110. De Godoy, L.M., et al., *Status of complete proteome analysis by mass spectrometry: SILAC labeled yeast as a model system.* Genome biology, 2006. **7**(6): p. 1.
111. Sury, M.D., J.-X.X. Chen, and M. Selbach, *The SILAC fly allows for accurate protein quantification in vivo.* Molecular & Cellular Proteomics, 2010: p. Mcp. M110. 000323.
112. Wu, C.C., et al., *Metabolic labeling of mammalian organisms with stable isotopes for quantitative proteomic analysis.* Analytical chemistry, 2004. **76**(17): p. 4951-4959.
113. Ross, P.L., et al., *Multiplexed Protein Quantitation in Saccharomyces cerevisiae Using Amine-reactive Isobaric Tagging Reagents.* Molecular & Cellular Proteomics, 2004. **3**(12): p. 1154-1169.
114. Hsu, J.L., et al., *Stable-isotope dimethyl labeling for quantitative proteomics.* Analytical chemistry, 2003. **75**(24): p. 6843-52.
115. Boersema, P.J., et al., *Multiplex peptide stable isotope dimethyl labeling for quantitative proteomics.* Nature protocols, 2009. **4**(4): p. 484-94.
116. Old, W.M., et al., *Comparison of Label-free Methods for Quantifying Human Proteins by Shotgun Proteomics.* Molecular & Cellular Proteomics, 2005. **4**(10): p. 1487-1502.
117. Link, A.J., et al., *Direct analysis of protein complexes using mass spectrometry.* Nature biotechnology, 1999. **17**(7): p. 676-82.
118. Washburn, M.P., D. Wolters, and J.R. Yates, 3rd, *Large-scale analysis of the yeast proteome by multidimensional protein identification technology.* Nature biotechnology, 2001. **19**(3): p. 242-7.
119. Metz, T.O., et al., *Characterization of the human pancreatic islet proteome by two-dimensional LC/MS/MS.* Journal of proteome research, 2006. **5**(12): p. 3345-3354.
120. Brunner, Y., et al., *Proteomics analysis of insulin secretory granules.* Molecular & Cellular Proteomics, 2007. **6**(6): p. 1007-1017.
121. Lu, H., et al., *The Identification of Potential Factors Associated with the Development of Type 2 Diabetes A Quantitative Proteomics Approach.* Molecular & Cellular Proteomics, 2008. **7**(8): p. 1434-1451.

122. Lu, H., et al., *Molecular and metabolic evidence for mitochondrial defects associated with β-cell dysfunction in a mouse model of type 2 diabetes.* Diabetes, 2010. **59**(2): p. 448-459.
123. Guo, Y., et al., *Quantitative proteomic and functional analysis of liver mitochondria from high fat diet (HFD) diabetic mice.* Molecular & Cellular Proteomics, 2013. **12**(12): p. 3744-3758.
124. Han, D., et al., *Detection of differential proteomes associated with the development of type 2 diabetes in the Zucker rat model using the itraq technique.* Journal of proteome research, 2010. **10**(2): p. 564-577.
125. Jin, J., et al., *Detection of differential proteomes of human β-cells during islet-like differentiation using itraq labeling.* Journal of proteome research, 2009. **8**(3): p. 1393-1403.
126. Levetan, C., et al., *Discovery of a human peptide sequence signaling islet neogenesis.* Endocrine Practice, 2008. **14**(9): p. 1075-1083.
127. Morrill, A.C. and C.D. Chinn, *The obesity epidemic in the United States.* Journal of Public Health Policy, 2004. **25**(3-4): p. 353-366.
128. Wang, Y. And M.A. Beydoun, *The obesity epidemic in the United States—gender, age, socioeconomic, racial/ethnic, and geographic characteristics: a systematic review and meta-regression analysis.* Epidemiologic reviews, 2007. **29**(1): p. 6-28.
129. Neuschwander-Tetri, B.A. and S.H. Caldwell, *Nonalcoholic steatohepatitis: summary of an AASLD Single Topic Conference.* Hepatology, 2003. **37**(5): p. 1202-1219.
130. Hou, X., et al., *Upregulation of pancreatic derived factor (FAM3B) expression in pancreatic beta-cells by MCP-1 (CCL2).* Mol Cell Endocrinol, 2011.
131. Mou, H., et al., *Knockdown of FAM3B triggers cell apoptosis through p53-dependent pathway.* Int J Biochem Cell Biol, 2013. **45**(3): p. 684-91.
132. Robert, C.E., Wu J, Burkhardt Br, Wolf B., *Transgenic mice overexpressing the novel islet specific cytokine, PANDER, exhibit glucose intolerance.* Diabetes, 2005. **54**((Suppl 1)): p. A400.
133. Xiang, J.N., D.L. Chen, and L.Y. Yang, *Effect of PANDER in betatc6-cell lipoapoptosis and the protective role of exendin-4.* Biochem Biophys Res Commun, 2012.
134. Yang, J., et al., *Structure-function studies of PANDER, an islet specific cytokine inducing cell death of insulin-secreting beta cells.* Biochemistry, 2005. **44**(34): p. 11342-52.

135. Zhuang, F., et al., *Levels of serum pancreatic derived factor (PANDER) and their correlations with islet beta cell function in newly diagnosed type 2 diabetic patients. .* Shandong Daxue Xuebao, 2011. **48**(5): p. 1-4.
136. Speliotes, E.K., et al., *Fatty liver is associated with dyslipidemia and dysglycemia independent of visceral fat: the Framingham Heart Study.* Hepatology, 2010. **51**(6): p. 1979-87.
137. Brown, M.S. and J.L. Goldstein, *Selective versus total insulin resistance: a pathogenic paradox.* Cell Metab, 2008. **7**(2): p. 95-6.
138. Robert-Cooperman, C.E., C.G. Wilson, and B.R. Burkhardt, *PANDER KO mice on high-fat diet are glucose intolerant yet resistant to fasting hyperglycemia and hyperinsulinemia.* FEBS Lett, 2011. **585**(9): p. 1345-9.
139. Biddinger, S.B., et al., *Hepatic insulin resistance is sufficient to produce dyslipidemia and susceptibility to atherosclerosis.* Cell Metab, 2008. **7**(2): p. 125-34.
140. Cao, X., et al., *Elevated circulating level of a cytokine, pancreatic-derived factor, is associated with metabolic syndrome components in a Chinese population.* Journal of Diabetes Investigation, 2015.
141. Meng, Z.X., et al., *Activation of liver X receptors inhibits pancreatic islet beta cell proliferation through cell cycle arrest.* Diabetologia, 2008. **52**(1): p. 125.
142. Helleboid-Chapman, A., et al., *Glucose regulates LXR[alpha] subcellular localization and function in rat pancreatic [beta]-cells.* Cell Res, 2006. **16**(7): p. 661-670.
143. Wilson-Grady, J.T., W. Haas, and S.P. Gygi, *Quantitative comparison of the fasted and re-fed mouse liver phosphoproteomes using lower ph reductive dimethylation.* Methods, 2013. **61**(3): p. 277-286.
144. Assimacopoulos-Jeannet, F., et al., *In vivo effects of hyperinsulinemia on lipogenic enzymes and glucose transporter expression in rat liver and adipose tissues.* Metabolism, 1995. **44**(2): p. 228-233.
145. Wanless, I.R. and J.S. Lentz, *Fatty liver hepatitis (steatohepatitis) and obesity: An autopsy study with analysis of risk factors.* Hepatology, 1990. **12**(5): p. 1106-1110.
146. Group, N.D.D., *Classification and diagnosis of diabetes mellitus and other categories of glucose intolerance.* Diabetes, 1979. **28**(12): p. 1039-1057.
147. Yoshikawa, T., et al., *Identification of liver X receptor-retinoid X receptor as an activator of the sterol regulatory element-binding protein 1c gene promoter.* Molecular and cellular biology, 2001. **21**(9): p. 2991-3000.

148. Dentin, R., et al., *Liver-specific inhibition of chrebp improves hepatic steatosis and insulin resistance in ob/ob mice.* Diabetes, 2006. **55**(8): p. 2159-2170.
149. Iizuka, K., *Recent progress on the role of chrebp in glucose and lipid metabolism.* Endocrine Journal, 2013. **60**(5): p. 543-555.
150. Calvo, D., et al., *Human CD36 is a high affinity receptor for the native lipoproteins HDL, LDL, and VLDL.* Journal of lipid research, 1998. **39**(4): p. 777-788.
151. Noguchi, N., et al., *Oxidation of lipids in low density lipoprotein particles.* Free radical research, 1998. **29**(1): p. 43-52.
152. Efanov, A., et al., *Liver X receptor activation modulates insulin secretion in pancreatic beta-cells.* Diabetologia, 2004. **47**: p. A172-A172.
153. Efanov, A.M., et al., *Liver X receptor activation stimulates insulin secretion via modulation of glucose and lipid metabolism in pancreatic beta-cells.* Diabetes, 2004. **53**: p. S75-S78.
154. Gerin, I., et al., *LXR beta is required for adipocyte growth, glucose homeostasis, and beta cell function.* Journal of Biological Chemistry, 2005. **280**(24): p. 23024-23031.
155. Choe, S.S., et al., *Chronic activation of liver X receptor induces beta-cell apoptosis through hyperactivation of lipogenesis.* Diabetes, 2007. **56**: p. A409-A409.
156. Zhang, H., et al., *Phosphoproteome analysis reveals an important role for glycogen synthase kinase-3 in perfluorododecanoic acid-induced rat liver toxicity.* Toxicology letters, 2013. **218**(1): p. 61-69.
157. Hong, K.U., et al., *Cdk1-cyclin B1-mediated phosphorylation of tumor-associated microtubule-associated protein/cytoskeleton-associated protein 2 in mitosis.* Journal of Biological Chemistry, 2009. **284**(24): p. 16501-16512.
158. Karthigeyan, D., et al., *Biology of Aurora A kinase: Implications in cancer manifestation and therapy.* Medicinal research reviews, 2011. **31**(5): p. 757-793.
159. Fedjaev, M., et al., *Global analysis of protein phosphorylation networks in insulin signaling by sequential enrichment of phosphoproteins and phosphopeptides.* Molecular biosystems, 2012. **8**(5): p. 1461-1471.
160. Soderling, T.R., et al., *Phosphorylation and inactivation of glycogen synthase by phosphorylase kinase.* Proceedings of the National Academy of Sciences, 1979. **76**(6): p. 2536-2540.

161. Cao, X., et al., *Elevated circulating level of a cytokine, pancreatic-derived factor, is associated with metabolic syndrome components in a Chinese population.* Journal of diabetes investigation, 2015.
162. Repa, J.J. and D.J. Mangelsdorf, *The role of orphan nuclear receptors in the regulation of cholesterol homeostasis.* Annual review of cell and developmental biology, 2000. **16**(1): p. 459-481.
163. Chiang, J.Y., R. Kimmel, and D. Stroup, *Regulation of cholesterol 7α-hydroxylase gene (CYP7A1) transcription by the liver orphan receptor (lxrα).* Gene, 2001. **262**(1): p. 257-265.
164. Sanyal, A.J., *AGA technical review on nonalcoholic fatty liver disease.* Gastroenterology, 2002. **123**(5): p. 1705-1725.
165. Mccullough, A.J., *Update on nonalcoholic fatty liver disease.* Journal of clinical gastroenterology, 2002. **34**(3): p. 255-262.
166. Angulo, P., *Nonalcoholic fatty liver disease.* New England Journal of Medicine, 2002. **346**(16): p. 1221-1231.
167. Reaven, G.M., *Role of insulin resistance in human disease.* Diabetes, 1988. **37**(12): p. 1595-1607.
168. Abbasi, F., et al., *Relationship between obesity, insulin resistance, and coronary heart disease risk.* Journal of the American College of Cardiology, 2002. **40**(5): p. 937-943.
169. Reaven, G.M., *Banting lecture 1988. Role of insulin resistance in human disease.* Diabetes, 1988. **37**(12): p. 1595-607.
170. Samuel, V.T., et al., *Mechanism of hepatic insulin resistance in non-alcoholic fatty liver disease.* Journal of Biological Chemistry, 2004. **279**(31): p. 32345-32353.
171. Ryysy, L., et al., *Hepatic fat content and insulin action on free fatty acids and glucose metabolism rather than insulin absorption are associated with insulin requirements during insulin therapy in type 2 diabetic patients.* Diabetes, 2000. **49**(5): p. 749-758.
172. Seppälä-Lindroos, A., et al., *Fat accumulation in the liver is associated with defects in insulin suppression of glucose production and serum free fatty acids independent of obesity in normal men.* The Journal of Clinical Endocrinology & Metabolism, 2002. **87**(7): p. 3023-3028.
173. Adiels, M., et al., *Overproduction of large VLDL particles is driven by increased liver fat content in man.* Diabetologia, 2006. **49**(4): p. 755-765.
174. Sanyal, A.J., et al., *Nonalcoholic steatohepatitis: association of insulin resistance and mitochondrial*

abnormalities. Gastroenterology, 2001. **120**(5): p. 1183-1192.
175. Kraegen, E.W., et al., *Development of muscle insulin resistance after liver insulin resistance in high-fat-fed rats.* Diabetes, 1991. **40**(11): p. 1397-1403.
176. Storlien, L., et al., *Fat feeding causes widespread in vivo insulin resistance, decreased energy expenditure, and obesity in rats.* American Journal of Physiology-Endocrinology And Metabolism, 1986. **251**(5): p. E576-E583.
177. Sandu, O., et al., *Insulin resistance and type 2 diabetes in high-fat-fed mice are linked to high glycotoxin intake.* Diabetes, 2005. **54**(8): p. 2314-2319.
178. Toye, A.A., et al., *A genetic and physiological study of impaired glucose homeostasis control in C57BL/6J mice.* Diabetologia, 2005. **48**(4): p. 675-686.
179. Freeman, H.C., et al., *Deletion of nicotinamide nucleotide transhydrogenase - A new quantitive trait locus accounting for glucose intolerance in C57BL/6J mice.* Diabetes, 2006. **55**(7): p. 2153-2156.
180. Den Boer, M., et al., *Hepatic steatosis: a mediator of the metabolic syndrome. Lessons from animal models.* Arteriosclerosis, thrombosis, and vascular biology, 2004. **24**(4): p. 644-649.
181. Pessayre, D., *Role of mitochondria in non-alcoholic fatty liver disease.* Journal of gastroenterology and hepatology, 2007. **22**(s1): p. S20-S27.
182. Spano, D., et al., *Changes of the hepatic proteome in hepatitis B-infected mouse model at early stages of fibrosis.* Journal of proteome research, 2008. **7**(7): p. 2642-2653.
183. Zhang, L., et al., *Proteomic analysis of fructose-induced fatty liver in hamsters.* Metabolism, 2008. **57**(8): p. 1115-1124.
184. Wang, X., et al., *Differential expression of liver proteins between obesity-prone and obesity-resistant rats in response to a high-fat diet.* British journal of nutrition, 2011. **106**(04): p. 612-626.
185. Eccleston, H.B., et al., *Chronic exposure to a high-fat diet induces hepatic steatosis, impairs nitric oxide bioavailability, and modifies the mitochondrial proteome in mice.* Antioxidants & redox signaling, 2011. **15**(2): p. 447-459.
186. Joo, J.I., et al., *Proteomic analysis for antiobesity potential of capsaicin on white adipose tissue in rats fed with a high fat diet.* Journal of proteome research, 2010. **9**(6): p. 2977-2987.

187. Meneses-Lorente, G., et al., *Identification of early proteomic markers for hepatic steatosis.* Chemical research in toxicology, 2006. **19**(8): p. 986-998.
188. Chanson, A., et al., *Proteomic analysis reveals changes in the liver protein pattern of rats exposed to dietary folate deficiency.* The Journal of nutrition, 2005. **135**(11): p. 2524-2529.
189. Miller, M., M. Ferguson, and J. Dillon, *Use of itraq in the discovery of non-invasive markers of NAFLD.* Liver and Metabolic Syndrome, 2009.
190. Xu, L., et al., *itraq-based proteomics for studying the effects of dioscin against nonalcoholic fatty liver disease in rats.* RSC Advances, 2014. **4**(58): p. 30704-30711.
191. Fraulob, J.C., et al., *A mouse model of metabolic syndrome: insulin resistance, fatty liver and non-alcoholic fatty pancreas disease (NAFPD) in C57BL/6 mice fed a high fat diet.* Journal of Clinical Biochemistry and Nutrition, 2010. **46**(3): p. 212-223.
192. Westerbacka, J., et al., *Genes involved in fatty acid partitioning and binding, lipolysis, monocyte/macrophage recruitment, and inflammation are overexpressed in the human fatty liver of insulin-resistant subjects.* Diabetes, 2007. **56**(11): p. 2759-2765.
193. Xu, E., et al., *Hepatocyte-specific Ptpn6 deletion promotes hepatic lipid accretion, but reduces NAFLD in diet-induced obesity: Potential role of pparγ.* Hepatology, 2014. **59**(5): p. 1803-1815.
194. Thumser, A.E., J.B. Moore, and N.J. Plant, *Fatty acid binding proteins: tissue-specific functions in health and disease.* Current Opinion in Clinical Nutrition & Metabolic Care, 2014. **17**(2): p. 124-129.
195. Sleno, L. And A. Emili, *Proteomic methods for drug target discovery.* Current opinion in chemical biology, 2008. **12**(1): p. 46-54.
196. Holly, M.K., et al., *Biomarker and drug-target discovery using proteomics in a new rat model of sepsis-induced acute renal failure.* Kidney international, 2006. **70**(3): p. 496-506.
197. Ryan, T.E. and S.D. Patterson, *Proteomics: drug target discovery on an industrial scale.* Trends in biotechnology, 2002. **20**(12): p. S45-s51.
198. Paradis, V., et al., *High glucose and hyperinsulinemia stimulate connective tissue growth factor expression: a potential mechanism involved in progression to fibrosis in nonalcoholic steatohepatitis.* Hepatology, 2001. **34**(4): p. 738-744.

199. Caldwell, S.H., C.K. Argo, and A.M. Al-Osaimi, *Therapy of NAFLD: insulin sensitizing agents.* Journal of clinical gastroenterology, 2006. **40**: p. S61-S66.
200. Hundal, R.S. and S.E. Inzucchi, *Metformin.* Drugs, 2003. **63**(18): p. 1879-1894.
201. Lin, H.Z., et al., *Metformin reverses fatty liver disease in obese, leptin-deficient mice.* Nature medicine, 2000. **6**(9): p. 998-1003.
202. Shadid, S. And M.D. Jensen, *Effects of pioglitazone versus diet and exercise on metabolic health and fat distribution in upper body obesity.* Diabetes Care, 2003. **26**(11): p. 3148-3152.
203. Kawaguchi, K., et al., *Pioglitazone prevents hepatic steatosis, fibrosis, and enzyme-altered lesions in rat liver cirrhosis induced by a choline-deficient L-amino acid-defined diet.* Biochemical and biophysical research communications, 2004. **315**(1): p. 187-195.
204. Yuan, G.-J., M.-L. Zhang, and Z.-J. Gong, *Effects of pparg agonist pioglitazone on rat hepatic fibrosis.* World journal of gastroenterology, 2004. **10**(7): p. 1047-1051.
205. Day, C.P. and O.F. James, *Steatohepatitis: a tale of two "hits"?* Gastroenterology, 1998. **114**(4): p. 842-845.
206. Day, C.P. and O.F. James, *Hepatic steatosis: innocent bystander or guilty party?* Hepatology, 1998. **27**(6): p. 1463-1466.
207. Choi, S.S. and A.M. Diehl, *Hepatic triglyceride synthesis and nonalcoholic fatty liver disease.* Current opinion in lipidology, 2008. **19**(3): p. 295-300.
208. Jou, J., S.S. Choi, and A.M. Diehl. *Mechanisms of disease progression in nonalcoholic fatty liver disease*. In *Seminars in liver disease*. 2008. © Thieme Medical Publishers.
209. Anderson, N. And J. Borlak, *Molecular mechanisms and therapeutic targets in steatosis and steatohepatitis.* Pharmacological reviews, 2008. **60**(3): p. 311-357.
210. Cheung, O. And A.J. Sanyal. *Abnormalities of lipid metabolism in nonalcoholic fatty liver disease*. In *Seminars in liver disease*. 2008. © Thieme Medical Publishers.
211. Cusi, K., *Role of insulin resistance and lipotoxicity in non-alcoholic steatohepatitis.* Clinics in liver disease, 2009. **13**(4): p. 545-563.
212. Nolan, C.J. and C.Z. Larter, *Lipotoxicity: why do saturated fatty acids cause and monounsaturates protect against it?* Journal of gastroenterology and hepatology, 2009. **24**(5): p. 703-706.
213. Garbarino, J. And S.L. Sturley, *Saturated with fat: new perspectives on lipotoxicity.* Current Opinion in Clinical Nutrition & Metabolic Care, 2009. **12**(2): p. 110-116.

214. Doege, H., et al., *Targeted deletion of FATP5 reveals multiple functions in liver metabolism: alterations in hepatic lipid homeostasis.* Gastroenterology, 2006. **130**(4): p. 1245-1258.
215. Doege, H. And A. Stahl, *Protein-mediated fatty acid uptake: novel insights from in vivo models.* Physiology, 2006. **21**(4): p. 259-268.
216. Silverstein, R.L. and M. Febbraio, *CD36, a scavenger receptor involved in immunity, metabolism, angiogenesis, and behavior.* Science signaling, 2009. **2**(72): p. Re3.
217. Greco, D., et al., *Gene expression in human NAFLD.* American Journal of Physiology-Gastrointestinal and Liver Physiology, 2008. **294**(5): p. G1281-G1287.
218. Makowski, L. And G.S. Hotamisligil, *The role of fatty acid binding proteins in metabolic syndrome and atherosclerosis.* Current opinion in lipidology, 2005. **16**(5): p. 543.
219. Newberry, E.P., et al., *Decreased hepatic triglyceride accumulation and altered fatty acid uptake in mice with deletion of the liver fatty acid-binding protein gene.* J Biol Chem, 2003. **278**(51): p. 51664-72.
220. Abu-Elheiga, L., et al., *Mutant mice lacking acetyl-coa carboxylase 1 are embryonically lethal.* Proceedings of the National Academy of Sciences of the United States of America, 2005. **102**(34): p. 12011-12016.
221. Jayakumar, A., et al., *Human fatty acid synthase: properties and molecular cloning.* Proceedings of the National Academy of Sciences, 1995. **92**(19): p. 8695-8699.
222. Wang, J., et al., *Characterization of HSCD5, a novel human stearoyl-coa desaturase unique to primates.* Biochemical and biophysical research communications, 2005. **332**(3): p. 735-742.
223. Jiang, G., et al., *Prevention of obesity in mice by antisense oligonucleotide inhibitors of stearoyl-coa desaturase-1.* The Journal of clinical investigation, 2005. **115**(4): p. 1030-1038.
224. Dorn, C., et al., *Expression of fatty acid synthase in nonalcoholic fatty liver.* Int J Clin Exp Pathol, 2010. **3**(5): p. 505-514.
225. Rivera, C.A., et al., *Toll-like receptor-4 signaling and Kupffer cells play pivotal roles in the pathogenesis of non-alcoholic steatohepatitis.* Journal of hepatology, 2007. **47**(4): p. 571-579.
226. Stienstra, R., et al., *Kupffer cells promote hepatic steatosis via interleukin-1β-dependent suppression of peroxisome proliferator-activated receptor α activity.* Hepatology, 2010. **51**(2): p. 511-522.

227. Huang, W., et al., *Depletion of liver Kupffer cells prevents the development of diet-induced hepatic steatosis and insulin resistance.* Diabetes, 2010. **59**(2): p. 347-357.
228. Bieghs, V., et al., *Role of scavenger receptor A and CD36 in diet-induced nonalcoholic steatohepatitis in hyperlipidemic mice.* Gastroenterology, 2010. **138**(7): p. 2477-2486. E3.
229. Baffy, G., *Kupffer cells in non-alcoholic fatty liver disease: the emerging view.* Journal of hepatology, 2009. **51**(1): p. 212-223.
230. Zhan, Y.-T. And W. An, *Roles of liver innate immune cells in nonalcoholic fatty liver.* World J Gastroenterol, 2010. **16**(37): p. 4652-4660.
231. Asanuma, T., et al., *Super paramagnetic iron oxide MRI shows defective Kupffer cell uptake function in non-alcoholic fatty liver disease.* Gut, 2010. **59**(2): p. 258-266.
232. Faggioni, R., et al., *Leptin deficiency enhances sensitivity to endotoxin-induced lethality.* American Journal of Physiology-Regulatory, Integrative and Comparative Physiology, 1999. **276**(1): p. R136-R142.
233. Solga, S.F. and A. Diehl, *Non-alcoholic fatty liver disease: lumen–liver interactions and possible role for probiotics.* Journal of hepatology, 2003. **38**(5): p. 681-687.
234. Thuy, S., et al., *Nonalcoholic fatty liver disease in humans is associated with increased plasma endotoxin and plasminogen activator inhibitor 1 concentrations and with fructose intake.* The Journal of Nutrition, 2008. **138**(8): p. 1452-1455.
235. Cheong, H., et al., *Phagocytic function of Kupffer cells in mouse nonalcoholic fatty liver disease models: Evaluation with superparamagnetic iron oxide.* Journal of Magnetic Resonance Imaging, 2015. **41**(5): p. 1218-1227.
236. Yoshikawa, S., et al., *Crucial role of impaired Kupffer cell phagocytosis on the decreased Sonazoid-enhanced echogenicity in a liver of a nonalchoholic steatohepatitis rat model.* Hepatology Research, 2010. **40**(8): p. 823-831.
237. Hidvegi, T., et al., *An autophagy-enhancing drug promotes degradation of mutant α1-antitrypsin Z and reduces hepatic fibrosis.* Science, 2010. **329**(5988): p. 229-232.
238. Amir, M. And M.J. Czaja, *Autophagy in nonalcoholic steatohepatitis.* Expert Review of Gastroenterology & Hepatology, 2011. **5**(2): p. 159-166.
239. Czaja, M.J., *Autophagy in health and disease. 2. Regulation of lipid metabolism and storage by autophagy: pathophysiological implications.* American Journal of Physiology-Cell Physiology, 2010. **298**(5): p. C973-C978.

240. Page, J.M. and S.A. Harrison, *Nash and HCC.* Clinics in liver disease, 2009. **13**(4): p. 631-647.
241. El-Serag , H.B., *Hepatocellular Carcinoma.* New England Journal of Medicine, 2011. **365**(12): p. 1118-1127.
242. Bugianesi, E., et al., *Expanding the natural history of nonalcoholic steatohepatitis: from cryptogenic cirrhosis to hepatocellular carcinoma.* Gastroenterology, 2002. **123**(1): p. 134-140.
243. White, E. And R.S. dipaola, *The double-edged sword of autophagy modulation in cancer.* Clinical cancer research, 2009. **15**(17): p. 5308-5316.
244. Xu, H., et al., *Chronic inflammation in fat plays a crucial role in the development of obesity-related insulin resistance.* The Journal of clinical investigation, 2003. **112**(12): p. 1821-1830.
245. King, G.L., *The role of inflammatory cytokines in diabetes and its complications.* Journal of periodontology, 2008. **79**(8S): p. 1527-1534.
246. Taniguchi, C.M., B. Emanuelli, and C.R. Kahn, *Critical nodes in signalling pathways: insights into insulin action.* Nature reviews Molecular cell biology, 2006. **7**(2): p. 85-96.
247. Bauer, C.D. and C.P. Berg, *The amino acids required for growth in mice and the availability of their optical isomers.* Journal of Nutrition, 1943. **26**: p. 51-63.
248. Allikmets, R., et al., *Characterization of the human ABC superfamily: isolation and mapping of 21 new genes using the expressed sequence tags database.* Human molecular genetics, 1996. **5**(10): p. 1649-1655.
249. Danielson, P., *The cytochrome P450 superfamily: biochemistry, evolution and drug metabolism in humans.* Current drug metabolism, 2002. **3**(6): p. 561-597.
250. Schwarz, M., et al., *Alternate pathways of bile acid synthesis in the cholesterol 7α-hydroxylase knockout mouse are not upregulated by either cholesterol or cholestyramine feeding.* Journal of lipid research, 2001. **42**(10): p. 1594-1603.
251. Nicholson, J., et al., *Proton-nuclear-magnetic-resonance studies of serum, plasma and urine from fasting normal and diabetic subjects.* Biochemical Journal, 1984. **217**(2): p. 365-375.
252. Iles, R., et al., *Phosphorylation status of liver by 31P-nmr spectroscopy, and its implications for metabolic control. A comparison of 31P-nmr spectroscopy (in vivo and in vitro) with chemical and enzymic determinations of ATP, ADP and Pi.* Biochemical Journal, 1985. **229**(1): p. 141-151.

253. Lenz, E.M. and I.D. Wilson, *Analytical strategies in metabonomics.* Journal of proteome research, 2007. **6**(2): p. 443-458.
254. Friedrich, N., *Metabolomics in diabetes research.* Journal of Endocrinology, 2012. **215**(1): p. 29-42.
255. Li, J., et al., *Pancreatic-derived factor promotes lipogenesis in the mouse liver: Role of the Forkhead box 1 signaling pathway.* Hepatology, 2011. **53**(6): p. 1906-1916.

Appendix I: Permissions

All previously published work contained within this dissertation was included with copyright permissions from the respective publishers. Use of previously published work has been noted within the text. This Appendix contains the terms and conditions of the license agreements for each previously published work.

The following license agreements are included:

Elsevier (*Molecular and Cellular Endocrinology*) [22]

BioScientifica Ltd (*Journal of Endocrinology*) [36]

Copyright permission for Elsevier (*Molecular and Cellular Endocrinology*):

ELSEVIER LICENSE
TERMS AND CONDITIONS
Nov 15, 2016

This Agreement between Mark G Athanason ("You") and Elsevier ("Elsevier") consists of your license details and the terms and conditions provided by Elsevier and Copyright Clearance Center.

License Number	3986051468407
License date	Nov 11, 2016
Licensed Content Publisher	Elsevier
Licensed Content Publication	Molecular and Cellular Endocrinology
Licensed Content Title	Quantitative proteomic profiling reveals hepatic lipogenesis and liver X receptor activation in the PANDER transgenic model
Licensed Content Author	Mark G. Athanason,Whitney A. Ratliff,Dale Chaput,Catherine B. MarElia,Melanie N. Kuehl,Stanley M. Stevens,Brant R. Burkhardt
Licensed Content Date	15 November 2016
Licensed Content Volume Number	436
Licensed Content Issue Number	n/a
Licensed Content Pages	9
Start Page	41
End Page	49
Type of Use	reuse in a thesis/dissertation

Portion	full article
Format	both print and electronic
Are you the author of this Elsevier article?	Yes
Will you be translating?	No
Order reference number	
Title of your thesis/dissertation	Quantitative Proteomic Investigation of Disease Models of Type 2 Diabetes
Expected completion date	Jan 2017
Estimated size (number of pages)	200
Elsevier VAT number	GB 494 6272 12
Requestor Location	Mark G Athanason 13032 Terrace Springs Drive TAMPA, FL 33637 United States Attn: Mark G Athanason
Total	0.00 USD

Terms and Conditions

INTRODUCTION

1. The publisher for this copyrighted material is Elsevier. By clicking "accept" in connection with completing this licensing transaction, you agree that the following terms and conditions apply to this transaction (along with the Billing and Payment terms and conditions established by Copyright Clearance Center, Inc. ("CCC"), at the time that you opened your Rightslink account and that are available at any time at http://myaccount.copyright.com).

GENERAL TERMS

2. Elsevier hereby grants you permission to reproduce the aforementioned material subject to the terms and conditions indicated.

3. Acknowledgement: If any part of the material to be used (for example, figures) has appeared in our publication with credit or acknowledgement to another source, permission must also be sought from that source. If such permission is not obtained then that material may not be included in your publication/copies. Suitable acknowledgement to the source must be made, either as a footnote or in a reference list at the end of your publication, as follows:

"Reprinted from Publication title, Vol /edition number, Author(s), Title of article / title of chapter, Pages No., Copyright (Year), with permission from Elsevier [OR APPLICABLE

SOCIETY COPYRIGHT OWNER]." Also Lancet special credit - "Reprinted from The Lancet, Vol. number, Author(s), Title of article, Pages No., Copyright (Year), with permission from Elsevier."

4. Reproduction of this material is confined to the purpose and/or media for which permission is hereby given.

5. Altering/Modifying Material: Not Permitted. However figures and illustrations may be altered/adapted minimally to serve your work. Any other abbreviations, additions, deletions and/or any other alterations shall be made only with prior written authorization of Elsevier Ltd. (Please contact Elsevier at permissions@elsevier.com)

6. If the permission fee for the requested use of our material is waived in this instance, please be advised that your future requests for Elsevier materials may attract a fee.

7. Reservation of Rights: Publisher reserves all rights not specifically granted in the combination of (i) the license details provided by you and accepted in the course of this licensing transaction, (ii) these terms and conditions and (iii) CCC's Billing and Payment terms and conditions.

8. License Contingent Upon Payment: While you may exercise the rights licensed immediately upon issuance of the license at the end of the licensing process for the transaction, provided that you have disclosed complete and accurate details of your proposed use, no license is finally effective unless and until full payment is received from you (either by publisher or by CCC) as provided in CCC's Billing and Payment terms and conditions. If full payment is not received on a timely basis, then any license preliminarily granted shall be deemed automatically revoked and shall be void as if never granted. Further, in the event that you breach any of these terms and conditions or any of CCC's Billing and Payment terms and conditions, the license is automatically revoked and shall be void as if never granted. Use of materials as described in a revoked license, as well as any use of the materials beyond the scope of an unrevoked license, may constitute copyright infringement and publisher reserves the right to take any and all action to protect its copyright in the materials.

9. Warranties: Publisher makes no representations or warranties with respect to the licensed material.

10. Indemnity: You hereby indemnify and agree to hold harmless publisher and CCC, and their respective officers, directors, employees and agents, from and against any and all claims arising out of your use of the licensed material other than as specifically authorized pursuant to this license.

11. No Transfer of License: This license is personal to you and may not be sublicensed, assigned, or transferred by you to any other person without publisher's written permission.

12. No Amendment Except in Writing: This license may not be amended except in a

writing signed by both parties (or, in the case of publisher, by CCC on publisher's behalf).

13. Objection to Contrary Terms: Publisher hereby objects to any terms contained in any purchase order, acknowledgment, check endorsement or other writing prepared by you, which terms are inconsistent with these terms and conditions or CCC's Billing and Payment terms and conditions. These terms and conditions, together with CCC's Billing and Payment terms and conditions (which are incorporated herein), comprise the entire agreement between you and publisher (and CCC) concerning this licensing transaction. In the event of any conflict between your obligations established by these terms and conditions and those established by CCC's Billing and Payment terms and conditions, these terms and conditions shall control.

14. Revocation: Elsevier or Copyright Clearance Center may deny the permissions described in this License at their sole discretion, for any reason or no reason, with a full refund payable to you. Notice of such denial will be made using the contact information provided by you. Failure to receive such notice will not alter or invalidate the denial. In no event will Elsevier or Copyright Clearance Center be responsible or liable for any costs, expenses or damage incurred by you as a result of a denial of your permission request, other than a refund of the amount(s) paid by you to Elsevier and/or Copyright Clearance Center for denied permissions.

LIMITED LICENSE

The following terms and conditions apply only to specific license types:

15. **Translation**: This permission is granted for non-exclusive world **English** rights only unless your license was granted for translation rights. If you licensed translation rights you may only translate this content into the languages you requested. A professional translator must perform all translations and reproduce the content word for word preserving the integrity of the article.

16. **Posting licensed content on any Website**: The following terms and conditions apply as follows: Licensing material from an Elsevier journal: All content posted to the web site must maintain the copyright information line on the bottom of each image; A hyper-text must be included to the Homepage of the journal from which you are licensing at http://www.sciencedirect.com/science/journal/xxxxx or the Elsevier homepage for books at http://www.elsevier.com; Central Storage: This license does not include permission for a scanned version of the material to be stored in a central repository such as that provided by Heron/XanEdu.

Licensing material from an Elsevier book: A hyper-text link must be included to the Elsevier homepage at http://www.elsevier.com . All content posted to the web site must maintain the copyright information line on the bottom of each image.

Posting licensed content on Electronic reserve: In addition to the above the following

clauses are applicable: The web site must be password-protected and made available only to bona fide students registered on a relevant course. This permission is granted for 1 year only. You may obtain a new license for future website posting.

17. **For journal authors:** the following clauses are applicable in addition to the above:

Preprints:

A preprint is an author's own write-up of research results and analysis, it has not been peer-reviewed, nor has it had any other value added to it by a publisher (such as formatting, copyright, technical enhancement etc.).

Authors can share their preprints anywhere at any time. Preprints should not be added to or enhanced in any way in order to appear more like, or to substitute for, the final versions of articles however authors can update their preprints on arXiv or RePEc with their Accepted Author Manuscript (see below).

If accepted for publication, we encourage authors to link from the preprint to their formal publication via its DOI. Millions of researchers have access to the formal publications on ScienceDirect, and so links will help users to find, access, cite and use the best available version. Please note that Cell Press, The Lancet and some society-owned have different preprint policies. Information on these policies is available on the journal homepage.

Accepted Author Manuscripts: An accepted author manuscript is the manuscript of an article that has been accepted for publication and which typically includes author-incorporated changes suggested during submission, peer review and editor-author communications.

Authors can share their accepted author manuscript:

- – immediately
    - via their non-commercial person homepage or blog
    - by updating a preprint in arXiv or RePEc with the accepted manuscript
    - via their research institute or institutional repository for internal institutional uses or as part of an invitation-only research collaboration work-group
    - directly by providing copies to their students or to research collaborators for their personal use
    - for private scholarly sharing as part of an invitation-only work group on commercial sites with which Elsevier has an agreement
- – after the embargo period
    - via non-commercial hosting platforms such as their institutional repository
    - via commercial sites with which Elsevier has an agreement

In all cases accepted manuscripts should:

- – link to the formal publication via its DOI
- – bear a CC-BY-NC-ND license - this is easy to do
- – if aggregated with other manuscripts, for example in a repository or other site, be shared in alignment with our hosting policy not be added to or enhanced in any way to appear more like, or to substitute for, the published journal article.

Published journal article (JPA): A published journal article (PJA) is the definitive final record of published research that appears or will appear in the journal and embodies all value-adding publishing activities including peer review co-ordination, copy-editing, formatting, (if relevant) pagination and online enrichment.

Policies for sharing publishing journal articles differ for subscription and gold open access articles:

Subscription Articles: If you are an author, please share a link to your article rather than the full-text. Millions of researchers have access to the formal publications on ScienceDirect, and so links will help your users to find, access, cite, and use the best available version.

Theses and dissertations which contain embedded PJAs as part of the formal submission can be posted publicly by the awarding institution with DOI links back to the formal publications on ScienceDirect.

If you are affiliated with a library that subscribes to ScienceDirect you have additional private sharing rights for others' research accessed under that agreement. This includes use for classroom teaching and internal training at the institution (including use in course packs and courseware programs), and inclusion of the article for grant funding purposes.

Gold Open Access Articles: May be shared according to the author-selected end-user license and should contain a CrossMark logo, the end user license, and a DOI link to the formal publication on ScienceDirect.

Please refer to Elsevier's posting policy for further information.

18. **For book authors** the following clauses are applicable in addition to the above: Authors are permitted to place a brief summary of their work online only. You are not allowed to download and post the published electronic version of your chapter, nor may you scan the printed edition to create an electronic version. **Posting to a repository:** Authors are permitted to post a summary of their chapter only in their institution's repository.

19. **Thesis/Dissertation**: If your license is for use in a thesis/dissertation your thesis may be submitted to your institution in either print or electronic form. Should your thesis be published commercially, please reapply for permission. These requirements include

permission for the Library and Archives of Canada to supply single copies, on demand, of the complete thesis and include permission for Proquest/UMI to supply single copies, on demand, of the complete thesis. Should your thesis be published commercially, please reapply for permission. Theses and dissertations which contain embedded PJAs as part of the formal submission can be posted publicly by the awarding institution with DOI links back to the formal publications on ScienceDirect.

Copyright permission for BioScientifica Ltd. (*Journal of Endocrinology*):

BIOSCIENTIFICA LTD. LICENSE
TERMS AND CONDITIONS
Nov 15, 2016

This Agreement between Mark G Athanason ("You") and BioScientifica Ltd. ("BioScientifica Ltd.") consists of your license details and the terms and conditions provided by BioScientifica Ltd. and Copyright Clearance Center.

License Number	3990291192726
License date	Nov 11, 2016
Licensed Content Publisher	BioScientifica Ltd.
Licensed Content Publication	Journal of Endocrinology
Licensed Content Title	PANDER transgenic mice display fasting hyperglycemia and hepatic insulin resistance
Licensed Content Author	Claudia E Robert-Cooperman, Grace C Dougan, Shari L Moak et al.
Licensed Content Date	Mar 1, 2014
Licensed Content Volume Number	220
Licensed Content Issue Number	3
Type of Use	Thesis/Dissertation
Requestor type	Author of requested content
Format	Print, Electronic
Portion	chapter/article
Rights for	Main product
Duration of use	Life of current edition
Creation of copies for the disabled	no
With minor editing privileges	no

For distribution to	Worldwide
In the following language(s)	Original language of publication
With incidental promotional use	no
The lifetime unit quantity of new product	0 to 499
The requesting person/organization is:	Mark G. Athanason
Order reference number	
Title of your thesis / dissertation	Quantitative Proteomic Investigation of Disease Models of Type 2 Diabetes
Expected completion date	Jan 2017
Expected size (number of pages)	200
Requestor Location	Mark G Athanason 13032 Terrace Springs Drive TAMPA, FL 33637 United States Attn: Mark G Athanason
Publisher Tax ID	GB 869 9945 28
Billing Type	Invoice
Billing Address	Mark G Athanason 13032 Terrace Springs Drive TAMPA, FL 33637 United States Attn: Mark G Athanason
Total	0.00 USD

Terms and Conditions

Introduction

The publisher for this copyrighted material is Bioscientifica Ltd. By clicking "accept" in connection with completing this licensing transaction, you agree that the following terms and conditions apply to this transaction (along with the Billing and Payment terms and conditions established by Copyright Clearance Center, Inc. ("CCC"), at the time that you opened your CCC account and that are available at any time at).

Limited License

The publisher hereby grants to you a non-exclusive license to use this material. Licenses are for one-time use only with a maximum distribution equal to the number that you identified in the licensing process.

Geographic Rights: Scope

Licenses may be exercised anywhere in the world.

Reservation of Rights
The publisher reserves all rights not specifically granted in the combination of (i) the license details provided by you and accepted in the course of this licensing transaction, (ii) these terms and conditions and (iii) CCC's Billing and Payment terms and conditions.

Limited Contingent on Payment
While you may exercise the rights licensed immediately upon issuance of the license at the end of the licensing process for the transaction, provided that you have disclosed complete and accurate details of your proposed use, no license is finally effective unless and until full payment is received from you (either by publisher or by CCC) as provided in CCC's Billing and Payment terms and conditions. If full payment is not received on a timely basis, then any license preliminarily granted shall be deemed automatically revoked and shall be void as if never granted. Further, in the event that you breach any of these terms and conditions or any of CCC's Billing and Payment terms and conditions, the license is automatically revoked and shall be void as if never granted. Use of materials as described in a revoked license, as well as any use of the materials beyond the scope of an unrevoked license, may constitute copyright infringement and publisher reserves the right to take any and all action to protect its copyright in the materials.

Copyright NoticeYou must include the following copyright and permission notice in connection with any reproduction of the licensed material: "Copyright [Original year of publication] [Copyright holder]."

Warranties: None
The publisher makes no representations or warranties with respect to the licensed material and adopts on its own behalf the limitations and disclaimers established by CCC on its behalf in its Billing and Payment terms and conditions for this licensing transaction.

Indemnity
You hereby indemnify and agree to hold harmless the publisher and CCC, and their respective officers, directors, employees and agents, from and against any and all claims arising out of your use of the licensed material other than as specifically authorized pursuant to this license. In no event shall the publisher or CCC be liable for any special, incidental, indirect or consequential damages of any kind arising out of or in connection with the use of the articles or other material derived from the journals, whether or not advised of the possibility of damage, and on any theory of liability.

No Transfer of License
This license is personal to you and may not be sublicensed, assigned, or transferred by you to any other person without the publisher's written permission.

No Amendment Except in Writing
This license may not be amended except in a writing signed by both parties (or, in the case

of the publisher, by CCC on publisher's behalf).

Objection to Contrary Terms
The publisher hereby objects to any terms contained in any purchase order, acknowledgment, check endorsement or other writing prepared by you, which terms are inconsistent with these terms and conditions or CCC's Billing and Payment terms and conditions. These terms and conditions, together with CCC's Billing and Payment terms and conditions (which are incorporated herein), comprise the entire agreement between you and publisher (and CCC) concerning this licensing transaction. In the event of any conflict between your obligations established by these terms and conditions and those established by CCC's Billing and Payment terms and conditions, these terms and conditions shall control.

STM Permissions Guidelines
The publisher is a signatory to the STM Guidelines and as such grants permission to other signatory STM publishers to re-use material strictly in accordance with the current STM Guidelines (http://www.stm-assoc.org/permissions-guidelines/).

Other Terms and Conditions:

V.1 10.26/12
Questions? customercare@copyright.com or +1-855-239-3415 (toll free in the US) or +1-978-646-2777.

Appendix II: Additional Data

Protein names and relative fold changes of proteins significantly differentially expressed after 1 week HFD:

Gene names	Relative fold change
Plcg1	0.381435
Stau1	2.13963
Apex2	0.596065
Arhgap1	0.6407519
Asph	1.765875
Surf1	1.947278
Fsip2	0.5817244
Mup13	4.154806
Slc4a4	0.4878055
Nfia	0.3760479
Baiap2	2.685986
Chchd2;2410018M08 Rik	1.662387
Abcc3	1.666087
Pdzd8	185.6285
Cgn	1.671586
Flnc	0.6711034
Sf1	0.6160217
Snrpa	1.472404
Fip1l1	1.510243
Cfh;Cfhr2	1.605301
Insig2	0.4657243
Dnm1l	7.330233
Arhgef1	1.921077
Xpo7	1.471547
Ttc39c	2.378669
Fga	1.459792
Evl	0.6587418
Agxt2l1	0.3559563
Larp4	2.530345
Itsn1	1.512999
Tns1	2.110816
Glod4	3.646272
Sep7	0.2648042
Kif13b	0.4754396
Rnf213	2.136759
Numa1	0.3630045
Zc3h4	1.994663
Cald1	2.691145
Mars	2.357934
Ighg2c	2.061309
Gstm1	0.6636925
Ube2m	1.728833
Hnrnpd	3.509085
Erc1	2.825798
Agl	1.547399
Eif1;Gm6900;Eif1b	0.6144141
Aox1	0.4023474
Sec23ip	3.53337
Akr1c19	0.5993993
Hnrnpa1;Gm7729	1.817484
Ate1	1.553319
Cyp3a25	0.6520976
Man2b1	0.5492947
Sod3	1.526737
Dhx15	0.5897455
Kpna6	0.6547235
Bhmt	1.827684
Slk	2.25369

Tpmt	1.877633
Pdlim1	2.977529
Ugdh	0.6157275
Pdk4	1.579193
Pfdn2	1.461094
Zfr	1.951703
Clpp	0.6554446
Cyp8b1	1.518638
Tpp1	0.2757733
Ighg1	1.836913
Apoa4	0.6535253
Spta1	1.693892
Apoa2	0.5342332
Scd1	0.6351788
Enpep	0.6631159
Sptan1	0.4039574
Gba	0.6727477
Gstp1;Gstp2	0.6149422
Rpl13a;Rpl13a-ps1	1.537478
Gstm3	0.461477
Gna11	14.8535
Pnp	0.6740907
Glb1	0.5712821
Gsta4	0.4628519
Gjb1	0.6035815
Mug1	1.64811
Mug2	0.4408822
Grn	0.5431889
Msr1	1.755044
Aimp1	1.847534
Saa4	2.044003
Stat1	1.465669
Stat3	10.21981
Plin2	0.5798625
Prox1	0.471484
Pctp	0.6361815
Rab2a	1.463263
Rad23b	10.9129
Ddx6	0.66936
Idi1	1.480901
Acot8	0.6652374
Bcl2l13	1.800706

Pcbp1	1.476236
Ube2n	0.2722801
Arf4	1.597499
Rps4x	2.105162
Hpcal1	1.830205
Ybx1	11.61314
Ppp2ca	2.252791
Pfkfb1	1.7803
Stam	0.6600952
Tceb1	0.6251504
Csrp1	2.755449
Ctsc	0.6354332
Apoa1	1.565434
Eif5b	1.646062
Clu	2.009331
Stt3b	1.456945
Mrps23	1.566648
Zc3h15	1.456376
Pcnp	0.3443391
Gm4951	5.038405
Dtx3l	1.810269
Thrap3	2.810547
Crk	1.781839
Cttn	0.6044632
Myl6;Myl6b	33.21538
Caprin1	1.743813
Cyp7b1	1.749647
Gstt2	0.6283621
Hp	0.4440044
Hsph1	0.6508555
Itih3	0.5484354
Dag1	0.5455048
Ifit1	1.454958
Cyp3a11;Cyp3a41a	0.6628979
Retsat	0.5154113
Gbf1	0.2244995
Tpm4	0.2171946
Cltb	0.6214236
Dusp23	0.5087084
Zc3h11a	1.472332
Abcf1	1.49008
Fam21	0.4245494

Paqr9	1.987115
Tex2	0.06754684
Rpl17;Gm6133	1.510082
Ccdc25	1.510886
Mtdh	0.5452358
Ubap2l	0.3041546
Eif4b	0.6744534
C8b	1.505575
Tiprl	1.642785
Mrps27	1.971511
Qars	4.113383
Scfd1	2.896938
Rmdn2	1.661653
Acot4	0.584224
Ttpa	0.5680761
Pgm3	1.65222
Etf1	0.3460988
Usp47	0.5203276
Yars2	0.6502735
Dnajb12	8.397686
Parp9	1.626375
Ufl1	2.44807
Nemf	1.498199
Ccar1	0.5146776
Fgb	1.659373
Lyrm4	0.3323779
Optn	1.615594
Afmid	0.6307501
Tat	0.5066439
Eif3l	0.4607333
Vmn1r81	0.1258778
Nags	0.2912511
Clptm1	0.6022055
Alas1	0.5096336
Cyp4f15	1.479559
Mavs	0.6691536
Fgg	1.50806
Rnpep	1.966123
Fam114a2	1.507987
Ppp2r5d	3.076226
Hnmt	1.605739

Cyp2c70	1.46422
Setd3	0.3494835
Sec16b	1.50422
Hnrpll	0.2606823
Psip1	2.914569
Adi1	1.489059
Arfgap2	0.5713199
Vwa5a	1.790802
Tmed9	0.655109
Cdk5rap3	0.386995
Nudt7	1.665034
Atp5l	0.5987753
Denr	1.799277
Smc3	0.6080589
Pin4	1.71839
Sugt1	2.482455
Dhrs7	5.154897
Gars	1.877612
Ephx1	0.6002197
Atad1	48.77322
Acad8	0.6030048
Pipox	0.6343673
Itpa	1.486199
Spcs1	1.697268
Csad	0.4896066
Ehhadh	0.6723068
Ethe1	0.602212
Aspdh	1.46729
Ranbp2	0.5426502
Tm9sf3	1.695559
Palmd	1.463614
Eny2	2.878258
Nudt5	0.5914416
Cd2ap	2.309652
Acsl4	0.6408588
Sult1b1	1.587632
Iigp1	1.69999
Srr	4.523575
Sqrdl	2.550393
Pmm2	0.1122382

Protein names and relative fold changes of proteins significantly differentially expressed after 2 weeks HFD:

Gene names	Relative fold change
Asph	1.520191
Surf1	0.4012588
Mup13	1.581039
Cgn	0.5362627
Flnc	3.149808
Ttc39c	1.62239
Fga	1.466956
Glod4	1.759611
Kif13b	0.424042
Zc3h4	0.6162452
Cald1	0.5453088
Gstm1	0.5925368
Eif1;Gm6900;Eif1b	1.58489
Akr1c19	0.5359498
Man2b1	2.267688
Bhmt	1.672241
Ugdh	0.5079002
Pfdn2	1.384016
Tpp1	0.5881704
Spta1	0.55989
Scd1	2.203455
Gna11	24.69589
Idi1	0.5049234
Ube2n	0.480821
Ctsc	0.5073419
Pcnp	2.218574
Dtx3l	1.47564
Cttn	0.3413381
Myl6;Myl6b	3.457103
Cyp7b1	1.800089
Hp	1.384247
Itih3	2.043431
Cyp3a11;Cyp3a41a	0.3255548
Retsat	1.464846
Abcf1	1.480091
Fam21	0.578999
Ccdc25	1.724578
Mtdh	0.4663262
Eif4b	0.4870172
Qars	1.395311
Scfd1	0.5498611
Rmdn2	1.365477
Pgm3	1.47092
Etf1	0.4714662
Yars2	0.6874558
Ufl1	2.201306
Fgb	1.633457
Tat	0.650875
Fgg	1.42869
Hnrpll	4.519113
Atp5l	1.662135
Ephx1	0.4425046
Itpa	1.375381
Csad	0.2105905
Eny2	1.920668
Nudt5	0.491861
Acsl4	0.5509092
Sult1b1	0.5092717
Sep9	2.282336
Nt5c	0.116789
Pir	0.6824492
Fubp3	1.450907
Acss2	0.6096534
Ttn	9.025482
Dhtkd1	1.420972
Btk	0.4266294
Hbb-b1	1.661538
Cobll1	1.626633
Hspg2	2.105071
Mylk	1.407685
Crat	2.068318
Col14a1	1.511459

Mup14	1.370881
Cfb;Gm20547;C2	0.6077403
Sumo3;Sumo2	0.5910952
Sgpl1	10.71338
Pxmp2	1.677597
Cp	1.384627
Tnxb	1.902963
Sptb	1.551577
Dsp	0.2959642
Muc5b	1.495581
Psmd13	0.672456
C6	1.619012
Plekhg4	1.524661
Tacc2	1.968936
Dlg1	0.6135224
Acbd5	0.3715609
Ide	1.92109
Pxn	0.6413723
Lamc1	1.568641
Aox3	1.401558
Psme2	0.5131395
Gstm6	0.6540459
Ces1e	0.644677
Adssl1	0.5385465
Larp1	2.585628
Akap1	1.457723
Cyp4a14	0.674463
Gpx4	0.648078
Ctss	0.6636455
Cops4	1.430214
Cyp1a2	1.410124
Igh-3	2.021223
Igh-6	0.6262731
Hbb-y	1.776248
Krt1	0.6105009
Fabp4	1.634037
Slc4a1	1.582153
Me1	0.4723189
Alb	1.372216
Polr2a	1.454335
Anxa1	1.412104
Ctsb	0.5513661

Gstm1	0.3707425
Gsn	1.550389
Ca1	1.407239
Bpgm	1.544704
Ugt2b5;Ugt2b17;Ugt2b37	0.5904676
Plg	1.383596
Eno3	14.10223
Serpina1b	1.375557
Ces1c	0.6498297
Hsd3b3	1.378858
Plaa	0.6599321
Bgn	1.847009
Atxn10	1.382918
Dpp4	0.4031897
Ahsg	1.444836
Fkbp4	2.370085
Des	4.12829
Ap1m1	0.688768
Cpox	1.561087
Inmt	0.6518477
Gfpt1	2.159464
Pfkm	6.371564
Cbr1	0.598063
Ndufs6	0.4115654
Slc16a1	1.616706
Rpl37a	0.5679144
Rpl30	0.5995435
Acta1;Actc1;Acta2;Actg2	6.720537
Psmb7	0.6828474
Urod	0.6084508
Cct4	1.737043
Serpina1e	1.428035
Egfr	1.414254
Apoh	1.639902
Fabp5	0.5283146
Serpina6	2.084544
Cd36	1.558558
Entpd5	0.6890399
Mcu	1.626438
Sult1d1	2.032893

Cyp2c67	0.6805737
Mup20	1.453761
Acaca	1.375513
Gm2a	0.6027935
Hars;Hars2	1.59032
Prdx2	1.37062
Mrps31	0.605942
Pon3	1.364828
Dbnl	1.993963
Selenbp2	1.853543
Sqstm1	1.46075
Isg15	1.64129
St8sia1	1.415362
Vcl	1.418062
Xpnpep1	1.602915
Rps27	1.551266
Acsm5	0.6864626
Acp6	0.5317355
Prkaa2	5.052769
Mzt1	2.010334
Tmx3	0.3868667
Tor1aip2	0.6197904
Ggt5	1.740589
Vwa8	1.416566
Pcdh1	0.4104605
Pdlim5	1.647413
Taco1	2.925275
Matr3	0.6450172
Ces2a	0.4863703
Blmh	2.101796
Gspt1;Gspt2	1.67325
Eif3c	1.530812
Cmbl	0.1375855
Rbpms2	0.2626331
Akr1c20	3.32357
Upb1	0.6069337
Hsd17b13	0.6831186
Hip1	2.054385
Lpcat3	0.5275787
Hba-a1;Hba	1.503392

Csde1	1.544548
Ces1f	0.656278
Lrp1	1.374426
Scpep1	0.6664485
Fdps	0.5978547
Steap4	0.5600349
Mvd	1.796615
Ufsp2	1.98497
Gstt3	0.6324927
Cisd2	0.6790795
Acot13	0.6882023
Ndufb3	1.61353
Ndufb7	1.573898
Ergic2	0.5723651
Cenpv	1.466036
Serbp1	1.631676
Spcs2	0.4282517
Mrpl45	1.715147
Sarnp	1.38444
Fkbp11	0.5593412
Chordc1	2.656504
Idh3a	2.040065
Fam210b	1.611108
Atg7	1.675447
Gng12	0.5303684
Keg1	0.6222575
Pik3ap1	0.5828943
Dpys	0.6844273
Cars	5.388743
Dkc1	2.289682
Galk1	2.099247
Naga	0.6842728
Ecsit	0.6707909
Hsd17b6	0.642907
Nsdhl	0.6587443
Coro1b	0.4238915
Ctsz	0.5692298
Npc2	0.5191967
Uba2	0.6191235

Protein names and relative fold changes of proteins significantly differentially expressed after 5 weeks HFD:

Gene names	Relative fold change
Fga	0.5565329
Eif1;Gm6900;Eif1b	4.64922
Akr1c19	0.6455268
Bhmt	1.586102
Ugdh	0.5426302
Spta1	0.618498
Scd1	0.6004217
Idi1	0.6038125
Myl6;Myl6b	2.029287
Hp	0.4751627
Itih3	0.4012391
Cyp3a11;Cyp3a41a	0.5873733
Retsat	0.2899573
Abcf1	0.07953208
Mtdh	2.600151
Rmdn2	0.6646559
Pgm3	1.379967
Etf1	0.6319894
Csad	2.012395
Nt5c	0.04433255
Sumo3;Sumo2	0.4332882
Pxmp2	1.540206
Dsp	0.5830574
Acbd5	2.108819
Pxn	2.059725
Cyp4a14	1.77883
Gpx4	1.422816
Hbb-y	1.591732
Gstm1	0.5883532
Ca1	0.2088533
Ugt2b5;Ugt2b17;Ugt2b37	0.6505102
Ces1c	1.631755
Cpox	1.557151
Cbr1	0.6257932
Ndufs6	0.5562072
Fabp5	0.4782128
Entpd5	0.6561843
Selenbp2	1.941571
Isg15	1.789426
Vwa8	1.617307
Pcdh1	1.408123
Blmh	0.1114469
Steap4	1.739158
Cisd2	0.6215038
Serbp1	2.631808
Sarnp	0.4003085
Chordc1	2.724179
Naga	0.6494528
Plcg1	2.640055
Stau1	1.407103
Evl	1.88667
Agxt2l1	0.2791096
Tns1	2.291259
Dhx15	0.6287116
Cyp8b1	1.916416
Apoa4	2.079067
Enpep	0.6379438
Stat3	0.6360878
Plin2	1.810392
Rad23b	0.6331703
Pcbp1	1.650051
Pfkfb1	1.570299
Tceb1	0.3995706
Apoa1	1.590551
Gm4951	1.739777
Crk	1.944579
Ifit1	1.40704
Paqr9	1.456485
Ttpa	0.100786
Nemf	2.038141
Clptm1	1.765388

Mavs	1.40735
Setd3	0.4788162
Sec16b	1.547328
Psip1	2.974812
Dhrs7	0.5088156
Palmd	18.86196
Sec24a	1.989405
Hsd17b10	1.586534
Ubr4	1.423306
Mlx	0.5862924
Itih4	0.1996279
Ccdc163	0.3035374
Macf1	5.142352
Gyk;Gk;Gykl1	1.532338
Tjp1	0.129243
Kng1	0.5652297
Mgll	2.896255
Cops6	1.41358
C4bp;C4bpa	0.4352296
Txndc5	0.6601502
Vmn2r18	1.521806
Mvp	0.4631629
Cul5	1.656223
Atxn2	1.403364
Myh11	3.087201
Prps1;Prps1l3	1.522675
Hnrnpl	6.022238
Carkd	0.612823
Slc27a2	1.408109
Cops5	0.6439772
Psma3	0.516611
Snx3	2.363112
Sp3	11.15369
Mtx2	1.528359
Soat2	0.5679289
Ttr	0.6546721
Apoe	1.843146
H2afv;H2afz	1.396456
Eif4a2	1.460119
Cfl1	0.5515693
Tgm2	0.6603783
Arsa	0.5973958

Cnbp	1.708198
Tango2	1.91618
Rab8a	0.5894765
Nudt2	2.029465
Nploc4	0.3513883
Cops2	1.507085
Arf2;Arf1;Arf3	17.16401
Abat	1.428664
Arf6	1.664782
Rpl32	1.762477
Tubb4b;Tubb4a	1.475187
Slc9a3r1	1.538232
Erh	0.6501374
Casp7	1.493398
Cyp2e1	1.680852
Pepd	0.4708975
Acss3	1.723395
Brd4	0.6229033
Irgm1	1.558377
Hsd3b5	1.642486
Tgtp;Tgtp1	2.886168
Tfrc	1.926037
Ugt1a6	0.5312187
Ecm29;AI314180	1.614732
Spcs3	0.195443
Usmg5	1.483233
Ldhd	1.429092
Cdc42bpb	1.535184
Plxna4	0.6180173
Pdk1	1.568133
Sep9	1.535167
Eif2a	0.2418695
Eea1	1.501697
Scfd2	0.6488068
Hmgcs1	0.4085626
Abca6	0.2605887
Sf3a1	1.488119
Hexim1	1.634173
Hpgd	2.072552
Prodh2	1.391638
Idh3b	1.582234
Ppa2	1.405769

Cyp4a12a;Cyp4a12b	1.47192
Gckr	1.559857
Cyp2c50	1.528956
Rtn4ip1	1.47229
Cds2	0.6181253
Prpf8	0.2757098
Btf3l4	0.4282234
Txndc12	0.4925236
Emc2	0.6134063
Xpot	2.838478
Smc1a	0.4501086
Pbld2	1.393424
Nsfl1c	0.4396557
Aldh1b1	0.5518795
Tomm70a	1.595674
Ccdc47	0.1405633
Cyc1	1.548082

Iyd	0.3596738
Hsd17b11	1.424516
Ehd4	1.492226
Lima1	2.381341
Cse1l	1.463295
Ddx21	1.503807
Cog8	0.5566417
Pdk2	0.5369678
Bag3	0.6163701
Edf1	1.447348
Txnrd1	0.645256
Tbl2	1.853377
Hebp1	1.406322
Myo1c	1.502757
Vapa	1.378392
Slc25a20	1.53385

Protein names and relative fold changes of proteins significantly differentially expressed after 9 weeks HFD:

Gene names	Relative fold change
Ugdh	0.5891099
Spta1	0.5784131
Idi1	0.3123715
Myl6;Myl6b	1.866926
Itih3	0.574432
Retsat	0.08500097
Rmdn2	1.887924
Dsp	0.3020843
Acbd5	2.229617
Pxn	0.3890634
Hbb-y	1.556997
Ces1c	1.568841
Ndufs6	1.9469
Fabp5	0.480027
Selenbp2	0.5083526
Blmh	0.303142
Chordc1	0.2528934
Tns1	0.2825769
Apoa4	0.3981675
Stat3	2.688463
Paqr9	1.724019
Nemf	0.5315067
Psip1	3.046514
Macf1	2.167337
Vmn2r18	2.949214
Myh11	0.3472071
Hnrnpl	5.94249
Nudt2	1.774392
Arf2;Arf1;Arf3	2.098171
Ldhd	0.4680342
Cdc42bpb	2.235204
Eif2a	1.988483
Hmgcs1	1.654925
Hpgd	5.033892
Cyp2c50	1.599537
Iyd	0.4577687
Lima1	1.919864
Ddx21	0.5620486
Pdk2	1.587814
Edf1	1.661237
Mup13	0.2916172
Kif13b	2.068748
Cald1	4.156598
Gna11	4.018547
Cyp7b1	0.5710642
Tat	0.2069451
Hnrpll	3.986255
Sult1b1	1.7032
Sep9	0.5072663
Cobll1	0.4869169
Plekhg4	0.4872091
Ide	2.734689
Krt1	0.04630987
Slc4a1	0.5679211
Me1	1.536843
Serpina1e	0.499966
Serpina6	0.1048201
Mzt1	0.4120255
Matr3	0.4479917
Dkc1	0.2974608
Ctsz	0.5764206
Uba2	29.40795
Slc4a4	0.2905559
Numa1	0.04206754
Pdlim1	2.270483
Pdk4	0.4979565
Gstp1;Gstp2	0.517442
Mug2	0.2840395
Saa4	2.415868
Bcl2l13	1.607058
Ybx1	7.352725
Stam	0.5341896
Csrp1	2.19096

Stt3b	1.864374
Zc3h15	0.5954136
Dag1	1.814263
Hnmt	1.539679
Acad8	0.5923195
Iigp1	1.929469
Cyp4a10	0.5185038
Rbmx;Rbmxl1	1.637656
Gpd2	1.523714
Tpd52l2	0.5863031
Gpcpd1	0.1907386
Dusp3	1.629201
Aldh3a2;Aldh3a1	1.522434
Eif2b3	3.538503
Ank1	0.5590422
9030624J02Rik	0.4259851
Sorbs2	0.5788537
Ier3ip1;Hdhd2	1.579509
Ces2g	1.960606
Luc7l2	0.5384802
Grsf1	1.536767
Acacb	8.891789
Pklr	1.663551
Utrn	1.806213
Lypla1l	3.197311
Sult1a1	1.610899
Gbe1	1.610307
Sympk	15.9032
Lamtor5	2.337684
Son	0.5651766
Aamp	3.437081
Atp6v0a1	1.933604
Faah	5.074807
Timm44	0.4295759
Copb2	1.616613
Snca	0.451253
Acot1	0.5924052
Nnmt	0.5163231
C4b	1.658415
	0.1829913
S100a10	0.5979404
H1f0	0.4980908

Gstm2	0.5002655
Fasn	1.818273
Vtn	0.5427374
Ldlr	1.703822
Fkbp2	0.4326515
Rab11b;Rab11a;Rab25	2.25317
Tbca	0.5228305
Tdo2	0.4152339
Inpp1	1.625695
Csrp3	2.599492
Fabp2	1.787468
Nucb1	2.729924
Gch1	0.5900288
Hp1bp3	0.3276092
Slco2b1	1.616068
Galns	0.4148191
Gm4952	1.643673
Mocs1	2.072997
Gcdh	1.551488
Gpam	1.88744
Ddx5	0.3415053
Atrx	0.5959773
Pdcd4	1.934485
Mrc1	2.233552
Trim28	0.4374858
Gstt1	2.0547
Dync1li2	2.541237
	1.692045
Sestd1	1.559453
Mogs	0.5716146
Vac14	1.642213
Tmem214	0.4690467
Clmn	2.260602
Fam160b1	0.2771389
Fam25c	0.5851889
Sltm	0.4088566
Ugt3a2	0.2512125
Agpat2	1.742233
Gale	1.839434
Kars	2.222318
Ces1	1.671457

Acaa1b	1.524465
Pla2g15	0.5986165
Acy3	1.53319
Tbrg4	0.4697535
Nono	3.288072
Aass	0.5112808
Arpc5	1.781187
Nubpl	5.048543
L3hypdh	2.759283
Nhp2l1	0.5768063
Oxsm	1.694731

Selo	1.538901
Baiap2l1	0.2501519
Crot	1.577842
Pygl	1.534469
Msrb1	1.993234
Adh4	1.873812
Fbxo6	0.4945161
Pex14	1.77883
Gbp2	0.2456626
Strap	0.3241378
Hnrnpc	1.601239